Acoustic sensing of the bacterium-substratum interface

Olsson, Adam Lars Johan

Acoustic sensing of the bacterium-substratum interface

Acoustic sensing of the bacterium-substratum interface

University Medical Center Groningen, University of Groningen
Groningen, The Netherlands

Cover: An artist's impression of quartz crystals. Quartz crystals, when of a certain cut, are used for acoustic sensing devices, such as the QCM-D used in this thesis. This cover was designed by Karl Rehnström.

Printed by Drukkerij van Denderen, Groningen, The Netherlands

ISBN (printed version): 978-90-367-5206-0
ISBN (electronic version): 978-90-367-5207-7

rijksuniversiteit
groningen

Acoustic sensing of the bacterium-substratum interface

Proefschrift

ter verkrijging van het doctoraat in de
Medische Wetenschappen
aan de Rijksuniversiteit Groningen
op gezag van de
Rector Magnificus, dr. E. Sterken,
in het openbaar te verdedigen op
woensdag 9 november 2011
om 14.30 uur

door

Adam Lars Johan Olsson
geboren op 16 juni, 1981
te Domkyrkoförs, Zweden

Promotores:	Prof. dr. ir. H.J. Busscher Prof. dr. H.C. van der Mei
Co-promotor:	Dr. P.K. Sharma
Beoordelingscommissie:	Prof. dr. A. Herrmann Prof. dr. ir. M.C.M. van Loosdrecht Prof. dr. ir. W. Norde

Paranimfen:	Gerwin Engels
	Arina Buizer

Contents

Chapter 1

General Introduction

Microbial adhesion

Microorganisms adhere to surfaces of widely different origin. Once adhering on a surface, microorganisms grow and encase themselves in extracellular polymeric substances creating a protective gel-like matrix. This forms into a three-dimensional structure called "biofilm" (Allison, 2003). Biofilms may be beneficial in, for instance, bioremediation and bioreactors,(Morikawa, 2006) but create problems when formed on industrial surfaces in terms of pipeline corrosion, plugging of filters and insulation in heat exchangers (Costerton et al., 1987). Furthermore, when biofilms form on biomedical devices, they not only impair their functionality, but also cause severe infections that are potentially lethal for the patient (Gristina, 1987). Desired or not, in order to influence the development of biofilms, fundamental knowledge of the mechanisms behind initial microbial adhesion as well as the mechanical properties the microbe-substratum interface is essential.

Theoretical mechanisms of microbial adhesion

Microbial adhesion is often explained based on the DLVO theory (named after Derjaguin, Landau, Verwey and Overbeek) (Hermansson, 1999). The DLVO theory describes the interaction between colloids and surfaces in terms of Lifshitz-Van der Waals and electrostatic interaction forces. Lifshitz-Van der Waals forces are directly proportional to the so-called Hamaker constant but reversibly proportional to distance. The Hamaker constant describes the interaction forces due to the dielectric properties of the colloid, the surface and the surrounding medium, and is therefore not universal, but unique for a specific colloid-substratum-medium combination. For bacterial cells interacting with substratum surface in water, the Hamaker constant is generally positive, which implies attractive Lifshitz-Van der Waals forces (Norde & Lyklema, 1989).

Electrostatic interactions occur between two electrically charged surfaces. In water, the surface electric charge is balanced by counter ions that arrange themselves in concentration gradient away from the surface, normally referred to as the electrical double layer. The size of the electrical double layer is dependent on the surface charge and the concentration (ionic strength) as well as the valence of the ions. In nature, the majority

of surfaces (including bacterial cell surfaces) are negatively charged. Therefore, when DLVO calculations are applied on bacterial adhesion, the electrostatic interaction term is mostly repulsive (Figure 1).

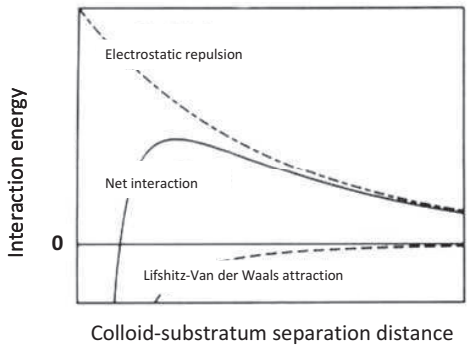

Figure 1. DLVO-curves showing the contribution of electrostatic repulsion and attractive Lifshitz-Van der Waals forces as a function of colloid-substratum separation distance. The units are arbitrary. In this example the electrostatic repulsion is large and the net-interaction is repulsive, which is normally the case at low ionic strengths.

Another theoretical approach towards bacterial adhesion is the thermodynamic one (Hermansson, 1999). In the thermodynamic approach, the Gibbs free energy is calculated simply by subtracting the free energies of the bacterium-liquid interface (γ_{bl}) and surface-liquid interface (γ_{bw}) from the free energies of the bacterium-surface interface (γ_{bs}) (Figure 2).

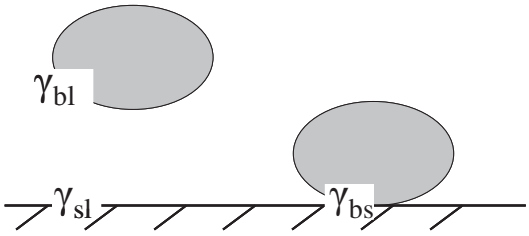

Figure 2. Thermodynamic approach toward bacterial adhesion: adhesion is favorable when the sum of the bacterium-liquid and liquid-substratum interfacial free energies (γbl + γls) is larger than the bacterium-substratum interfacial energy γbs.

If the Gibbs free energy is negative, the interaction is favorable and adhesion is expected. The thermodynamic approach assumes a minimal separation distance between the interacting surfaces and covers strong acid-base interactions, as e.g. hydrogen bonding which are active at only very short distances.

The Dutch scientist Van Oss eventually combined the two approaches in the so called extended DLVO-theory (Van Oss, 2003). Although the extended DLVO-theory provides a good starting point in order to understand colloidal particle adhesion to surfaces, its application toward bacterial adhesion assumes bacteria to behave like inert particles, which is by no means guaranteed. The similarity between microorganisms and rigid colloidal particles stops at about their shape and size. Not surprisingly, there are about just as many examples in literature for which (extended) DLVO calculations are successful as unsuccessful in explaining microbial adhesion.

Microbes are living organisms possessing a vast variety of cell surface appendages that affect their adhesion to surfaces. Appendages may both offer steric hindrance (Rijnaarts et al., 1995) or stretch out and overcome net-repulsive forces mediating adhesion from a distance via a bridging process (Heckels et al., 1976). In nature, practically all surfaces are quickly covered by a layer of adsorbed macromolecular components, which may either increase or decrease microbial adhesion (Dunne, 2002). Microbes can adhere via specific protein-ligand interactions with proteins present in conditioning films formed in, for instance, the oral cavity (Gong et al., 2000) or the blood stream (Saravia-Otten et al., 1997). Theoretical predictions become even more troublesome giving the fact that the conformation of bacterial cell surface appendages can be strongly influenced by environmental factors, such as ionic strength and pH (Sonohara et al., 1995). Furthermore, neither of the theoretical approaches accounts for the possibility of time dependence in the bacterial adhesion forces due molecular rearrangements within the interface into a more energetically favorable conformation. As a consequence, in the end, all theoretical approaches for microbial adhesion require experimental validation.

Methods to study microbial adhesion

Flow displacement devices are frequently used to gain insight in microbial adhesion or desorption kinetics (Boks et al., 2008; Katsikogianni & Missirlis, 2010). Microbial adhesion kinetics provides the researcher with valuable information about the tendency of the examined microbe to adhere to a substratum surface, but does not address the properties of the adhesive bond. The strength of the adhesive bond is sometimes estimated in flow displacement devices from the shear forces required to cause

detachment of adhering bacteria (De La Fuente et al., 2007; Katsikogianni & Missirlis, 2010). Similarly there are ways to estimate the adhesive force using rotating discs (De Jong et al., 2002) or centrifugal force assays (Prakobphol et al., 1995). However, these are indirect methods only showing the consequence of an applied force.

Optical techniques such as total internal reflection aqueous fluorescence microscopy and total internal reflection microscopy can be used to visualize bio-interfaces at nm scale (Vigeant et al. 2001 & 2002; Walz, 1997), but do not address the mechanical characteristics of the bond. Only a few methods exist to directly measure the mechanical properties of the interface. Optical tweezers (Klein et al, 2003) and atomic force microscopy (AFM) (Camesano & Logan, 2000) do measure adhesive forces by pushing and pulling a microbe towards and away from a substratum surface. Unfortunately this only gives information of the adhesive bond near its failure point, *i.e.* bond breakage. Also, since the microbial cells are fixed, either by a light trap or by glueing to the AFM cantilever, the microbes can no longer move freely, and thus the adhesion process is forced and unnatural and therefore potentially invasive. Detachment forces required to detach adhering bacteria using AFM are orders of magnitude larger than the shear forces required to detach bacteria in flow displacement devices (Boks et al., 2008). It is difficult to judge whether this discrepancy is due to an increased number of contact points caused by the applied load during forced adhesion in AFM, or if a larger force is required to detach microbes perpendicularly rather than latterly from a substratum surface. Perpendicularly directed forces must break multiple bonds simultaneously, whereas lateral shear forces could induce a rolling movement of the adhering microbe in which the bonds could break individually, one by one, from side to side. On the other hand, optical tweezers that also operate perpendicularly to a substratum surface, have measured adhesion forces within the same range as found in flow displacement devices (Boks et al., 2008). One major disadvantage with optical tweezers is that the light intensity of the optical trap may cause physiological damage to the microbes (Rasmussen et al., 2008).

Even though these techniques continuously reveal new aspects of microbial adhesion, the disadvantage of these techniques is that they are destructive and invasive. Therefore an experimental technique to study the mechanical properties of the interface between an adhering microbe and a substratum surface non-destructively and non-invasively is needed. One potential technique could be acoustic sensing.

Acoustic sensing of bacterial adhesion

Among the family of acoustic sensing devices, the Quartz Crystal Microbalance (QCM) has been widely used to measure adhesion kinetics as well as the mass of molecules adsorbed at solid-liquid interfaces (Andersson et al., 2005; Johannsmann et al., 1992; Voinova et al., 2002). QCM senses adsorbed mass at a ng/cm^2 scale, in terms of negative shifts in the resonance frequency of an oscillating quartz-crystal sensor-surface. QCM is not only very sensitive to adsorbed mass but it also possesses the ability to monitor changes in resonance frequency and dissipative energy losses in real time. This together with the fact that it does not need any further labeling for analysis have been strong arguments for using the QCM as a rapid biosensor for bacterial presence. Several papers in the literature describe bacterial adhesion based on QCM experiment and these include a variety of different strains and species, such as *Escherichia coli* (Muramatsu et al., 1989; Poitras & Tufenkji, 2009a; Serra et al., 2008), *Staphylococcus aureus* (He et al., 1995; Serra et al., 2008) *Staphylococcus epidermidis* (Pavey et al., 2001)*, Mycobacterium phlei* (Serra et al., 2008) *Edwardsiella tarda* (Hong et al., 2009)*,* and the shrimp pathogen *Vibrio harveyi* (Buchatip et al., 2010).

Since the QCM senses adhering bacteria via their connection to the surface, QCM can also be used to gain information about the processes within the microbe-substratum interface (Figure 3) (Olofsson et al., 2005; Otto et al., 1999). QCM studies showed differences in the adhesive properties between different bacterial strains as well as differences due to substratum surface characteristics. The interpretation of the experimental outcome has been difficult. Some studies report positive frequency shifts due to bacterial adhesion (Olofsson et al., 2005; Olsen et al., 2003; Poitras & Tufenkji, 2009b; Su & Li, 2005; Vaughan et al., 2001) which according to conventional QCM-theory indicate mass loss. In order to fully exploit the potential of QCM for bacterial adhesion studies, there is an urgent need for a model that is able to unambiguously explain the QCM outcomes of bacterial adhesion experiments.

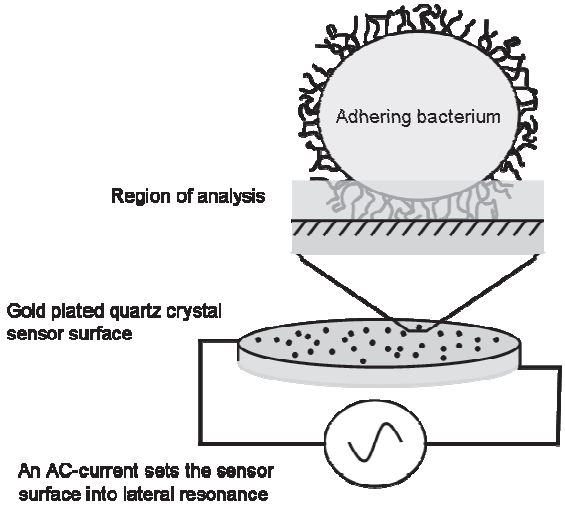

Figure 3. Schematic illustration of the potential benefit of using QCM to study bacterial adhesion. The QCM senses the bacteria via its adhesive bond towards the sensor surface, making it an ideal tool to monitor processes confined to the bacterium-substratum interface.

Aim of this thesis

QCM has been forwarded as a non-destructive and non-invasive technique to study dynamic processes within bacterium-substratum interfaces, but its implementation towards bacterial adhesion has been hampered due to the lack of an unambiguous interpretation of positive frequency shifts in conventional QCM-theory.

The aim of this thesis is to develop an interpretation of positive frequency shifts in the study of bacterial adhesion using QCM. Subsequently, positive frequency shifts are used to study mechanical properties of bacterium-substratum interface according to the newly developed interpretation for selected bacterial strains and environmental conditions.

Chapter 2

Influence of cell surface appendages on the bacterium-substratum interface measured real-time using QCM-D

Adam. L. J. Olsson, Henny. C. van der Mei, Henk J. Busscher, Prashant K. Sharma, *Langmuir*, **2009**, 25, 1627-1632

Abstract

QCM-D (Quartz Crystal Microbalance with Dissipation) utilizes an oscillating quartz crystal to register adsorption of rigid masses through a decrease in its resonance frequency *f*. In addition, QCM-D has the ability to measure the dissipative nature of non-rigid masses adhering to the crystal surface in the form of oscillation amplitude decay time. Although QCM has been applied to register bacterial adhesion to the crystal surface, full interpretation of the frequency change and dissipation signal has hitherto been impossible due to the complex interactions within the distance of 250 nm between the substratum and the bacterial cell surface. Here, we study adhesion of a series of *Streptococcus salivarius* mutants, possessing various surface appendages of known lengths, as a function of time using QCM-D. In addition, the number of bacteria adhering to the crystal surface was determined. The results show that adhesion of a "bald" bacterium, completely devoid of surface appendages, is registered as a frequency decrease. Adhesion of bacteria possessing surface appendages either yield much smaller decrease or increase in frequency, despite the fact they adhere in higher numbers. Furthermore, the magnitude of frequency and dissipation shifts was found to be influenced by the distance at which the cell body was held from the sensor surface by its surface appendages.

Introduction

Biofilms can be advantageous, such as in waste water treatment, soil and plant ecology, but are disadvantageous on e.g. ship hulls, and in food and paper industry. Moreover, biofilms can be fatal in biomedical implant-related infections. Bacterial adhesion constitutes the starting point for biofilm formation and is initially reversible, but due to interfacial rearrangements becomes irreversible within minutes after first contact (Van der Mei et al., 2008). The interfacial events occurring in initial bacterial adhesion and their time sequence are poorly understood and have only been speculated upon. Poisson analysis of adhesion forces revealed in Atomic Force Microscopy have suggested that overtime the number of acid-base pairs formed between a substratum surface and a bacterial cell surface may rapidly increase due to removal of interfacial water to cause irreversible adhesion (Boks et al., 2008).

In early physico-chemical approaches of bacterial adhesion to surfaces, bacteria were often compared with inert colloidal particles, possessing a certain charge and hydrophobicity, and the influence of structural cell surface appendages was usually neglected, as is still often the case due to experimental difficulties in assessing microscopic or nanoscopic cell surface features. Yet these surface appendages, usually present in different lengths and composition, may play an important role in the interfacial phenomena leading to irreversible adhesion.

QCM-D (Quartz Crystal Microbalance with Dissipation) is a technique by which complex interfacial processes, as occurring during bacterial adhesion, can be monitored (Olofsson et al., 2005; Otto et al. 1999; Otto & Hermansson, 2003). In essence, a QCM is a sensitive balance with a resolution of several ng/cm^2 and an additional capability to measure the dissipative nature of the attached mass. A voltage across a gold plated AT-cut quartz crystal sets the crystal into lateral resonance at a frequency f (approximately 5 MHz) giving rise to an evanescent wave in the adjacent medium. Resonance frequency decreases (Δf) upon mass deposition (Δm) according to the Sauerbrey's equation (Eq. 1) (Sauerbrey, 1959)

$$\Delta m = -\frac{C_{QCM}}{n}\Delta f \qquad (1)$$

where C_{QCM} is a sensitivity constant and n is the overtone number of the oscillating frequency (1, 3, 5, 7, 9, 11 or 13). The Sauerbrey equation is valid when a rigid mass attaches to the crystal surface, but when a flexible mass attaches, non-rigidity causes deformation during oscillation, resulting in dissipative energy losses. This so-called dissipation (D) yields information about the interfacial coupling of the attached mass to the crystal surface. In highly dissipative systems ($\Delta D > 10^{-6} / \Delta f$), the Sauerbrey equation underestimates the attached mass (the "missing mass" effect), as explained by Voinova et al. (Voinova et al., 1997 & 2002; Voinova et al., 1999). A fast decay of the evanescent shear wave due to dissipation in an aqueous environment results in a maximum penetration depth (k) of 250 nm (Kanazawa & Gordon, 1985) at 5 MHz according to

$$k = \sqrt{\pi f \rho / \eta} \qquad (2)$$

where ρ is the density and η the viscosity of the fluid surrounding the crystal vibrating at a frequency f.

Although the output parameters of a QCM-D experiment are well defined, their interpretation is often difficult, especially in bacterial adhesion. Many studies on bacterial adhesion and biofilm formation report a decrease in resonance frequency upon bacterial adhesion in line with the Sauerbrey equation (Nivens et al., 1993; Otto et al., 1999; Otto & Hermansson, 2003; Schofield et al., 2007), although some studies report an increase in resonance frequency (Chen et al., 1996; Olofsson et al., 2005; Reipa et al., 2006) which according to the Sauerbrey equation indicates a mass loss. It is unknown at present, why some strains give positive or negative frequency shifts. Proposed mechanisms include biosurfactant release by adhering bacteria, increased fluid viscosity in the interfacial region and different degrees of bacterial cell surface hydrophobicity (Olofsson et al., 2005). Full and unambiguous interpretation of the QCM-D output parameters yielding support for any of the above hypotheses, however, is hampered by lack of knowledge of the

number of bacteria adhering to the crystal surface as a function of time during measurements. Moreover, these studies have all been performed with strains that have not been characterized with respect to the lengths and composition of possible cell surface appendages.

Therefore, the aim of this study was to determine QCM-D output parameters (Δf and ΔD) as a function of time during adhesion of different *Streptococcus salivarius* strains, with cell surface appendages of known lengths (Van det Mei et al., 1987). In addition, the number of adhering bacteria to the crystal surface was measured as a function of time. The combined results of both sets of experiments were employed to provide an interpretation of QCM-D output parameters based on the absence or presence of bacterial cell surface appendages of various lengths.

Materials and Methods

Bacterial Strains, Culture Conditions, and Harvesting

S. salivarius HB, HB7, HBV5, HBV51 and HBC12 were used in this study. In the past, these strains have been shown to be equally hydrophilic and negatively charged, but different in their possession of cell surface appendages (Van det Mei., 1987). Strains are either completely devoid of any surface appendages, such as the "bald" mutant HBC12, or are "hairy" possessing cell surface appendages, formally designated as fibrils, of 4 different antigens B, C, D and F and with different lengths (see Figure 1 for a schematic presentation of the cell surfaces). Bacteria were cultured in Todd Hewitt Broth (THB, OXOID, Basingstoke, UK) at 37°C in ambient air. For each experiment, the strains were inoculated from blood agar in 10 ml THB for 24 h. This pre-culture was added to 200 ml of THB to prepare a main culture, which was grown for 16 h before harvesting. Bacteria were harvested by centrifugation (5 min at 5000 *g*), washed twice and resuspended in adhesion buffer (50mM potassium chloride, 2 mM potassium phosphate and 1 mM calcium chloride, pH 6.8). To break bacterial chains, cells were sonicated intermittently 3 times for 10 s at 30 W on ice (Vibra Cell model 375; Sonics and Materials, Danbury, CT). The bacterial concentration was determined by Bürker-Türk counting chamber counting. Finally, bacteria were diluted in adhesion buffer to a concentration of 3×10^8 bacteria ml^{-1}.

QCM-D Experiments

Bacterial adhesion was studied under flow using a QCM-D device, model Q-sense E1 (Q-sense, Gothenburg, Sweden) together with a window module for optical monitoring of the sensor surface. A flow system was built using two 60 ml reservoirs connected to each other via the QCM-D module. At the start of each measurement, the crystal sensor was incubated in adhesion buffer. When stable base lines for both *f* and *D* were achieved, the bacterial suspension was allowed to flow through the system under hydrostatic pressure, yielding a pulse-free flow by pumping the suspension from the outlet to inlet reservoir using a peristaltic pump (Ismatec SA, Glattbrugg, Switzerland). Experiments were conducted at 23℃ under a flow rate of 300 µl/min and bacterial adhesion was observed for 4 h. The QCM-D flow chamber is disc shaped with a volume of approximate 100 µl and a diameter of 14 mm with inlet and outlet facing the crystal surface, and the flow applied creates an approximate shear rate of 7.5 s^{-1}. Gold plated AT-cut quartz crystals, with a sensitivity constant of 17.7 ng/cm^2 (Q-sense, Gothenburg, Sweden), were used as substratum. Before each experiment, the crystals were cleaned by 10 min UV/Ozone treatment, followed by immersion into a 3:1:1 mixture of ultrapure water, NH_3 and H_2O_2 (Merck, Darmstadt, Germany) at 70℃ for 10 min and 10 min UV/Ozone treatment. The evanescent shear wave penetration depth into the adjacent medium decreases with increasing overtone number (Eq. 2). This provides the ability to slice the bacterium-substratum interface into sections and grab the signal from these sections separately. Therefore, frequency shift and dissipation were measured and recorded at all harmonics (fundamental frequency, 3^{rd}, 5^{th}, 7^{th}, 9^{th}, 11^{th} and 13^{th} overtone) with the QSoft 401 software (Q-sense, Gothenburg, Sweden) in real-time throughout the adhesion process. The responses from the 7^{th} overtone and beyond were nearly the same, both qualitatively and quantitatively, and therefore the 9^{th} to the 13^{th} overtone are not presented. Further data analyses were done with QTools (Q-sense, Gothenburg, Sweden) and Excel 2003 (Microsoft Corporation). Each experiment was carried out in triplicate.

In order to clean the crystal and remove adhering bacteria after each measurement, crystals were immediately sonicated in SDS 2% (w/v) and ethanol (70%) for 10 min followed by ultrapure water rinse. Between measurements, 10 ml SDS (2%) followed by 20 ml ultrapure water was pumped through the system to clean the QCM-D crystal holder.

Bacterial Adhesion in the QCM-D Chamber

Simultaneously with the *f*- and *D*-signal, bacterial deposition onto the sensor surface was observed with a metallurgical microscope (Leica DM2500 M, Rijswijk, The Netherlands) equipped with a 20x objective (Leica HCXPL FLUOTAR). Using a CCD camera (Model A101, Basler vision technologies, Ahrensburg, Germany) mounted to the microscope and coupled to an image analyzer (TEA, Difa, Breda, The Netherlands), images were grabbed at regular time intervals during the adhesion process. The number of adhering bacteria as a function of time was subsequently enumerated from these images using in-house software based on the MATLAB platform.

Results

Bacterial Adhesion Kinetics

The adhesion kinetics of the five streptococcal strains to the crystal sensor surface is presented in Figure 1. Initial bacterial deposition rates, i.e. the tangent towards the lines in the origin, are similar for all strains, but after 4 h of adhesion, significant ($p<0.05$, pairwise between all strains, Student t-test) differences in the number of adhering bacteria become evident, dependent on the type of surface appendage present. HB and HBV5 express the highest fibril density and adhere in highest numbers, followed by the less densely fibrillated strains HB7 and HBV51. The mutant strain HBC12 adheres in the lowest numbers.

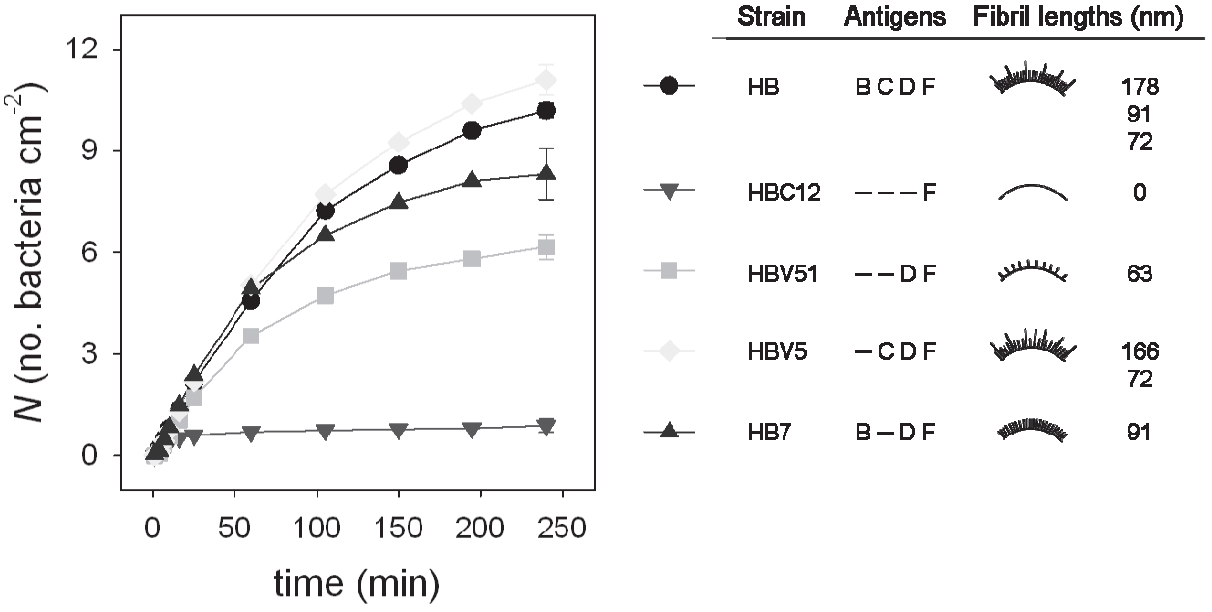

Figure 1. The number of streptococci adhering to a gold-coated quartz crystal sensor in a QCM-D chamber as a function of time for *Streptococcus salivarius* strains with different surface appendages, as indicated (Data on surface appendages are taken from Van der Mei et al. (1987). Error bars represent SD over 3 measurements with separately cultured bacteria.

QCM: Dissipation versus Frequency

Figure 2 presents the dissipation ΔD as a function of the frequency shift Δf for the streptococci with different types of surface appendages. Strains possessing surface appendages cause non linearity between ΔD and Δf and positive frequency shifts up till the 3rd overtone, whereas the "bald" mutant strain HBC12 expresses a linear correlation between ΔD and Δf with negative frequency shifts. At the 7th overtone all strains exhibit a linear correlation between ΔD and Δf and negative frequency shifts.

Dissipation versus Number of Adhering Bacteria

Figure 3 summarizes the dissipation ΔD as a function of the number of adhering streptococci for the different frequencies considered. All strains exhibit a linear correlation between ΔD and the number of adhering bacteria. Dissipation is dependent on the type of surface appendage present. Strain HB7, solely expressing the 91 nm fibril (antigen B), yields the highest dissipation per adhering bacterium. Strain HB possesses a mixture of fibrils (including the 91 nm fibril) and shows the second highest dissipation. Strains HBV5 and HBV51 possessing 72 nm (antigen C) and 63 nm fibrils respectively, but lacking the 91 nm fibrils, show the lowest dissipation among the strains carrying surface appendages. Figure 3 also shows a dramatic decrease in the absolute values of dissipation per adhering bacterium with increasing overtone number although the plots are similar and the ranking of the strains remains the same. The bald strain HBC12 deviates from this behavior and shows the same dissipation at all overtones.

Frequency Shift versus Number of Adhering Bacteria

Figure 4 shows the frequency shift Δf as a function of the number of adhering streptococci for the different frequencies considered. Frequency shift is dependent on the type of surface appendage present. At the fundamental frequency, all strains possessing surface appendages yield a slightly negative frequency shift during the initial part of the measurement where the bacterial deposition rate is the highest and cause positive frequencies shifts after 4 h of adhesion. At the 3rd overtone, only the strains HB and HB7, both possessing the 91 nm fibril, exhibit positive frequency shifts whereas the strains HBV5 and HBV51 (72 and 63 nm fibril, respectively) exhibit small negative frequency shifts. Above the 3rd overtone, a negative frequency shifts is observed for all strains. HBC12, which lack surface appendages, diverges from this behavior and yields a negative frequency shift at all overtones.

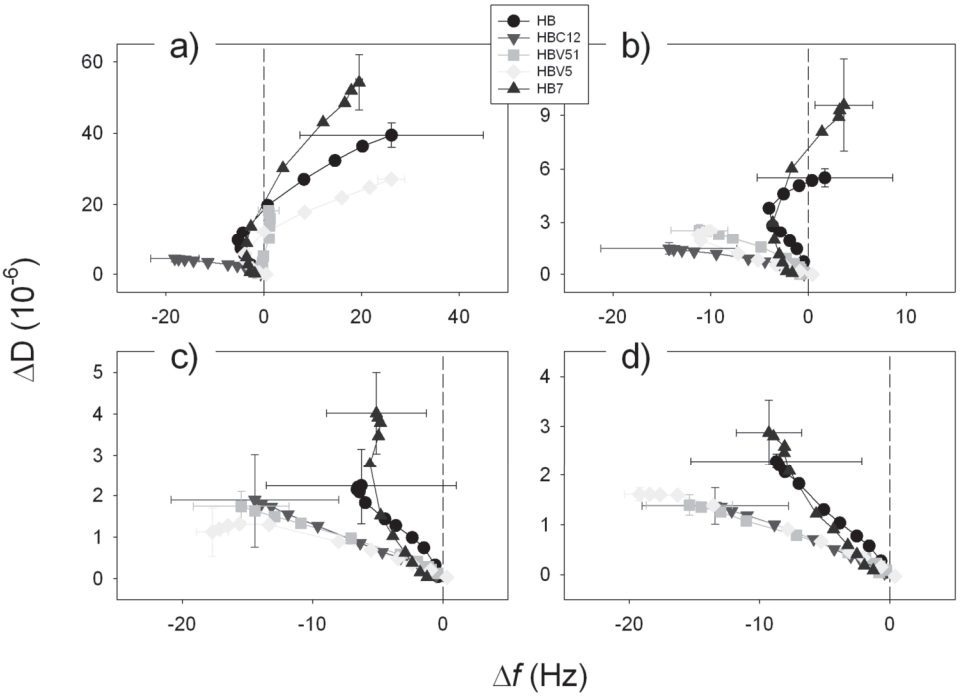

Figure 2. Change in dissipation, *ΔD* as a function of the frequency shift *Δf* during 4 h of streptococcal adhesion at the fundamental frequency (panel a), 3rd (panel b), 5th (panel c) and 7th overtone (panel d). Note the difference in scales of the axes for the different panels. Error bars represent SD at 4 h of adhesion over 3 measurements with separately cultured bacteria.

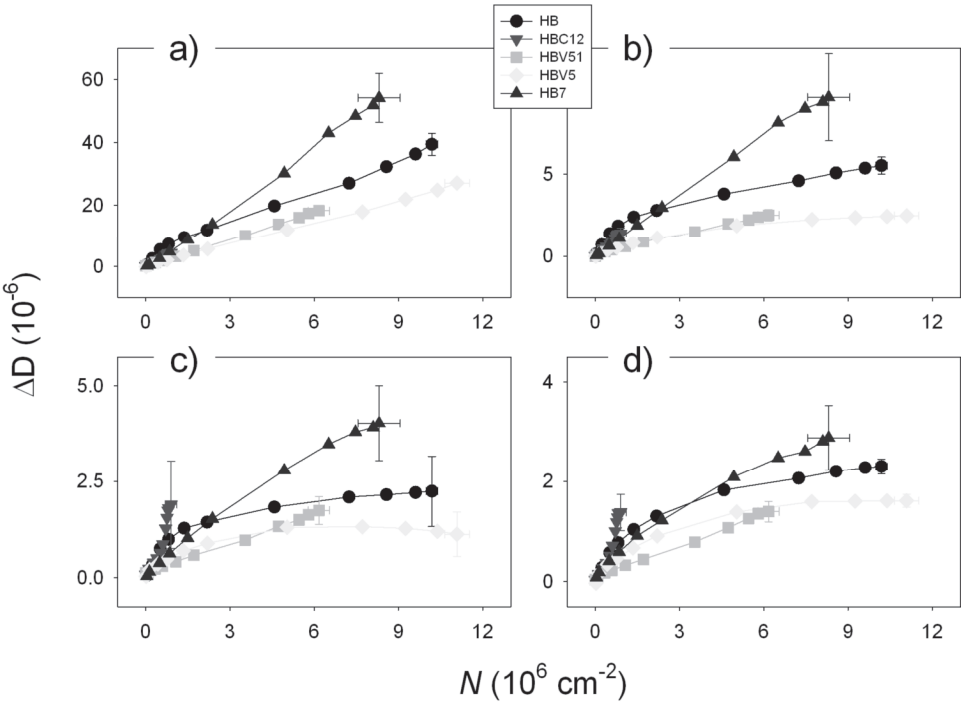

Figure 3. Change in dissipation, ΔD as a function of number of adhering streptococci N at the fundamental frequency (panel a), 3rd (panel b), 5th (panel c) and the 7th overtone (panel d). Note the difference in scales of the y-axes for the different panels. Error bars represent SD over 3 measurements with separately cultured bacteria.

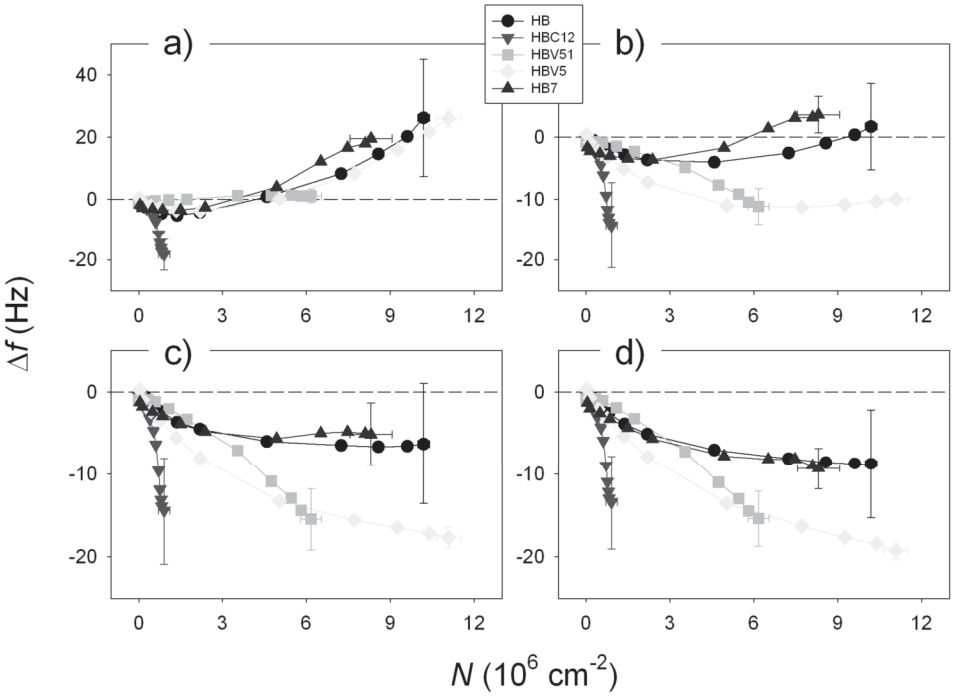

Figure 4. Frequency shift, Δf as a function of number of adhering streptococci N at the fundamental frequency (panel a), 3rd (panel b), 5th (panel c) and the 7th overtone (panel d). Note the difference in scales of the y-axes for the different panels. Error bars represent SD over 3 measurements with separately cultured bacteria.

Discussion

In the present study, we have used QCM-D in combination with microscopic enumeration of bacterial adhesion in order to find an interpretation of the QCM-D output parameters. Streptococcal strains with various lengths of surface appendages were included to facilitate this interpretation and to relate the findings with interfacial phenomena occurring during bacterial adhesion. Although in QCM a negative frequency shift is generally associated with an increased adsorbed mass, this appeared not to be true in streptococcal adhesion and only a strain completely devoid of surface appendages showed a negative frequency shift, despite the fact that other strains adhered in higher numbers. Strains with surface appendages caused positive frequency shifts till 3rd overtone above which small negative frequency shifts occurred up till the 7th overtone.

Surface appendages usually act as anchoring tools, enhancing bacterial adhesion as evident from the rate of adhesion and surface coverage after 4 h which correlate to the fibril density on the bacterial cell surface (Figure 1). Surface appendages also offer steric hindrance and immobilize the bacterial cell body at a certain distance from the sensor surface. The “bald” nature of the HBC12 mutant allows direct interaction between the cell body and the sensor surface. This is in sharp contrast to the type of contact established by strains possessing surface appendages where the bacterium is separated from the sensor surface by an interfacial region constituted by its appendages, either fully stretched or collapsed to some extent (see Figure 5). The depth to which the shear evanescent wave penetrates into the fluid adjacent to the crystal surface constitutes the analysis depth and is strongly dependent on the magnitude of frequency considered (Eq. 2), providing an excellent tool to slice the bacterium-substratum interface into different sections by analyzing multiple overtones.

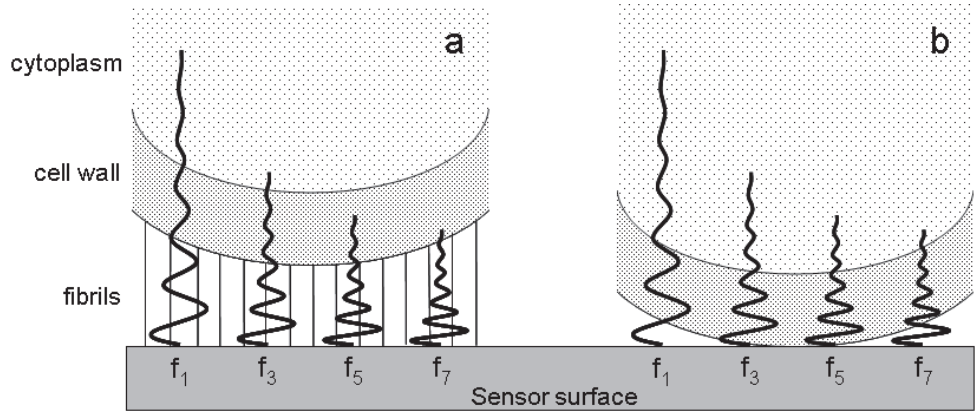

Figure 5. Interface between the crystal sensor surface and a bacterium with (a) and without ("bald") surface appendages (b). Superimposed in this schematic are the shear wave penetration depths at the fundamental frequency (f_1), 3rd (f_3), 5th (f_5) and the 7th (f_7) overtone.

The thickness of the interfacial region between the bacterial cell body and the sensor surface is not exactly known, but can be speculated upon based on the known lengths of the cell surface appendages. For HB and HBV5, the 178 and 166 nm fibrils are considered to be too sparsely distributed to significantly affect the distance between bacterial cell body and the sensor surface, and it is assumed that HB7, possessing a dense layer of 91 nm fibrils, is positioned furthest away from the surface followed by HBV5 (72 nm) and HBV51 mutant (63 nm). The wild type (HB) possesses a mixture of the 91 and 72 nm fibrils and is assumed to maintain a distance of 80 nm. Absence of fibrils, positions HBC12 in direct contact with the sensor surface (i.e. at a distance of 0 nm).The effect of the above argued distances between bacterial cell body and sensor surface on the QCM-signal is presented in Figure 6 for the end values of $\Delta f/N$ and $\Delta D/N$. Interestingly there is a correlation between length of the surface appendages and frequency shift. If the appendages keep the bacterial cell body further away from the sensor surface, $\Delta f/N$ tends to become less negative (Figure 6a). This is in agreement with a previous study where less negative frequency shifts for fimbriated *Escherichia coli* were observed as compared to a non-fimbriated one (Otto et al., 1999). A similar correlation is observed for dissipation, provided that the bald mutant is excluded (Figure 6b).

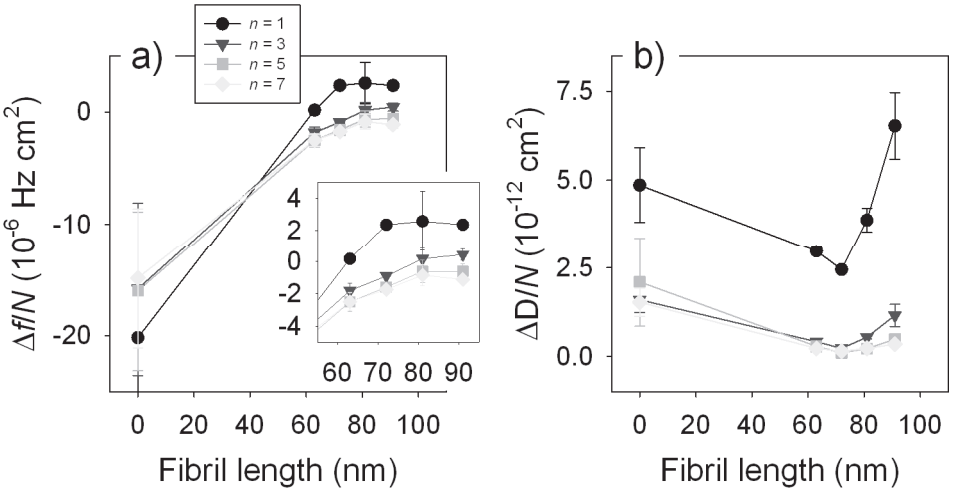

Figure 6. *Δf/N* (panel a) and *ΔD/N* (panel b) as a function of the average length of the surface appendages of the strains after 4 h of adhesion. Fundamental frequency (circles), 3rd overtone (triangles), 5th overtone (squares), 7th overtone (diamonds) are shown. The error bars represent SD over 3 measurements with separately cultured bacteria.

Due to the high sensitivity of the QCM-D to detect molecular adsorption events, even low concentrations of molecules present in the bacterial suspension (biomolecules released from bacteria, remnants of culture medium etc.) could affect the *Δf*- and *ΔD*-signal during bacterial adhesion. However, molecular adsorption always causes a negative frequency shift and the positive frequency shifts observed here for the fibrillated strains would even be larger. The cause for positive frequency shifts frequently observed upon adhesion of bacteria (Chen et al., 1996; Olofsson et al., 2005; Reipa et al., 2006), is not systematically studied, and has hitherto been attributed to biosurfactant release by adhering bacteria, different degrees of bacterial cell surface hydrophobicity or increased fluid viscosity in the interfacial region. Positive frequencies seen for diatoms (Molino et al., 2008) and mammalian cells (Marx et al., 2001; Marxer et al., 2003) are attributed to the effect of drug treatment on cellular structures and differences in cell morphology. In the present study, QCM-D output parameters and enumeration of adhering streptococci with cellular appendages of known lengths enables us to propose two plausible hypotheses which may explain positive frequency shifts upon bacterial adhesion. In the first hypothesis, the evanescent shear wave, traveling away from the crystal surface incidences on a denser medium (i.e. the cell wall) which causes a reflection of the shear wave. If the

shear wave travels far enough, it can potentially create a standing wave between bacteria and the sensor surface facilitating oscillation. This hypothesis would explain why positive frequencies only appear at low harmonics where deeper shear wave penetration increases the possibility of a standing wave. In the second hypothesis, bacteria can be regarded as masses (i.e. their cell body) connected to the oscillating surface by a string (i.e. their cell surface appendages), creating a resonating pendulum, enhancing the crystal oscillation.

The energy by which a wave or a pendulum could affect the sensor, would be dictated by the interfacial region thickness (i.e. the separation distance due to the cellular appendages) and the oscillation frequency, possibly explaining the relation between frequency shift and the length of the appendages present on the bacterial cell surface, as well as the differences in frequency shifts between overtones. Previous studies have shown that adhesion of a-biotic nylon micro-particles, that were held at distance from the sensor surface due to polymer coatings covering the sensor surface, caused positive frequency, (Berglin et al., 2008) and that increasing thickness of a multilayer of adsorbing vesicles induces positive frequency shifts (Granéli et al., 2004).

Conclusion

The influence of bacterial cell surface appendages on a bacterium-substratum interface during adhesion has been monitored with a QCM-D. The number of adhering bacteria is not directly related to the change in frequency shift Δf, but instead the thickness of the interfacial region as defined by the length of the surface appendages dictates the QCM-D output parameters. Positive frequency shifts are observed when the bacterial cell body is not in direct contact with the crystal sensor surface and held at a distance, dependent on the length of the surface appendages.

Acknowledgement

We like to thank ZON-MW for grant 91107008 enabling the purchase of the quartz crystal microbalance Qsense-E1 & E4

Chapter 3

Novel analysis of bacterium-substratum bond-maturation measured using a quartz crystal microbalance

Adam L. J. Olsson, Henny C. van der Mei, Henk J. Busscher, Prashant K. Sharma, *Langmuir*, **2010**, 26, 11113-11117

Abstract

Studies in flow displacement systems have shown that the reversibility of bacterial adhesion decreases within seconds to minutes after initial contact of a bacterium with a substratum surface. Atomic Force Microscopy (AFM) has confirmed that the forces mediating bacterial adhesion increase over a similar time span. The interfacial rearrangements between adhering bacteria and substratum surfaces responsible for this bond-maturation have never been studied. Quartz Crystal Microbalance with Dissipation (QCM-D) senses the interfacial region real-time and non-disruptively up to 250 nm from the sensor surface. In this paper, QCM-D is combined with real-time observation of bacterial adhesion in a flow displacement system, in order to analyze resident-time-dependent changes in dissipation. Three different *Streptococcus salivarius* strains showed a non-linear relation between total dissipation shift (ΔD) and number of adhering bacteria, whereas inert and rigid silica particles demonstrated a linear relation between ΔD and the number of adhering particles. This suggests removal of interfacial water, due to residence-time-dependent deformation of the non-rigid bacterium-substratum interface, during bond-maturation. Dissipation could be described by an exponentially decaying function, which combined with adhesion data allowed to extract the dissipation shifts per bacterium upon initial contact (ΔD_0), after bond-maturation (ΔD_∞) as well as a characteristic time constant (τ_{bm}). All bacterial strains showed significant bond-maturation within one minute after arrival of an individual bacterium at the substratum surface, which was not observed for silica particles. Dissipation analysis at the level of individually adhering bacteria would have been impossible without the simultaneous real-time analysis of bacterial adhesion numbers.

Introduction

Biofilms are unique results of interactions occurring mostly between biotic and abiotic surfaces. Biofilms can be beneficial, such as in wastewater treatment or soil and plant ecosystems, but cause problems, for example on ship hulls, water pipelines, heat exchangers and in food and paper processing. Biofilms grown on biomedical implants cause infections that may be potentially life-threatening (Costerton et al., 1987). The first important step in biofilm formation to surfaces is bacterial adhesion. Bacterial adhesion is initially reversible, but bond-maturation transforms the bond from a reversible to a more irreversible one.

Bond-maturation has been demonstrated from residence-time-dependent desorption of bacteria from surfaces in flow displacement systems (Boks et al., 2008) and bacterial desorption probabilities were found to decrease by a factor 100 to 1000 within one minute after arrival of an individual bacterium at a substratum surface. Atomic force microscopy (AFM) has been used to measure the forces responsible for bacterial adhesion and analysis of retract force-distance curves as a function of the surface delay time has shown that bond-maturation occurs exponentially overtime within seconds to minutes after initial contact of a bacterium with a substratum surface (Vadillo-Rodríguez et al., 2004).

The existence of bond-maturation suggests a residence-time-dependent rearrangement in the bacterium-substratum interface that may involve the removal of interfacial water facilitating closer contact, an increase in the number of contact points, or the release of extracellular polymeric substances (EPS) when bacteria are under metabolically active conditions. Accordingly, the interface between an inert and rigid particle is unlikely to undergo the same degree of rearrangement as does the interface between a bacterial cell and a substratum surface. The exact physico-chemical processes occurring in the interfacial region between a substratum surface and a bacterium in the first minutes after its arrival have never been studied and require non-disruptive, real-time measurement of interfacial rearrangement in combination with bacterial adhesion numbers.

Quartz Crystal Microbalance with Dissipation (QCM-D) is an acoustic technique which measures both the amount and the visco-elastic properties of an adhering mass on an oscillating quartz-crystal sensor-surface, in terms of shifts in the resonance frequency

(Δf) and in dissipation (ΔD). A fast decay in the amplitude of the evanescent shear wave, into the adjacent aqueous environment, results in a maximum analysis depth of 250 nm (Kanazawa & Gordon, 1985). This depth further decreases with increasing overtone number. Few studies have used QCM to study bacterial adhesion. Shifts in the resonance frequency (Δf) have been reported for adhering spores, starving and exponentially growing bacteria (Olofsson et al., 2005). Also, differences in resonance frequency shifts (Δf) have been observed between bacteria with and without surface appendages (Olsson et al., 2009; Otto et al., 1999), as well as differences due to substratum hydrophobicity (Otto & Hermansson, 2003). Bacterial adhesion to the sensor surface however, has been associated with both negative and positive frequency shifts which complicates interpretation since positive frequency shifts indicate desorption according to the Sauerbrey equation in which the frequency decreases linearly with the adsorbing mass. The reasons behind positive frequency shifts observed during adsorption of bacteria, nylon microparticles and adsorbing vesicles have been discussed in terms of an acoustic standing wave or self resonance of the adsorbing mass (Berglin et al., 2008; Granéli et al., 2004; Olsson et al., 2009). The cause for positive frequency shifts during bacterial adhesion is, however, still unclear and recent work has indicated that frequency shifts are unsuitable to quantify number of adhering bacteria (Olsson et al., 2009). In fact it has been suggested that dissipation is a better parameter for quantifying bacterial adhesion (Poitras & Tufenkji, 2009). Thus, unambiguous interpretation of QCM-D data on bacterial adhesion to a sensor surface is impossible without additional information on the exact number of bacteria adhering to the sensor surface. This study is the first to combine QCM-D with real-time image analysis of bacterial adhesion numbers on the sensor surface, in order to investigate bacterial bond-maturation. Since the dissipation term describes dissipative energy losses due to visco-elastic behavior of the adsorbed layer, i.e. the bacterium-substratum interface, this combination may allow rigorous interpretation of the dissipation changes during bacterial bond-maturation.

The aim of this study was to investigate how time-dependent bond-maturation after initial contact of a bacterium with a substratum surface affects the visco-elastic properties of bacterium-substratum interface using QCM-D combined with real-time image analysis of bacterial adhesion. An exponentially decaying function describing bacterial desorption as a function of bacterial-residence time, as proposed by Dabros and Van de Ven (1982) was adapted to describe the changes in dissipation shifts as a function of residence-time during bond-maturation. By combining the bacterial deposition rates to the surface with

the residence-time-dependent dissipation shifts, an initial dissipation shift upon contact ΔD_0, a final dissipation shift ΔD_∞, per adhering bacterium and a bond-maturation time constant τ_{bm}, could be obtained for three different strains of *Streptococcus salivarius*, each possessing different lengths of surface appendages and for micron-sized silica particles, included as an inert and rigid non-biological control.

Materials and Methods

Bacterial Strains, Culture Conditions and Harvesting

S. salivarius HB7, HBV51 and HBC12 were cultured in Todd Hewitt Broth (THB, OXOID, Basingstoke, UK) at 37°C in ambient air. For each experiment, the strains were inoculated from blood agar in 10 ml THB for 24 h. This pre-culture was added to 200 ml of THB to prepare a main culture, which was grown for 16 h. Bacteria were harvested by centrifugation (5 min at 5000 *g*) and resuspended in adhesion buffer (50 mM potassium chloride, 2 mM potassium phosphate and 1 mM calcium chloride, pH 6.8). To break bacterial chains, cells were sonicated intermittently 3 times for 10 s at 30 W (Vibra Cell model 375; Sonics and Materials, Danbury, CT) while cooling the suspension in a water/ice bath and washed twice in 100 ml adhesion buffer. Prior to the experiments, the bacterial concentration was determined with a Bürker-Türk counting chamber and diluted with adhesion buffer to a concentration of 10^9 bacteria ml^{-1}. Previously, these strains have been shown to be equally hydrophilic and negatively charged, but possess cell surface appendages of different lengths and density (Van det Mei., 1987). Furthermore, these strains are known not to produce EPS. Silica particles with a diameter of 1 µm were used as an inert and rigid non-biological control as suspended in adhesion buffer to a concentration 3 x 10^8 particles ml^{-1}, i.e. slightly lower than the bacterial concentrations in suspension in order to minimize differences in deposition rates between particles and bacteria.

QCM-D Experiments

Adhesion of bacteria and silica particles was studied under flow in the QCM-D device, model Q-sense E1 (Q-sense, Gothenburg, Sweden) equipped with a window module for optical monitoring of the sensor surface. Gold-plated AT-cut quartz crystals (Q-sense, Gothenburg, Sweden), were used as substratum. Before each experiment, the crystals were cleaned by immersion in a 3:1:1 mixture of ultrapure water, NH_3 and H_2O_2 (Merck, Darmstadt, Germany) at 70°C for 10 min followed by 10 min UV/Ozone treatment, yielding a water contact angle of 16 ± 3 degrees. The dissipation shifts (ΔD) were measured for the 3rd overtone, corresponding to an oscillation frequency of 15 MHz, throughout the adhesion process using the QSoft 401 software (Q-sense, Gothenburg, Sweden). The 3rd overtone was chosen to get the deepest shear wave penetration (150 nm) and largest area of the sensor surface without getting interference from the O-ring which holds the sensor surface in place. Before measurements, the crystal sensor was first incubated in adhesion buffer. When stable base lines for both Δf and ΔD were achieved, the bacterial suspensions were perfused under negative pressure through the QCM-D chamber for 13 min using a peristaltic pump (Ismatec SA, Glattbrugg, Switzerland). Experiments were conducted at 23°C at a flow rate of 300 µl/min. The QCM-D flow chamber is disc-shaped with a volume of approximate 100 µl and a diameter of 12 mm with inlet and outlet facing the crystal surface, giving an estimated shear rate of 2.8 s^{-1}. Each experiment was carried out in triplicate.

In order to clean the crystal surface and remove adhering bacteria between the measurements, crystals were immediately sonicated after an experiment in a 2% (w/v) sodium dodecyl sulphate (SDS) solution for 10 min and rinsed with ultrapure water. The QCM-D chamber was cleaned by perfusion of 10 ml SDS (2%) followed by 20 ml ultrapure water through the system.

Bacterial deposition on the sensor surface was observed with a metallurgical microscope (Leica DM2500 M, Rijswijk, The Netherlands) equipped with a 20x objective (Leica HCXPL FLUOTAR). Using a CCD camera (Model A101, Basler vision technologies, Ahrensburg, Germany) mounted to the microscope and coupled to an image analyzer (TEA, Difa, Breda, The Netherlands), images of the sensor surface were recorded throughout the experiments, while simultaneously recording the ΔD-signal.

Data Analysis

Residence-time-desorption studies in flow displacement systems have shown that the rate of both colloidal particle and bacterial desorption decrease exponentially with the residence-time of the particles or bacteria on a surface (Boks et al., 2008; Dabros & Van de Ven, 1982). Similarly, AFM studies have shown that the required force to pull an adhering bacterium free from substratum surface increases exponentially towards a maximum as a function of the surface delay time (Vadillo-Rodríguez et al., 2004). The above studies indicate that the bacterium-substratum interface changes exponentially with time after the arrival of a bacterium on a substratum. Additionally, Figure 2 ($\Delta D/N$ versus t) shows a finite dissipation shift upon initial contact of a bacterium with a substratum surface followed by an exponential decrease towards a stable value. Therefore, in the present study, the residence-time-dependent dissipation shift $\Delta D(t-\tau)$ caused by an individual adhering bacterium on a QCM-D sensor surface was modeled by Eq. 1

$$\Delta D(t-\tau) = \Delta D_{\infty} - (\Delta D_{\infty} - \Delta D_0) e^{-(t-\tau)/\tau_{bm}} \qquad (1)$$

where ΔD_0 is the shift in dissipation caused by a single bacterium upon initial contact (i.e. at 0 s) and ΔD_{∞} is the final shift in dissipation and τ_{bm} is a characteristic bond-maturation time constant, t is the actual time and τ denotes the time of arrival, i.e. first contact, of a bacterium with the substratum surface.

Ideally, if all bacteria arrive on the surface at the same time point, Eq. 1 can be fitted to the plot shown in Figure 2. Since in practice, however, bacteria arrive at the surface at different points in time, the measured dissipation shift is the result of adhesion of bacteria, each with their own time of arrival and consequently their own residence-time. The measured dissipation shift is the sum of the dissipation shifts from all individual bacteria adhering to the sensor surface, and can therefore be described as

$$\Delta D(t-\tau) = \int_0^t j \left[\Delta D_{\infty} - (\Delta D_{\infty} - \Delta D_0) e^{-(t-\tau)/\tau_{bm}} \right] d(t-\tau) \qquad (2)$$

where j is the bacterial deposition rate. Note that Eq. 2 is valid as long as adhesion numbers increase linearly with time (Figure 1) i.e. j is an integer and independent of time. Because only under these conditions it is possible to know the number of bacteria present on the surface and their residence-times (t-τ) without registering individual arrivals.

In order to obtain the constants ΔD_0, ΔD_∞ and τ_{bm}, the integral is fitted to the total dissipation shift during which adhesion increases linearly with time. The deposition rate, j, can be easily obtained from the linear relation between time and the number of adhering bacteria using linear regression.

Results

The adhesion kinetics together with corresponding dissipation shifts are presented in Figure 1 for silica particles (panel a) and a bacterial strain (*S. salivarius* HB7, panel b). A linear increase in the number of adhering silica particles is concurrent with a linear increase in total dissipation shift, indicating that within the timeframe of the experiment all adhering particles contribute equally to the total dissipation shift regardless of their residence-time on the surface. Oppositely, for the bacterial strain, a linear increase in numbers of adhering bacteria was not accompanied by a linear increase in total dissipation shift, but rather by an exponentially decaying one, indicative of time-dependent rearrangements in the interface between the bacterial cell and the substratum surface. A similar behavior was observed for the other two bacterial strains included (*S. salivarius* HBV51 and HBC12, data not shown). Dividing the measured dissipation shift by the number adhering particles or bacteria yields the average contribution $\Delta D/N$ of each particle or bacterium to the total dissipation shift as a function of time (see Figure 2 for an example).

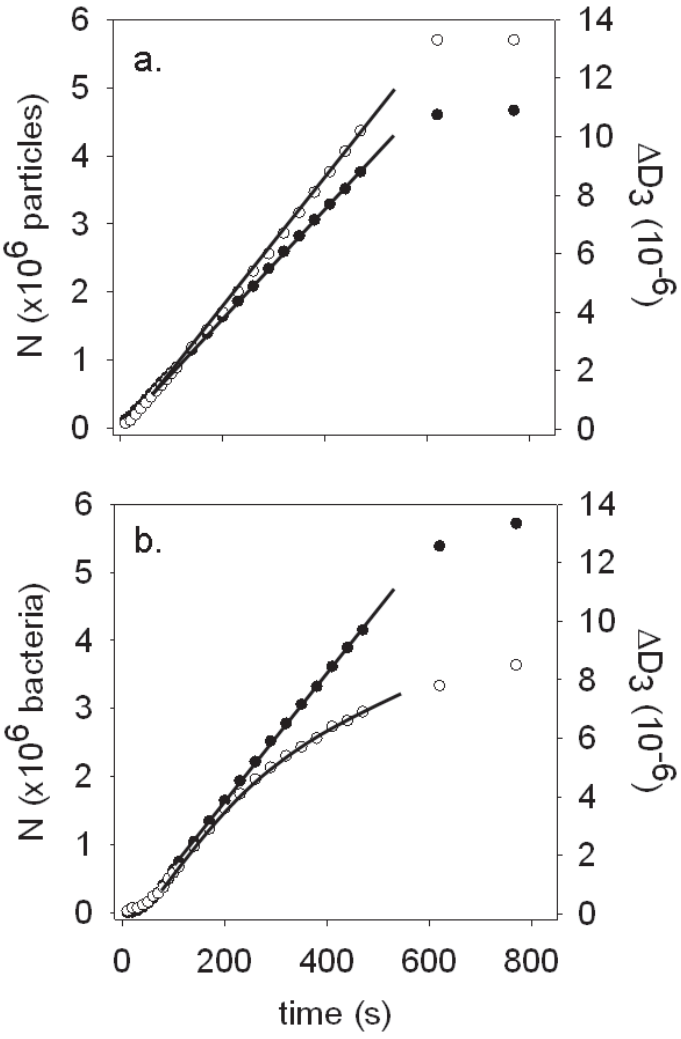

Figure 1. Increase in the number of adhering particles and bacteria *N* (●, left axis) and measured dissipation shift *ΔD* (○, right axis) as a function of time, for silica particles (panel a) and *S. salivarius* HB7 (panel b). A linear increase in the number of adhering silica particles is accompanied by a linear increase in measured dissipation shift, whereas a linear increase in bacterial numbers is accompanied by a non-linear change in dissipation, indicating a time-dependent rearrangement in the bacterium-substratum interfacial region.

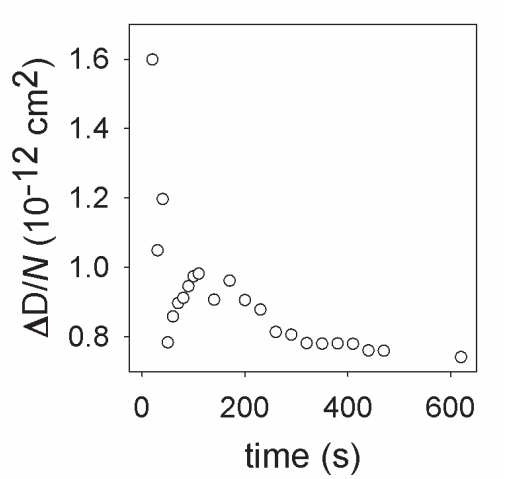

Figure 2. Exponential decrease in the total dissipation ΔD, divided by the number of adhering bacteria N, as a function of time, during linear increase of the number of adhering *S. salivarius* HB7 with time.

The measured dissipation shift is the result of adhering particles or bacteria that have all arrived at different points in time at the surface. Therefore the dissipation shift per particle or bacterium $\Delta D/N$ as presented in Figure 2 neglects the differences in residence-time as existing over the population of adhering particles or bacteria. Thus residence-time-dependent dissipation can not be directly derived from Figure 2. Figure 2 does indicate, however, that dissipation decreases exponentially overtime, similar to the exponentially decaying function describing residence-time-dependent desorption, as proposed by Dabros & Van de Ven (1982). Accordingly, this equation was rewritten for dissipation shifts (Eq. 1, see Materials and Methods section) and integrated over the time interval during which adhesion numbers increase linearly, yielding the integral Eq. 2 (see Materials and Methods section). Fitting of Eq. 2 to the measured dissipation shift (see Figure 3) directly yields ΔD_0 and ΔD_∞ as well as the characteristic time constants τ_{bm} for residence-time-dependent bond-maturation (Table 1). For adhering silica particles, no statistically significant differences between ΔD_0 and ΔD_∞ were found indicating the absence of interfacial rearrangements, whereas for all three bacterial strains initial dissipation shifts ΔD_0 were significantly higher than the final dissipation shifts ΔD_∞ ($p<0.05$, one-way, paired Student t-test) indicating interfacial rearrangements responsible for bond-maturation, occurring with a time-constant of around 55 s. No statistically significant differences were observed between residence-time-dependent dissipation among the three bacterial strains.

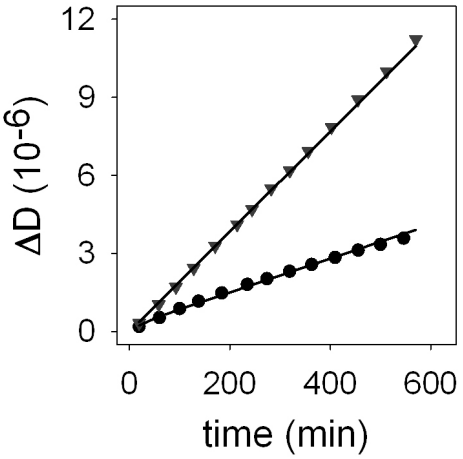

Figure 3. Measured (symbols) and modeled (lines) dissipation shift for silica particles (triangles) and *S. salivarius* HB7 (circles) during the linear increase of adhesion.

Table 1. Surface morphology and average fibrillar lengths of the bacterial strains used, together with their dissipation shift and standard deviation over three separately grown cultures upon initial contact ΔD_0 and at infinity ΔD_∞, together with the characteristic time constant for bond-maturation τ_{bm} for the three *S. salivarius* strains included in this study and silica particles. † indicates statistically significant differences between ΔD_0 and ΔD_∞ ($p < 0.05$, paired Student t-test). No statistically significant differences were found between different bacterial strains for any of the three fitting parameters ($p > 0.05$, two tailed Student t-test, assuming equal variances).

	Surface morphology	Fibril length	ΔD_0 (10^{-12})	ΔD_∞ (10^{-12})	τ_{bm} (s)
HB7		91 nm Dense layer	2.7 ± 1.0	1.2 ± 0.4†	55 ± 26
HBC12		0 nm Fuzzy layer	2.1 ± 1.3	0.7 ± 0.7†	53 ± 49
HBV51		63 nm Sparse layer	3.5 ± 1.5	1.0 ± 0.4†	57 ± 47
Silica		0 nm Rigid surface	2.4 ± 0.7	2.6 ± 0.3	-

Discussion

This paper describes a novel analysis of QCM-D data, in combination with real-time observation of bacterial adhesion numbers, to determine residence-time-dependent bond-maturation of individual bacteria due to rearrangements in the bacterium-substratum interface. This bond-maturation is important, as it governs the transition from reversible to irreversible adhesion. All bacterial strains included in this study express a significant exponential decrease in dissipation shift after initial contact with the sensor surface with a characteristic time constant of around 55 s. This is in distinct contrast to the behavior of micron-sized silica particles, not exhibiting any time dependent change in dissipation after initial contact.

Bacteria are often assumed to be inert and rigid colloidal particles obeying the basic principles of colloid and interface science with respect to their adhesion to substratum surfaces (Hermansson, 1999). There are, however, essential differences between the surface of a smooth, homogeneous, inert and rigid colloidal particle and the surface of a bacterium, and colloidal models often fail in explaining bacterial adhesion. The surface morphology of a bacterium is highly complex, with a vast variety of cell surface structures and appendages, creating a rugged, inhomogeneous and non-rigid surface. Accordingly, an inert and rigid particle is not easily deformed after adhesion and the interface between two rigid surfaces, like the surfaces of silica particles and the gold-coated QCM sensor in this study, remains relatively unchanged. Constituents of bacterial cell surfaces are neither inert nor rigid surface structures and appendages will rearrange during adhesion until the bacterium is positioned in the energetically most favorable conformation.

In QCM-D studies on molecular adsorption, a decrease in dissipation is associated with a decreasing water content within the adsorbed layer of molecules (Berglin et al., 2009; Vörös, 2004). Hence, a decrease in dissipation shift as measured here during bacterial adhesion reflects removal of water from the bacterium-substratum interface, due to an increase in the density of cell surface structures in the interface over time (Figure 4). This interfacial rearrangement consequently leads to an increasing number of contact points and short-range interactions that increase the adhesion strength between the bacterial cell and the substratum surface. This is in agreement with AFM-studies in which Poisson analyses suggest that during bond-maturation interfacial water is removed,

allowing a higher number of acid-base pairs to form between a bacterium and a substratum surface (Abu-Lail & Camesano, 2006; Boks et al., 2008).

This study shows no differences in bond-maturation between the three *S. salivarius* strains, although they express surface appendages of different lengths (Olsson et al., 2009), implying that the surface morphology of these bacterial strains plays an insignificant role in bond-maturation under the present experimental conditions. Other desorption- and AFM- studies (Boks et al., 2008a; Boks et al., 2008b), also report insignificant differences between different strains of bacteria with respect to their bond-maturation over time. The time constants obtained from QCM-D in this study are, however, higher than the time constants mostly obtained from AFM (Boks et al., 2008; Van der Mei et al., 2008) suggesting that forced adhesion during AFM-measurements causes bacteria to overcome electrostatic and steric repulsion in the interfacial region more quickly than during unforced adhesion in QCM-D.

Summarizing, the present study describes a novel methodology to study bacterial bond-maturation, using a QCM-D in combination with real-time observation of bacterial adhesion to the sensor surface, from the time-dependent change in the dissipation signal. The measured dissipation caused by all adhering bacteria, regardless of their residence-times, was modeled using an exponentially decaying function. Modeling yielded the dissipation upon initial contact ΔD_0 and after bond-maturation ΔD_∞ per adhering bacterium as well as a bond-maturation time constant τ_{bm}. Whereas adhering micron-sized silica particles showed no significant bond-maturation, all bacterial strains showed significant bond-maturation in approximately 55 s after initial contact with the QCM gold-coated sensor surface, indicating rearrangements in the interfacial region.

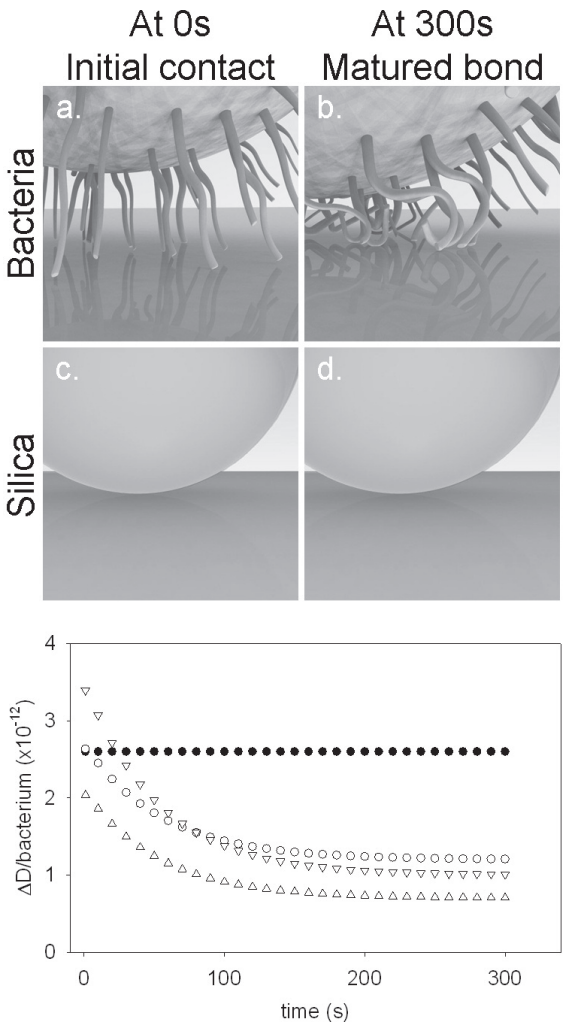

Figure 4. Illustration of bacterial-bond maturation. Initial shift in dissipation upon initial contact of bacteria (impression a) is decreasing over time due rearrangements in the bacterium-substratum interface until the energetically most favorably conformation is reached (impression b). The rigid surface of silica particles is unable to undergo rearrangements and keeps its original shape from initial contact (impression c) and forward over time (impression d). The plot shows calculated values of *ΔD* per bacterium as a function of time, using Eq. 1 and the constants listed in Table 1 for *S. salivarius* HB7 (○), HBV51 (▽), HBC12 (△) and micron-sized silica particles (●).

Acknowledgements

We would like to thank Zon-MW for Grant 91107008 which enabled the purchase of the quartz crystal microbalance Qsense-E1 & E4 and Karl Rehnström for graphical help.

Chapter 4

Acoustic sensing of the bacterium-substratum interface using QCM-D and the influence of extracellular polymeric substances

Adam L. J. Olsson, Henny C. van der Mei, Henk J. Busscher, Prashant K. Sharma, *J. Colloid Interface Sci.*, **2011**, 357, 135-8

Abstract

It is commonly assumed that bacterial presence on a QCM sensor-surface is associated with a negative frequency shift according to conventional mass-loading theory. Here, we demonstrate that bacteria adhering to QCM sensor-surface may yield positive frequency shifts up to 1.9×10^{-6} Hz per bacterium according to a coupled-oscillator theory. Furthermore, it is demonstrated that the excretion of extracellular polymeric substances (EPS) by adhering bacteria can change the frequency shift in the negative direction by 1.7×10^{-6} Hz per bacterium, according to conventional mass-loading theory. The difference in frequency shifts between an EPS-producing and a non-EPS producing staphylococcal strain correlated with the excretion of 3×10^{-14} g EPS per bacterium, representing only a few percent of the weight of a bacterium. Thus an adsorbed molecular mass as low as a few percent of the mass of an adhering bacterium significantly alters the QCM-signal. Since adhesion of many different bacterial strains is accompanied by molecular adsorption of EPS, with potentially opposite effects on the QCM-signal, a combination of the coupled-oscillator and normal mass-loading theory has to be applied for proper interpretation of QCM frequency shifts in bacterial detection.

Introduction

Biofilms are matrix enclosed populations of microorganisms that can adhere to biological as well as non-biological surfaces of widely varying origin. Biofilms are ubiquitous and form amongst others in the environment, on industrial surfaces and on biomaterial implants and devices, where they pose a life-threatening condition for a growing patient population that rely on these implants and devices for the restoration of function. Adhesion of microorganisms to substratum surfaces constitutes one of the initial steps in biofilm formation. Upon adhesion, bacteria may subsequently release extracellular polymeric substances (EPS) in order to adhere more firmly and provide shelter against environmental attacks. The role of these initial colonizers is not to be underestimated as they link the entire biofilm that grows on top of them to the substratum surface. Understanding the fundamental mechanisms of microbial adhesion is required to pave the way for the development of non-adhesive surfaces, minimizing the risk of biofilm formation. In spite of the use of techniques like flow-displacement devices, Atomic Force Microscopy (AFM) and calorimetry, the mechanisms of microbial adhesion, especially at the sub-micron level, are still not completely understood. This study investigates the potential use of Quartz Crystal Microbalance with dissipation (QCM-D) to study the dynamics of the interface between adhering bacteria and a surface in a non-destructive and non-disruptive manner.

The QCM is a popular technique to study the adsorption kinetics and mechanical properties of thin molecular films at the solid-liquid interface (Macakova et al., 2010). In essence, QCM measures the amount of adhering mass by means of shifts in the resonance frequency (Δf) of an oscillating quartz-crystal sensor. In addition, the amplitude of oscillation is influenced by dissipative energy losses due to visco-elastic properties of the adsorbed film. These energy losses can be quantified from the frequency bandwidth or the oscillation decay time (dissipation, ΔD) (Rodahl & Kasemo, 1996). Since the penetration depth of the oscillation-induced shear-waves for a 5 MHz crystal in QCM is limited to 250 nm in aqueous environments (Kanazawa & Gordon, 1985), QCM provides an unique ability to study interactions confined to the bacterium-substratum interface (Olofsson et al., 2005; Olsson et al., 2009 & 2010; Otto et al., 1999; Otto & Silhavy, 2002). It is commonly assumed that bacterial presence on a QCM sensor-surface follows conventional mass-loading theory, i.e. that the adsorbed mass is detected as negative frequency shift.

For rigid layers, the frequency shift is negatively proportional to the adsorbed mass according to the Sauerbrey relation (Eq. 1) (Sauerbrey, 1959)

$$\Delta m = -\frac{C_{QCM}}{n}\Delta f \qquad (1)$$

in which Δm is the amount of adsorbed mass, Δf is the shift in resonance frequency, C_{QCM} is a mass sensitivity constant (17.7 ng/cm^2 for a 5 MHz crystal) and n is the resonance frequency overtone number. For non-rigid layers, dissipation must be included in the analysis in order to estimate the adsorbed mass (Johannsmann et al., 1992; Voinova et al., 2002).

However, there are numerous examples of colloidal particle adhesion, including bacteria and diatoms, resulting in positive frequency shifts (Berglin et al., 2008; Molino et al., 2008; Olofsson et al., 2005; Olsson et al., 2009; Pomorska et al., 2010). Conventional mass loading theory cannot explain the occurrence of positive frequency shifts which means that colloidal particles do not adhere to the sensor surface as molecules. Positive frequency shifts due to particle adhesion have been explained in terms of a coupling between two oscillators via a small point-contact, which in contrast to the normal mass-loading theory, may increase the resonance frequency (Dybwad, 1985). In this so-called coupled-oscillator theory, resonance frequency is not only dictated by the magnitude of adsorbed mass, but also by the stiffness of the bond between the adsorbed mass and the crystal-sensor-surface according to

$$2(2\pi f)^2 = \left(\frac{K}{M}+\frac{k}{M}+\frac{k}{m}\right) \pm \sqrt{\left(\frac{K}{M}+\frac{k}{M}+\frac{k}{m}\right)^2 - 4\frac{K}{M}\times\frac{k}{m}} \qquad (2)$$

in which f is the resonance frequency of the quartz-crystal sensor, K is the spring constant and M the mass of the quartz-crystal sensor-surface, k is a spring constant describing the stiffness of the particle-sensor contact point and m is the mass of the adhering particle. This equation is derived for attachment of a single particle in air, hence not directly applicable for a population of particles adhering at the solid-liquid interface.

Finite element modeling however, suggests that coupled-oscillation is the cause behind positive frequency shifts during colloidal particle adhesion also in liquid (Pomorska et al. 2010).

Adhering bacteria are of the size and shape of large colloidal particles and are therefore likely to affect the QCM-frequency shift according to the coupled-oscillator theory. In contrast to colloidal particles, bacteria are living organisms that can excrete EPS, which is important for their adhesion to surfaces (Tsuneda et al. 2003) and subsequent biofilm formation (Sutherland, 2001). The major components of EPS are exopolysaccharides, nucleic acids, proteins, glycoproteins and phospholipids (Allison, 2003). Hence, although it is within reason to interpret bacterial adhesion to QCM sensor-surfaces according to coupled-oscillator theory, bacterial adhesion may be accompanied by molecular adsorption of excreted EPS, affecting the QCM-response in line with conventional mass-loading theory (Long et al., 2009; Zhu et al., 2009). In order to differentiate between the QCM-D signals arising due to bacterial adhesion and EPS, two strains of *Staphylococcus epidermidis* were used in the study: a non-EPS-producing (*S. epidermidis* ATCC 12228) and an EPS-producing (*S. epidermidis* ATCC 35984) one.

Materials and methods

Bacterial Strains, Culture Conditions and Harvesting

The bacterial strains *S. epidermidis* ATCC 35984 and *S. epidermidis* ATCC 12228 have previously been used as model organisms for an EPS-producing strain (*S. epidermidis* ATCC 35984) and a non-EPS-producing strain (*S. epidermidis* ATCC 12228) and were therefore chosen for this study (Katsikogianni & Missirlis, 2010). Both strains were grown in tryptone soya broth (TSB), harvested by centrifugation (5 min at 5000 g) and resuspended in PBS buffer (10 mM potassium phosphate, 150 mM sodium chloride, pH 6.8) Suspensions were sonicated, while on ice, three times for 10 s at 30 W (Vibra Cell model 375; Sonics and Materials, Danbury, CT) and washed twice in 100 ml PBS before dilution to a final concentration of 3×10^8 bacteria per ml.

Bacterial Adhesion in QCM and Fluorescence Microscopy

Bacterial adhesion was allowed in a window-equipped QCM-D device (model E1, Q-sense, Gothenburg, Sweden) for 20 min followed by 140 min PBS buffer rinse at 23°C and a flow rate of 300 µl/min, using hydrophilic gold-plated QCM sensor-surface as substratum surface. Number of adhering bacteria was microscopically determined and related to the shifts in frequency (Δf) and dissipation (ΔD) for 3rd, 5th and 7th overtone. After each measurement, staphylococci and EPS on the sensor-surfaces were stained with LIVE/DEAD *Bac*light viability stain and calcofluor white for EPS, respectively. The presence of bacteria and EPS was then evaluated by fluorescence microscopy (Leica DM4000B Leica Microsystems Heidelberg GmbH, Heidelberg, Germany). All experiments were carried out in triplicates.

Results and Discussion

The results are presented in terms of staphylococcal adhesion kinetics to the sensor-surface (Figure 1a) together with the corresponding shifts in dissipation (Figure 1b) and frequency (Figure 1c) of the 3rd overtone (15 MHz) for *S. epidermidis* ATCC 35984 (EPS-producing) and *S. epidermidis* ATCC 12228 (non-EPS-producing). *S. epidermidis* ATCC 35984 adhered to an average density of 3.8 x 10^6 bacteria cm^{-2}, while *S. epidermidis* ATCC 12228 adhered to an average density of 3.5 x 10^6 bacteria cm^{-2}, which does not represent a statistically significant difference ($p = 0.59$, two-tailed t-test, assuming equal variances), allowing direct comparison of ΔD and Δf shifts for the two strains. Neither bacterial cell division nor detachment was observed during the whole duration of the experiment. The observed dissipation shifts (Figure 1b) were also not significantly different between the two strains ($p = 0.70$, two-tailed t-test, assuming equal variances), indicating that the presence of the bacterial cell bodies on the sensor-surface is the main source to dissipation during staphylococcal adhesion.

Frequency shifts (Figure 1c) increased linearly in the positive direction during the adhesion phase (initial 20 min), which was concurrent with a linear increase in numbers of adhering bacteria. However, the frequency shift caused by adhesion of the non-EPS-producing strain is approximately two-fold more positive than the shift in frequency accompanying adhesion of the EPS-producing strain. After initial adhesion, the frequency

continued to shift in the positive direction for the non-EPS-producing strain, although at much slower rate than during adhesion. For the EPS-producing strain, the frequency began to decrease, indicating molecular adsorption according to conventional mass-loading theory. Consequently, the difference in Δf between the two strains increased with time. After 140 min, the EPS-producing strain yielded a positive frequency shift of 0.7 Hz, corresponding to 1.8×10^{-7} Hz per adhering bacterium. This is significantly lower than the positive frequency shift of 6.6 Hz caused by the non-EPS producing strain, corresponding to 1.9×10^{-6} Hz per adhering bacterium ($p = 0.03$, one-tailed t-test, assuming equal variances). Fluorescence images of the QCM sensor-surface (Figure 2) confirmed the difference in EPS excretion and only showed EPS around adhering *S. epidermidis* ATCC 35984 and not around *S. epidermidis* ATCC 12228.

The positive frequency shifts observed for both strains indicate that staphylococci adhere to the sensor-surface according to the coupled-oscillator theory (Eq. 2), rather than according to conventional mass-loading theory (Eq. 1). The resonance frequency of this coupled-oscillator is mathematically described by Eq. 2 and is presented in Figure 2c as a function of the characteristic spring constant k, describing the contact point stiffness (see also the insert in Figure 2a and 2b). Less stiff contact (small k-values) yields positive frequency shifts that increase non-linearly with stiffness. Stiffer contact points (large k-values) on the other hand, yield negative frequency shifts that decrease non-linearly with stiffness. The sudden change from positive to negative frequency shift occurs when the attached particle and sensor-surface are oscillating at the same frequency. For bacterial adhesion, this means that the magnitude of the frequency shift is strongly influenced by the stiffness of the bacterium-substratum interface, which in turn can alter due to bond–maturation (Olsson et al., 2010). In this particular case, the adhesive bond between bacteria and surface possesses a stiffness which allows the bacteria to oscillate at a frequency below 15 MHz, yielding positive frequency shifts for the 3rd, 5th and 7th overtone.

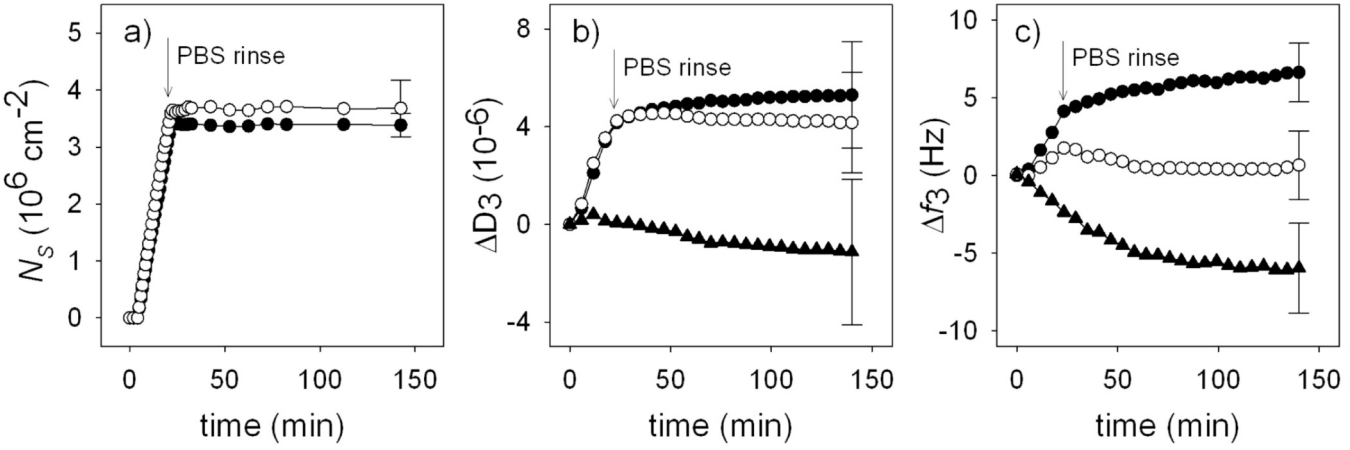

Figure 1. Adhesion kinetics of staphylococci to the QCM sensor-surface (a), together with the dissipation shift *ΔD* (b) and frequency shift *Δf* (c) of the third overtone as a function of time. *S. epidermidis* ATCC 35984 (open circles) is an EPS-producing strain, while *S. epidermidis* ATCC 12228 (closed circles) is a non-EPS producing strain. Closed triangles represent the difference in *ΔD* and *Δf* between the two strains. Arrows indicate the time-point at which flow with a bacterial suspension is changed to flow with a PBS-buffer. Error bars indicate the standard error at 140 min over three measurements with separately cultured bacteria.

The fact that most bacteria produce and excrete EPS complicates the analysis. EPS consists of molecules that adsorb directly on the sensor-surface, increasing its effective mass *M* (see insert in Figure 2b). A closer inspection of Eq. 2 reveals that an increase of *M*, at constant value of *k*, decreases the resonance frequency of the sensor-surface, analogous to the conventional mass-loading theory described by Eq. 1. Hence, an increase in *M* dislocates the coupled-oscillator frequency curve towards less positive or more negative frequency shifts (see Figure 2c). This indicates that for EPS-producing strains, the frequency shift is due to an interplay between bacterial adhesion and molecular adsorption yielding a lower (less positive or more negative) shift in frequency than for a similar, non-EPS-producing strain. Accordingly, subtraction of the positive frequency and dissipation shift caused by non-EPS-producing ATCC 12228 from that of EPS producing ATCC 35984 describes the molecular adsorption kinetics of excreted EPS (Figure 1c). The differential curve for dissipation shifts (Figure 1b) is not significantly different from zero, suggesting that EPS is rigidly adsorbed to the crystal surface and that the difference in frequency shift can be analyzed according to Sauerbrey relation (Eq. 1). In addition, there is no significant difference in the differential frequency shift caused by the adsorbed EPS between the 3rd, 5th and 7th overtone after 140 min (Table 1), which is another indication that EPS is rigidly adsorbed.

Employing the Sauerbrey relation for each overtone at 140 min, yields the conclusion that approximately 1 x 10^{-7} g EPS is adsorbed per cm^2 (Table 1). Considering that there are roughly 3.5 x 10^6 bacteria cm^{-2}, it can be calculated that one bacterium excretes about 3 x 10^{-14} g EPS. This amount of EPS corresponds to a few percent of the average bacterial weight (10^{-12} g) and is excreted by *S. epidermidis* ATCC 35984 within 140 min in the absence of any additional nutritional sources but its internal reserve.

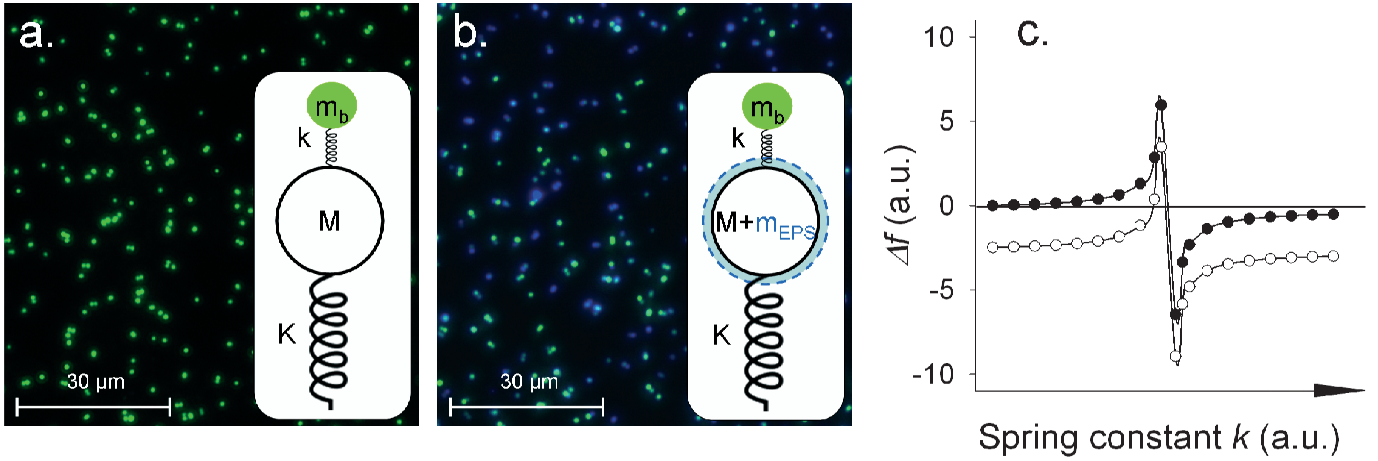

Figure 2. Fluorescent images of non-EPS-producing *S. epidermidis* ATCC 12228 (a) and of EPS-producing *S. epidermidis* ATCC 35984 (b) on the QCM sensor-surface. Live bacteria appear in green and EPS in blue. Inserts represent the coupled-oscillator model (see Eq. 2) as valid in the absence (a) and presence (b) of EPS. The graph (c) schematically presents the resonance frequency for a coupled-oscillator as a function of contact point stiffness for an unloaded (closed circles, m_b attached to M through k) and a mass-loaded (open circles, m_b attached to $M+m_{EPS}$ through k) sensor-surface, according to Eq. 2. The solid line indicates the resonance frequency of the unloaded crystal-sensor-surface, represented by M and K.

Table 1. Average values of dissipation shifts ΔD and frequency shifts Δf for *S. epidermidis* ATCC 12228 (non-EPS producing; EPS-) and *S. epidermidis* ATCC 35984 (EPS producing; EPS+) for the 3rd, 5th and the 7th overtone, observed after 140 min. Additionally, the average difference in ΔD and Δf between the strains is given, together with the corresponding mass calculated according to Sauerbrey relation. ± indicates the standard error over three measurements with separately grown cultures.

	EPS-	EPS+	EPS+ - EPS-
Δf_3 (Hz)	6.6 ± 1.9	0.7 ± 2.2	-6.0 ± 2.9
ΔD_3 ($\times 10^{-6}$)	5.3 ± 2.2	4.2 ± 2.0	-1.1 ± 3.0
m_{EPS} (ng/cm^2)			106 ± 51
Δf_5 (Hz)	5.2 ± 1.7	-0.2 ± 1.9	-5.4 ± 2.6
ΔD_5 ($\times 10^{-6}$)	2.6 ± 1.2	2.2 ± 1.2	-0.4 ± 1.7
m_{EPS}(ng/cm^{-2})			96 ± 46
Δf_7 (Hz)	4.9 ± 1.5	-0.5 ± 1.8	-5.4 ± 2.3
ΔD_7 ($\times 10^{-6}$)	1.4 ± 0.5	1.7 ± 0.7	0.3 ± 0.9
m_{EPS}(ng/cm^2)			96 ± 41

The above analysis demonstrates that QCM has the potential to acoustically sense the dynamics occurring within the sub-micron bacterium-substratum interface during adhesion. Positive frequency shift caused by adhering bacteria can be described by a coupled-oscillator theory and is influenced by the bacterium-substratum interface stiffness, but we here show that EPS-excretion introduces a component of molecular adsorption next to the coupling of bacteria adhering to the crystal. Bacterial adhesion to QCM sensor-surfaces should therefore be considered as a combination of a coupled-oscillator, due to the bacterial cell body, and conventional mass-loading, due to molecular adsorption of excreted EPS. Molecular adsorption, even when confined to only a few percent of the mass of the bacterial cell body, significantly influences the QCM-frequency shift. This is most important when QCM is to be used to study bacterial adhesion and great care should be taken when analyzing QCM-frequency shifts, as they can be due to opposing influences of bacterial adhesion and molecular adsorption.

Acknowledgement

We like to thank ZON-MW for grant 91107008 enabling the purchase of the quartz crystal microbalance Qsense-E1 & E4.

Chapter 5

Coupled resonance analysis using QCM of the adhesive bond stiffness of streptococci with different surface appendages at different ionic strength

Adam L. J. Olsson, Narasimhan Arun, Johannes S. Kanger,
Henk J. Busscher, Henny C. van der Mei, Prashant K. Sharma

Submitted to *Soft matter*

Abstract

Positive frequency shifts during bacterial adhesion in a quartz crystal microbalance (QCM) have been difficult to interpret according to conventional mass-loading theory, which considers adhering bacteria as masses coupled to the sensor-surface. The explanation for positive frequency shifts lies in the fact that bacteria possess their own resonance that couples to the sensor-surface resonance. The resonance frequency of adhering bacteria not only depends on their mass but also on their adhesive bond stiffness. The aim of this study was to investigate whether the coupled resonance model could be applied to compare the adhesive bond stiffness of bacteria with different surface appendages. To this end, we used two *Streptococcus salivarius* strains possessing fibrillar surface appendages of different lengths (91 and 63 nm). Positive frequency shifts (Δf) indicated that both streptococcal strains adhered to the QCM sensor-surface according to the coupled resonance model. In the coupled resonance model, stiffer bonds yield zero-crossing in a graph of Δf as a function of QCM resonance frequency f_s at higher frequencies. Accordingly, reduction of the ionic strength caused extension of the fibrillar surface appendages, as measured using total internal reflection microscopy, which decreased the adhesive bond stiffness for both streptococcal strains. This indicates that a more densely packed configuration of the fibrils within the bacterium-substratum interface increased the stiffness of the bond, which caused the QCM response to move in the direction of conventional mass-loading, although observed frequency shifts remained positive.

Introduction

Microbial adhesion takes place on virtually all natural and man made surfaces, as one of the initial steps in the formation of a biofilm. Biofilms can pose considerable health threats in food-processing, drinking water systems and human health, while at the same time, depending on the strains and substrata involved, biofilms can be used for waste-water treatment or as probiotics in health. In order to influence initial microbial adhesion, understanding of the adhesive bond at the bacterium-substratum interface is essential. According the physico-chemical modelling, adhesion is achieved by an interplay between attractive Lifshitz-Van der Waals forces in combination with attractive or repulsive electrostatic and acid-base interactions (Hermansson, 1999). Bacterial cell surfaces however, are difficult if not impossible to compare with the surfaces of inert colloidal particles, as bacteria usually possess cell surface appendages of different lengths that may affect the adhesive bond. Moreover, the conformation of these cell surface appendages changes with time during initial adhesion (Olsson et al., 2010) and is influenced by environmental factors, such as ionic strength and pH (Sonohara et al., 1995).

Characterization of the adhesive bond between a bacterium and a substratum surface is experimentally challenging and only possible through the use of atomic force microscopy (Abu-Lail & Camesano, 2003) or optical tweezers (Klein et al., 2003). Both techniques are invasive and potentially destructive and rely on forcing bacteria into contact with a substratum surface, followed by pulling them away from the surface in order to measure the force required to break the bond, but are not able to determine the stiffness of the adhesive bond.

The Quartz Crystal Microbalance (QCM) is a well established instrument to study adsorption kinetics and mechanical properties of molecular films at solid-liquid interfaces in terms of shifts in resonance frequency of an AT-cut quartz-crystal sensor and its dissipative energy losses (Berglin et al., 2009; Macakova et al., 2010). Colloidal particles, including bacteria, are too large to couple to the sensor-surface as a mass (*i.e.* conventional Sauerbrey-type mass-loading (Sauerbrey, 1959) and their adhesion to the QCM sensor-surface has given rise to positive frequency shifts that are hitherto hard to explain by a generalized theory (Berglin et al., 2008; Fatisson et al., 2009; Olofsson et al., 2005; Olsen et al., 2003; Olsson et al., 2009; Poitras & Tufenkji, 2009b; Su & Li, 2005; Vaughan et al., 2001) It has been suggested however, that instead of mass-loading to the

sensor-surface, adhering particles (Dybwad, 1985) or bacteria (Olsson et al., 2011) possess a resonance frequency of their own that couples to the resonance of the sensor-surface to yield positive frequency shifts together with large dissipative energy losses.

Bacterial cell surface appendages often form the coupling between a substratum surface and a bacterium. The adhesive bond stiffness may not only depend on the length and density of these surface appendages, but also on whether they are stretched or more collapsed depending on ionic strength. Shifts in QCM resonance frequency (Δf) and its dissipative energy loss (dissipation, ΔD) have recently been correlated with fibrillar lengths in a collection of *Streptococcus salivarius* strains (Olsson et al., 2009). Positive frequency shifts occurred for fibrillated strains and their magnitude appeared dependent on fibril length.

The aim of this study was to investigate whether the coupled resonance model is applicable to assess the adhesive bond stiffness of two oral *S. salivarius* strains with different lengths of fibrils on their surfaces. Stretching or collapse of fibrillar cell surface appendages was induced by changing the ionic strength of the suspending fluid. In addition, it was investigated whether the separation distance between adhering streptococci and the QCM sensor-surface varied upon changing the ionic strength using total internal reflection microscopy (TIRM). Since the coupled resonance model is not very well known, even not among QCM users, we first briefly describe the coupled resonance model.

Coupled Resonance Model in QCM

Particle adhesion on the QCM sensor-surface operating in air has previously been described according to a coupled resonance model (Dybwad, 1985). In the coupled resonance model, a particle adhering to the sensor-surface is depicted as a resonator with its own resonance frequency (f_p) according to Eq. 1 that couples to the resonance frequency of the QCM sensor-surface (f_s) given by Eq. 2

$$2\pi f_P = \sqrt{\frac{k}{m}} \tag{1}$$

$$2\pi f_S = \sqrt{\frac{K}{M}} \tag{2}$$

in which *k, m* and *K, M* are the stiffness and mass respectively for the particle and QCM sensor-surface. The shift in sensor resonance frequency Δf is determined by the ratio between sensor-surface resonance frequency and the particle resonance frequency. At relatively low sensor frequencies the particles can move along with the movement of the sensor. The sensor then senses the adhering particle as an increase in its effective mass, yielding negative frequency shifts (mass-loading). At relatively high sensor frequencies the particles can not follow with the movement of the sensor. The sensor now senses counteracting forces during movement that are proportional to the stiffness of the contact point (coupled resonance).

The use of the original coupled resonance model is restricted to a single particle in air (Dybwad, 1985) where dissipative energy losses are minor. Dissipative energy losses can be introduced easily by taken the spring constant as a complex number, representing a viscous component (dash pot) as part of the coupling (D'Amour et al., 2006) provided that the loading is small. Dissipative energy losses in QCM are quantified by the bandwidth Γ of the resonance peak at half maximum, or the decay of the oscillation amplitude with time, as expressed in the dissipation, *D*. Dissipation and bandwidth are related to each other via

$$\Gamma = \frac{Df_s}{2} \tag{3}$$

The small-load approximation has been shown to be generally applicable, i.e. to populations of particles adhering to a QCM sensor-surface in air (Vittorias et al., 2010) as well as in liquid through modeling using finite element analysis (Pomorska et al., 2010). Figure 1 presents a prediction according to the small-load approximation of Δf and $\Delta\Gamma$ for adhering particles as a function of the ratio between the QCM sensor-surface resonance frequency (f_s) and the particle resonance frequency (f_p).

The location of the zero-crossing frequency f_{ZC} (where Δf changes sign) depends on the ratio between the quartz crystal resonance frequency and the particle resonance frequency (f_s/f_p). The zero-crossing frequency is accompanied by a maximum in bandwidth. Herewith, theoretical predictions of the coupled resonance model can be described over an unlimited range of frequencies.

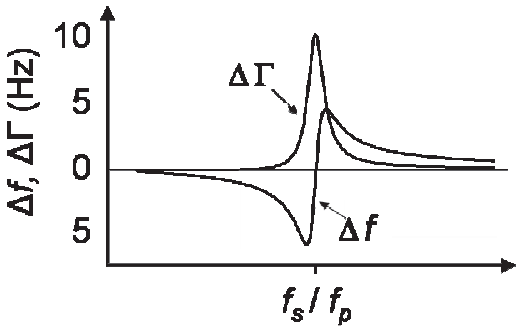

Figure 1. Theoretical prediction of the shifts in frequency (Δf) and bandwidth ($\Delta\Gamma$) for particles adhering to a QCM sensor-surface in a coupled resonance model. The asymptotic shift from negative to positive Δf occurs when the particle resonance frequency (f_p) equals the QCM resonance frequency (f_s) and is accompanied with a maximum in $\Delta\Gamma$.

Experimentally however, one can only probe resonance frequencies equal to the QCM sensor's fundamental frequency and its higher harmonics (3rd, 5th, 7th, 9th, 11th and 13th overtone). Zero-crossing frequencies are only observed in experiments if the particles possess an adhesive bond stiffness which allows them to oscillate at frequencies within the accessible window, usually ranging from 5 to 65 MHz (see Figure 2). When the zero-crossing occurs outside this window, data points may seem to scatter randomly, while also zero-crossing within the accessible window may not always be easy to fit into a coupled resonance model due to the fact that only discrete overtone frequencies can be measured.

Note, the coupled resonance model, as displayed in Figure 1, describes the appearance of un-normalized frequency shifts, whereas QCM-D users usually display frequency shifts that are normalized with respect to resonance frequency overtone number ($\Delta f/n$).

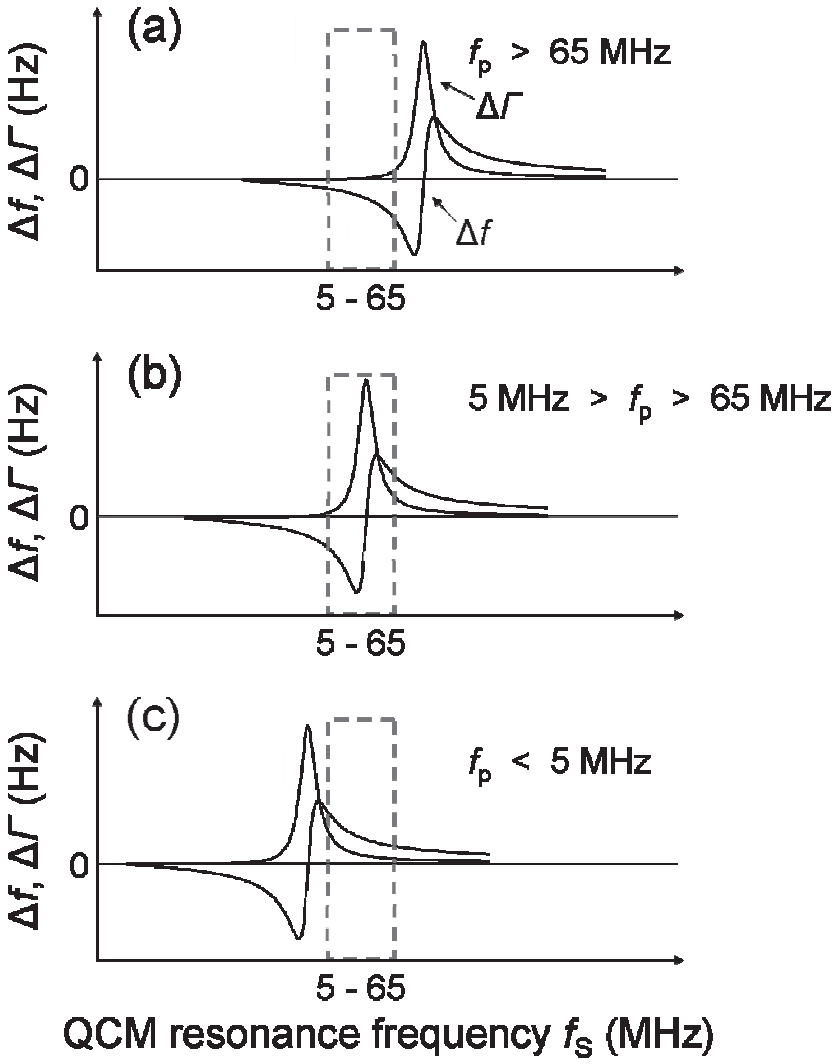

Figure 2. Theoretical shifts in frequency (Δ*f*) and bandwidth (ΔΓ) for particles adhering with different adhesive bond stiffness to a QCM sensor-surface in a coupled resonance model as a function of the QCM resonance frequency (f_S). Particle resonance frequency (f_p) increases with adhesive bond stiffness. Cross-over points at $f_s = f_p$ can only be observed when within the window of the QCM fundamental resonance frequency and its overtones, indicated by the dashed rectangles.

Materials and Methods

Bacterial Strains and Growth Conditions

S. salivarius mutant strains HB7 and HBV51 were cultured aerobically at 37 °C in Todd Hewitt broth (Oxoid, Basingstoke, UK), according to previously described protocols (Olsson et al., 2009). Bacteria were harvested by centrifugation (5 min at 5000 *g*) and washed in 100 ml adhesion buffer (50 mM potassium chloride, 2 mM potassium phosphate and 1 mM calcium chloride, pH 6.8). Bacteria were sonicated intermittently 3 times for 10 s at 30 W (Vibra Cell model 375; Sonics and Materials, Danbury, CT) while cooling on ice, and once again washed in 100 ml buffer before being diluted in buffer to a final concentration of 3 x 10^8 bacteria ml^{-1}. Both strains are hydrophilic and known not to produce any extracellular polymeric substances, but they possess fibrillar surface appendages of different lengths and density (van det Mei et al., 1987). In demineralized water, HB7 possesses a dense layer of 91 nm long fibrils, whereas HBV51 a sparse layer of 63 nm long fibrils.

QCM Experiments and Analysis

Bacterial adhesion was carried out in a window-equipped QCM-D device (model Q-sense E1, Q-sense, Gothenburg, Sweden) on gold-plated QCM sensor-surfaces. Before each experiment, the sensor-surfaces were cleaned by immersion in a 3:1:1 mixture of ultrapure water, NH_3 and H_2O_2 (Merck, Darmstadt, Germany) at 70°C for 10 min followed by 10 min UV/Ozone treatment, yielding a water contact angle of 16 ± 3 degrees. Bacterial adhesion was allowed from adhesion buffer (ionic strength 57 mM) for 1 h at 20°C and a flow rate 300 µl/min. The QCM-D flow chamber is disc-shaped with a volume of approximate 100 µl and a diameter of 12 mm with inlet and outlet facing the crystal surface, giving an estimated shear rate of 2.8 s^{-1}. After adhesion, the bacterial suspension in 57 mM ionic strength buffer was replaced by 12.5 or 5.7 mM buffer, with no suspended bacteria, in intervals of 5 min. Changes in Δf and $\Delta\Gamma$ due to differences in conductivity of the buffers were accounted for by subtracting the QCM responses Δf and $\Delta\Gamma$ upon changing ionic strength in the absence of bacteria from the ones measured in a 57 mM buffer in presence of bacteria.

Images of the bacterial deposition on the QCM sensor-surface were collected 30 s before each reduction in ionic strengths, using a CCD camera (Model A101, Basler vision technologies, Ahrensburg, Germany), mounted on a metallurgical microscope with a 20x objective (Leica DM2500 M, Rijswijk, The Netherlands). The bacterial density, i.e. the number of bacteria adhering per unit area N_S (N/cm^2), were calculated from these images using in-house image analysis software (written on MATLAB platform). All measurements were performed in triplicate with separately cultured bacteria.

TIRM Experiments and Analysis

For TIRM, streptococci were allowed to adhere at room temperature for 5 min in 57 mM adhesion buffer to a glass cover slip in a disc-shaped parallel plate flow chamber, with an inner height of 0.5 mm and an inner diameter of 12 mm. TIRM measurements were made in stagnant condition at 57, 12.5 and 5.7 mM. The buffers were replaced using a peristaltic pump at a flow rate of 150 µl per min,

An inverted microscope (Olympus, IX71, Tokyo, Japan) in combination with a 100x apochromat TIRF-objective (NA 1.45, Olympus) and EMCCD camera (Andor iXon DU-885 Belfast, Northern Ireland) was used for observing the scattered intensity from the adhering bacteria in the different ionic strength buffers. A laser (Coherent Innova 70 Santa Clara, CA USA) with wavelength λ of 488 nm was used for illumination, focused by a custom-made TIRM condenser onto the back-focal plane of the objective. The lateral distance of the focus in the back-focal plane could be varied using a nano-positioning stage that in order to adjust the angle of incidence (AOI) of the laser beam at the substratum surface. The laser power measured at the substratum surface was 200 µW at an AOI of 0 degrees. The AOI for TIRM measurements was set to 63 degrees resulting in an evanescent light field penetration depth of d_p = 191 nm according to

$$d_p = \frac{\lambda_o}{4\pi\sqrt{n_1^2 \sin^2\theta - n_2^2}} \qquad (5)$$

where λ_0 is the wavelength of the light in vacuum, θ the incident angle at the glass-water interface and n_1 and n_2 the refractive indices of glass and water, respectively. A mirror, placed between the filter turret and the objective, in combination with a beam

dump was used to remove the reflected light from entering the EMCCD camera, therewith allowing detection of scattered light from the evanescent field only. The scattering intensity was measured on 100 frames for 5 ms at each step. Changes in distance due to changes in ionic strength were calculated from the intensity of the evanescent field (i.e. the intensity of the scattered light) according to (Walz, 1997)

$$I(z) = I_o e^{-z/d_p} \qquad (4)$$

where z denotes the distance from the interface, I_o is the intensity of the field at the interface (z=0) and d_p is the evanescent field penetration depth.

Results

The QCM-D shifts in frequency and bandwidth normalized with respect to bacterial density N_S (N/cm^2) at the sensor-surface ($\Delta f/N_S$ and $\Delta\Gamma/N_S$) are presented as a function of QCM resonance frequency for all ionic strengths in Figure 3. Both strains express positive frequency shifts at all overtones and at all ionic strengths, suggesting adhesion to the QCM sensor-surface according to the coupled resonance model with resonance frequencies below 5 MHz. Whereas both shifts in frequency and bandwidth are similar in 5.7 and 12.5 mM suspension fluids, deviations occur in the highest ionic strength suspension. In a 57 mM suspension, HB7 yields a maximum positive frequency shift Δf of roughly 5 x 10^{-6} Hz cm^2 at a QCM resonance frequency of 45 MHz, although the standard deviation is high. Despite the fact this might indicate, that 45 MHz is close to the zero-crossing frequency, no maximum in bandwidth shift is observed. HBV51 also yields a maximum in positive frequency shifts in the 57 mM suspending fluid of roughly 7 Hz cm^2 at a QCM resonance frequency of 25 MHz and it also possesses a large standard deviation. It is accompanied however, by a minimum in bandwidth shift instead of, as in the coupled resonance model, by a maximum.

TIRM data in Figure 4 present the change in bacterium-surface separation distance upon decreasing the ionic strength of the suspending fluid from 57 to 12.5 and 5.7 mM. Note that, as a limitation of TIRM, the reported values only describe the increase in separation distance upon a decrease in ionic strength. The actual separation distance for the bacteria at 57 mM is unknown. The largest increase in separation distance is observed

when ionic strength is reduced from 57 to 5.7 mM. For HB7, this increase amounts 90 nm, which corresponds with the stretching of its 91 nm length fibrils. HBV51, with fibrillar lengths of 63 nm, moves about 43 nm further from the substratum surface upon reducing the ionic strength of the suspending fluid to 5.7 mM.

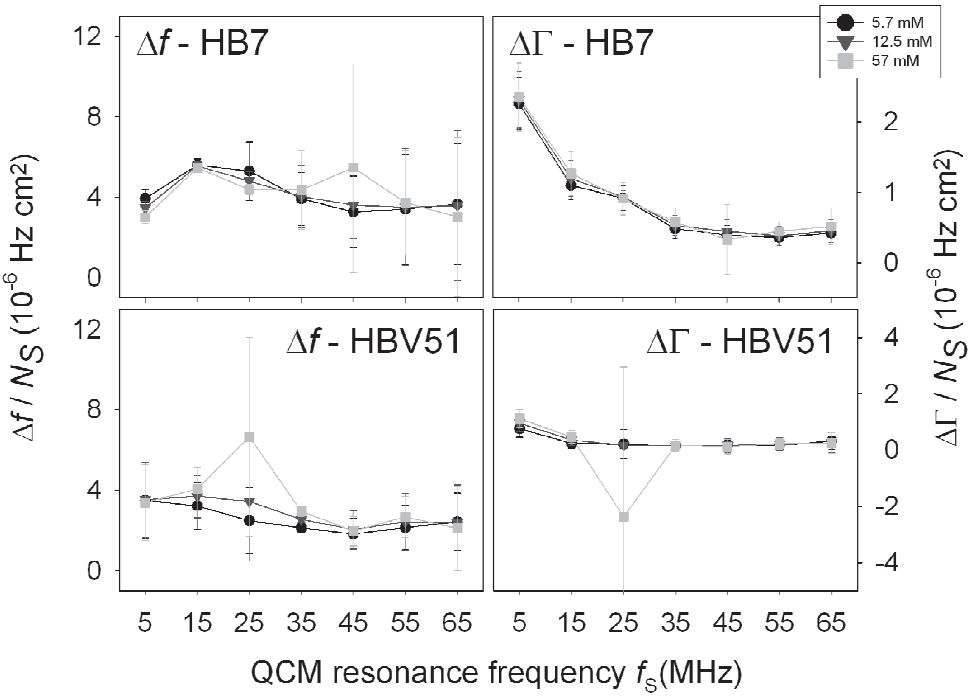

Figure 3. Shifts in frequency (Δ*f*, left panels) and bandwidth (ΔΓ, right panels) per adhering bacterium as a function of QCM resonance frequency (f_S) for *S. salivarius* HB7 and *S. salivarius* HBV51 at different ionic strengths. Error bars represent SD over 3 data points from 3 separately grown bacterial cultures.

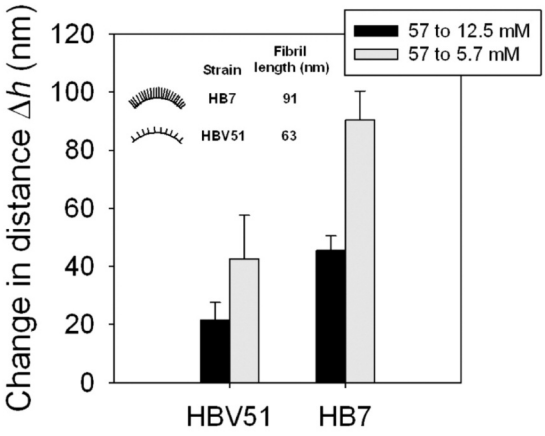

Figure 4. Change in the distance between a bacterial cell and substratum surface from its initial distance at 57 mM, when ionic strength of the suspending fluid is reduced to 12.5 and subsequently to 5.7 mM for *S. salivarius* HB7 and HBV51, possessing fibrillar surface appendages with different lengths. Error bars represent SD over at least 5 individual bacteria, divided over 3 experiments with separatly grown cultures.

Discussion

Window-equipped QCM-D, in combination with a microscope for direct observation of bacterial deposition on the QCM sensor-surface, was used to study the adhesion of two fibrillated *S. salivarius* strains with the aim of assessing the adhesive bond stiffness using a coupled resonance model. According to the coupled resonance model, bacterial resonance frequencies can be derived from the zero-crossing frequencies f_{ZC} when the frequency shift Δf is plotted as a function of QCM resonance frequency f_s. Neither of the two streptococcal strains yielded zero-crossing frequencies accompanied by bandwidth maxima, as required in the coupled resonance model, within the accessible range of 5-65 MHz at any ionic strength. However, positive frequency shifts indicate that these streptococci do not adhere according to Sauerbrey's mass-loading theory. The general appearance of the $\Delta f/N_S$ and $\Delta\Gamma/N_S$ curves in Figure 3, within the window of accessible frequencies in QCM (compare Figure 1), suggests that both strains have zero-crossing frequencies f_{ZC} below 5 MHz for all ionic strengths, as displayed in figure 5. Extrapolation suggests that whereas the zero-crossing frequency of HBV51 dramatically decreases from roughly 1.1 MHz to somewhere below 100 kHz, the zero-crossing frequency of HB7 decreases from roughly 1.1 to 0.7 MHz when the ionic strength is decreased from 57 to 12.5 and subsequently to 5.7 mM. Increasing zero-crossing frequencies indicate that the

adhesive bond stiffness increases. The zero-crossing frequency increases over a much wider frequency range for HBV51 than for HB7, although its separation distance changes less upon reducing ionic strength (see Figure 4). Thus it can be concluded that the stiffness of the adhesive bond between a bacterium and a substratum surface is not *a priori* determined by separation distance. More likely, the adhesive bond stiffness is determined by the fibrillar density. When the fibrils are stretched to their full length (5.7 mM), HB7 possesses a denser layer of fibrils and therefore possesses a stiffer bond than HBV51. As the ionic strength increases, reduced electrostatic repulsion causes the fibrils to collapse into a more densely packed configuration, leading to stiffer bonding.

The above, neglects the maxima in frequency shifts observed for both strains at higher frequencies. Particularly since they are associated with high standard deviations, these maxima might be indicative of a second zero-crossing frequency, although they are not accompanied by a maximum in dissipation bandwidth. Occurrence of a second zero-crossing frequency could be due to a minor sub-population of bacteria with different bonding characteristics or an unknown binding factor. For the time being, we prefer to neglect these maxima as being the result of statistical variations.

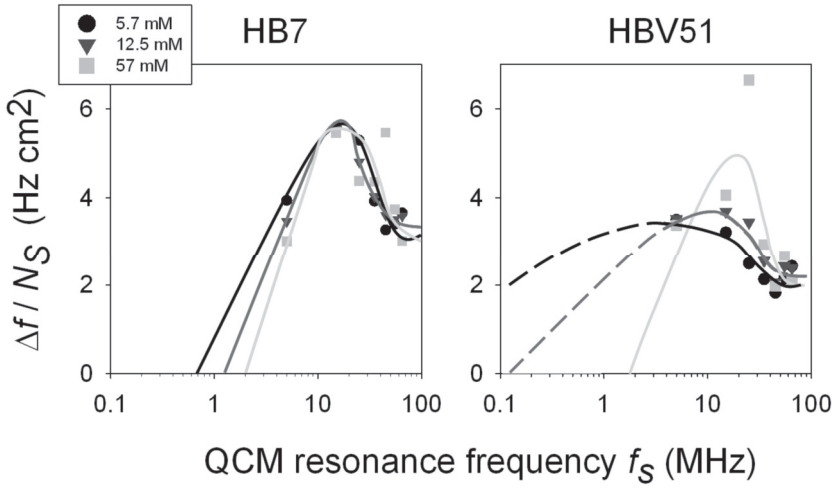

Figure 5. Shifts in frequency Δ*f* per adhering bacterium as a function of QCM resonance frequency (f_S), presented on a logarithmic scale for HB7 and HBV51 at different ionic strengths. Lines are inserted and extrapolated manually in order to estimate the zero-crossing frequencies f_{ZC} for the streptococci at the different ionic strengths. Extrapolations too long to be considered reliable are dashed.

There are currently no data available on other bacterial strains to compare the present results with, but resonance frequencies of inert TiO_2 particles are available for comparison (Pomorska et al., 2010). When comparing resonance frequencies of particles and bacteria however, differences in their effective masses must be taken into consideration, as an increase in mass will decrease the particle resonance frequency (Eq. 1). TiO_2 particles have approximately a 4 times higher density than the bacteria, while the particles used by Pomorska et al. (Pomorska et al., 2010) were also larger in size. Yet TiO_2 particles possessed zero-crossing frequencies between 5-15 MHz, which would only increase if the higher density as compared with bacteria is accounted for. This leads to the conclusion that bacteria, most notably the current two streptococcal strains, adhere through a much less stiff bond than the TiO_2 particles

In conclusion, the QCM-response upon adhesion of fibrillated *S. salivarius* strains show that streptococci do not adhere according to Sauerbrey's mass-loading theory, but rather act as resonators coupled to the sensor-surface. Their adhesive bond stiffness depends on the density of fibrils at the bacterial-substratum interface.

Acknowledgements

We like to thank ZON-MW for grant 91107008 enabling purchase of the quartz crystal microbalance Qsense-E1 & E4, and Prof. Diethelm Johannsmann for valuable discussions on QCM theory.

Chapter 6

Adhesive bond stiffness of *Staphylococcus aureus* with and without fibronectin-binding proteins to an adsorbed fibronectin film

Adam L. J. Olsson, Prashant K. Sharma, Henny C. van der Mei, Henk J. Busscher

Abstract

Staphylococcus aureus is known to cause biomaterials-associated-infections of implants and devices once it has breached the skin and mucosal barriers. Adhesion is the initial step in the development of biomaterials-associated-infections and strategies to prevent staphylococcal adhesion and therewith biomaterials-associated-infections require understanding of the adhesive bond. The aim of this study was to compare the adhesive bond stiffness of two *S. aureus* strains with and without fibronectin binding proteins (FnBP) adhering to a fibronectin-coated quartz crystal microbalance (QCM) sensor-surface, on the basis of a coupled resonance model. Both fibronectin adsorption and staphylococcal adhesion were accompanied by negative frequency shifts, regardless of the absence or presence of FnBPs on the staphylococcal cell surfaces. This is opposite to the positive frequency shifts often observed for other bacterial strains adhering to bare sensor-surfaces, and may indicate that staphylococcal adhesion to the soft adsorbed fibronectin-coating occurs through stiff binding due to an increased bacterium-substratum contact area as the adhering staphylococci sink into and deform the adsorbed protein layer. *S. aureus* 8325-4 possessing FnBPs, yields less negative frequency shifts Δf, further away from the zero-crossing frequency than *S. aureus* DU5883 and must therefore adhere through a stiffer bond to the fibronectin-coating. Due to a limited window of observation, as defined by the available resonance frequencies in QCM, we could not determine exact stiffness values.

Introduction

Pathogenic *Staphylococcus aureus* can be found in 30 to 50% of all healthy adults. Severe infections may be initiated once staphylococci breach the skin or mucosal barriers of the body and enter adjoining tissues or the bloodstream, where they can adhere to many different surfaces, including endothelial and epithelial cells, fibroblasts as well as to plasma exposed biomaterials implant surfaces. Alarming increases in antibiotic resistance among *S. aureus* strains force researchers and clinicians towards other alternative treatments (Lowy, 1998). One strategy to avoid biomaterial-associated-infection is to prevent initial bacterial adhesion, which requires detailed understanding of the mechanisms governing the adhesion process, including the nature of the adhesive bond and its stiffness between a bacterium and the substratum surface.

S. aureus can bind to plasma exposed surfaces through the use of fibronectin binding proteins (FnBP) (Fowler et al., 2000; Greene et al., 1995; Peacock et al., 1999; Saravia-Otten et al., 1997; Vaudaux et al., 1984). Xu et al. (2008) have determined adhesion kinetics, desorption rates, adhesion enthalpies as well as adhesion forces and energies of *S. aureus* strains with and without FnBPs (Xu et al., 2008). Strain 8325-4, known to possess FnBPs, adhered to Fn-coated glass in higher numbers than strain DU5883, lacking FnBPs. More intriguingly, although the kinetics of FnBP-mediated adhesion in parallel flow was clearly reduced upon exposing the Fn-coating with a blocking agent, both adhesion enthalpies and adhesion force measurements appeared much less, if at all, affected. It was suggested that whereas bacterial adhesion in parallel flow was mediated through only Fn-FnBP interactions at the outermost bacterial cell surface, atomic force microscopy and calorimetry were able to probe interactions deeper within the bacterial electrophoretically soft surfaces to reveal hidden Fn-binding sites also for strain DU5883. Thus, although analysis of retraction-force distance curves in atomic force microscopy reveal adhesion forces upon approach, force microscopy is invasive and the measured forces are difficult, if not impossible, to relate to the natural ability of staphylococci to adhere.

Recently, it was suggested that a Quartz Crystal Microbalance (QCM) can be used as sensor for the non-invasive assessment of the adhesive bond stiffness of bacteria adhering to the sensor-surface (Olsson et al., 2011) The more common application of QCM is the sensing of the adsorption of molecular mass (Kwon et al., 2006; Rawle et al., 2007). In

conventional mass-loading theory, the adsorbed mass is assumed to couple directly to the sensor-surface, increasing its effective mass, which reduces its resonance frequency according to Sauerbrey's relation (Sauerbrey, 1959). Sauerbrey's relation is valid only for rigid molecular films. For visco-elastic films, dissipative energy losses, as derived from increased resonance frequency bandwidths (ΔΓ) or reduced oscillation decay times (dissipation, ΔD), must be taken into account for proper derivation of the adsorbed mass (Voinova et al., 2002). Whereas the conventional mass-loading theory assumes thin and homogeneously adsorbed films, as valid for adsorbed protein films, bacteria are discrete objects adhering via a relatively small contact point. The QCM response upon bacterial adhesion to bare substrata, i.e. in the absence of an adsorbed protein film, has been demonstrated to obey a coupled resonance model (Olsson et al., 2011). This model depicts an adhering bacterium as a resonator of its own that resonates together with the QCM sensor-surface (see Figure 1) (Dybwad, 1985; Pomorska et al., 2010). The frequency shift of this coupled resonance is determined by the ratio between the sensor-surface's resonance frequency f_s and the particle's resonance frequency f_p, as determined by its mass m and contact point stiffness k. Soft contact points yield positive frequency shifts, whereas stiff contact points yield negative frequency shifts (see also Figure 1).

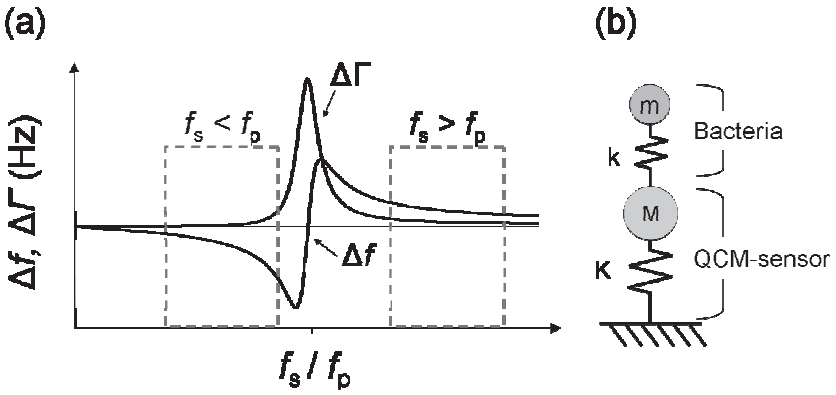

Figure 1. Theoretical shifts in frequency (Δf) and increases in bandwidth (ΔΓ) for bacteria adhering to a QCM sensor-surface as a function of the ratio between the sensor-surface's and particle's resonance frequency (f_s/ f_p) in a coupled resonance model (panel a), as schematically displayed in panel b. The asymptotic shift from negative to positive Δf occurs when the particle resonance frequency (f_p) equals the QCM resonance frequency (f_s) and is accompanied with a maximum in ΔΓ. Rectangles indicate potential windows of observable resonance frequencies, for particles with a resonance frequency (f_p) above the QCM-resonance frequency (f_s).

The QCM resonance-frequency at which Δf crosses zero (f_{ZC}) is accompanied with a peak in bandwidth/dissipation and equals the particle's resonance frequency, from which the stiffness k of the adhesive bond can be determined according to

$$f_{ZC} = f_p = \frac{1}{2\pi}\sqrt{\frac{k}{m}} \quad (1)$$

Importantly, f_{ZC} can be directly observed when the frequency shifts are plotted as a function of the QCM resonance frequency, but only if it falls within the range of available frequencies (i.e. fundamental and its corresponding overtones), as illustrated in Figure 1.

The aim of this study was to analyze the adhesive bond stiffness of two *S. aureus* strains with and without FnBP adhering to an adsorbed fibronectin coating on the QCM sensor-surface on the basis of the coupled resonance model.

Materials and Methods

Bacterial Culture Conditions and Harvesting

FnBP expressing *S. aureus* 8325-4, and its isogenic and non-FnBP expressing mutant DU5883, were maintained on beads at -80°C. For culturing, both strains were plated onto tryptone soy broth (TSB; OXOID, Basingstoke, UK) agar plates overnight at 37°C. These agar plates were maintained at 8°C for maximum 1 week. Pre-cultures were prepared by inoculation of a single colony into 10 ml TSB that was allowed to grow overnight at 37°C under rotation. Pre-cultures were subsequently used to inoculate a main-culture of 200 ml TSB and maintained under similar conditions for an additional 2 h to yield early exponential phase staphylococci, with a peak expression of FnBPs in *S. aureus* 8325-4 (Saravia-Otten et al., 1997). Staphylococci were harvested by centrifugation at 6500g for 5 min at 10°C and washed 2 times in 100 ml PBS (10 mM potassium phosphate, 150 mM sodium chloride, pH 6.8). Bacterial aggregates were broken by sonication while on ice for 3 x 10 s at 30 W (Vibra Cell model375, Sonics and Material Inc., Danbury, Connecticut, USA)

and finally diluted in PBS to a final concentration of 3 x 10^8 cells per ml, as determined by counting in a Bürker-Türk counting chamber.

QCM Preparation and Experiments

Gold plated quartz-crystal sensor-surfaces were cleaned by immersion in a 3:1:1 mixture of ultrapure water, NH_3 and H_2O_2 (Merck, Darmstadt, Germany) at 75°C for 10 min followed by 10 min UV/ozone treatment. Experiments were carried out in a window equipped QCM-D module (E1, Q-sense, Gothenburg, Sweden), that was mounted underneath a microscope enabling direct observation of the QCM sensor-surface. This set-up utilizes an AT-cut quartz crystal operating a fundamental frequency of 5 MHz and its 3rd, 5th, 7th, 9th, 11th and 13th overtone *n*, which corresponds to resonance frequencies of 15, 25, 35, 45, 55 and 65 MHz, respectively and that defines our window of observation (see Figure 1). The sensor-surface was first incubated at a flow rate of 200 µl/min in PBS until the QCM yielded a constant baseline for Δf and $\Delta\Gamma$. The sensor-surfaces were then coated using a fibronectin solution (0.5 µg/ml human fibronectin in PBS, Sigma Aldrich BV, Zwijndrecht, The Netherlands) at a flow rate of 200 µl/min for 20 min. Next, the sensor-surface was once again incubated in PBS, but at a flow rate of 300 µl/min, until constant Δf and $\Delta\Gamma$ values were obtained and a staphylococcal suspension was introduced to the chamber at a flow rate of 300 µl/min for 1 h at room temperature. The QCM-D flow chamber is disc-shaped with a volume of approximate 100 µl and a diameter of 12 mm with inlet and outlet facing the crystal surface, giving an estimated shear rate of 1.9 s^{-1} and 2.8 s^{-1} at flowrates of 200µl/min and 300µl/min, respectively. Images of the bacteria on the sensor-surface were made using the microscope (Leica DM2500 M, Rijswijk, The Netherlands) mounted CCD camera (Model A101, Basler vision technologies, Ahrensburg, Germany). Numbers of adhering bacteria per unit area N_{1h} after 1 h of adhesion were determined from these images using image analysis software (written in-house on a Matlab platform).

Results

The conventional way of presenting QCM-D data is by plotting the shifts in frequency Δf and changes in dissipative energy losses (expressed either as ΔD or $\Delta \Gamma$) as a function of time for the 3rd overtone, as done in Figures 2a and 2b. Fibronectin adsorption yielded a negative frequency shift of around 160 Hz and a bandwidth increase of 14 Hz. As staphylococci subsequently adhered to the fibronectin-coated surface, the frequency shift became more negative and bandwidth further increased. *S. aureus* 8325-4, possessing FnBPs, yielded a negative frequency shift after 1 h of adhesion of around 8 Hz and a bandwidth increase of 18 Hz, whereas DU5883, without FnBPs, yielded a much more negative frequency shift of 30 Hz and a bandwidth increase of 25 Hz.

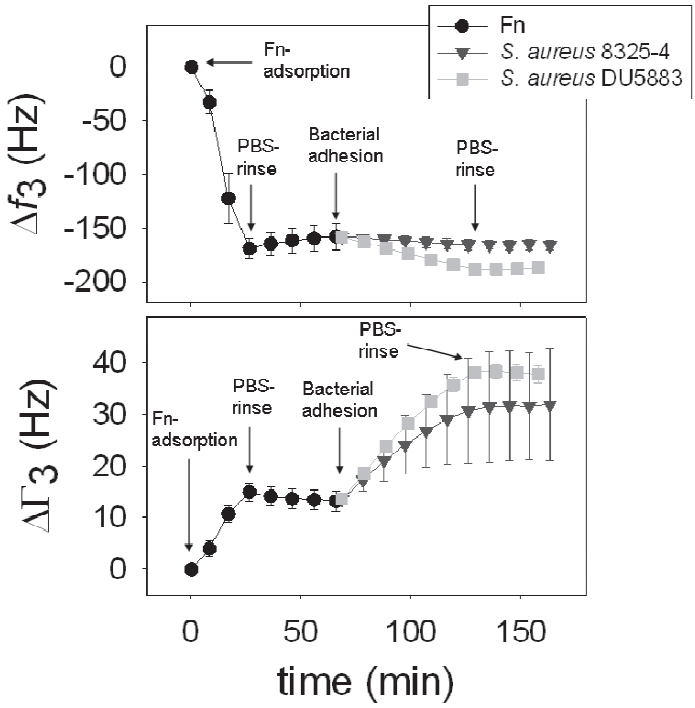

Figure 2. Shifts in frequency (top) and bandwidth increase (bottom) during Fn-adsorption and subsequent staphylococcal adhesion as a function of time. For Fn-adsorption, error bars represent SD over five separate measurements, while for *S. aureus* 8325-4 and DU5883 adhesion, the error bars represent SD over 3 experiments with separately grown staphylococcal cultures.

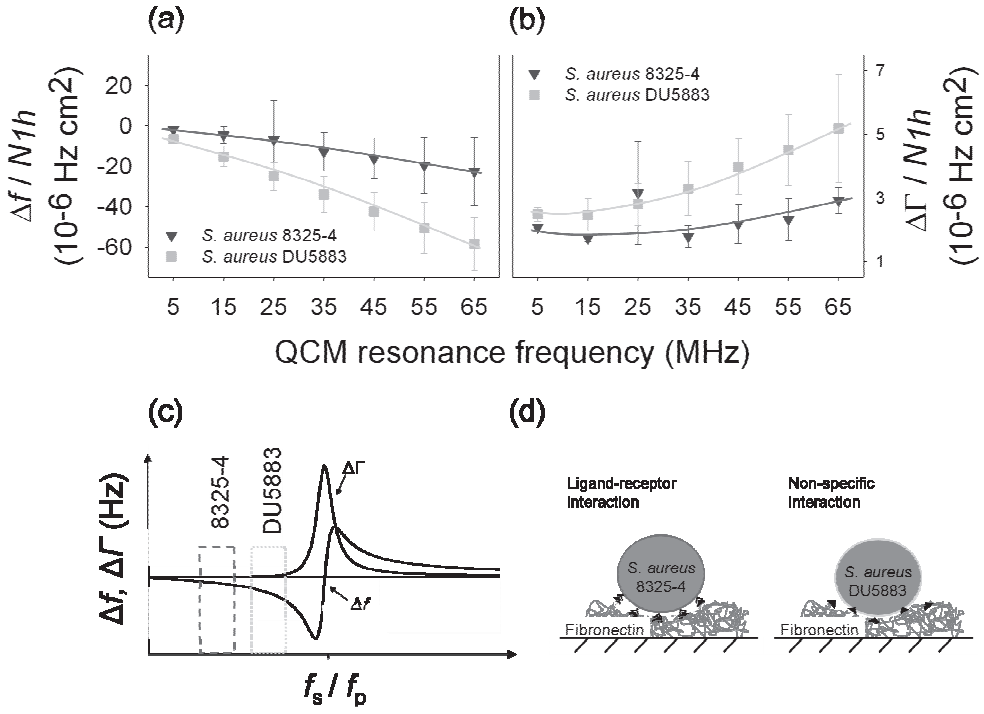

Figure 3. Normalized frequency shifts $\Delta f/N_{1h}$ (a) and bandwidth increases $\Delta\Gamma/N_{1h}$ (b) as a function of QCM resonance frequency after 1 h of staphylococcal adhesion to Fn-coated QCM-surfaces. Panel c shows Δf and $\Delta\Gamma$ as a function of (f_s/f_p) according to the coupled resonance model, together with potential positions of the window of observable frequencies in QCM, fitting the measured data. Error bars represent SD over 3 experiments with separately grown staphylococcal cultures. Lines in panels a and b are inserted manually. Panel d schematically displays how staphylococci adhering to a fibronectin-coating increase their contact area by sinking into the protein layer, and how in addition the adhesive bond of strain 8325-4 becomes stiffer by specific ligand-receptor bonds (Note: schematics not drawn to scale).

In order to analyze staphylococcal adhesion according to the coupled resonance model, we display the frequency shifts and bandwidth increases after 1 h staphylococcal adhesion as a function of QCM resonance frequency (Figures 3a and 3b). The number of staphylococci adhering on the sensor-surface after 1 h amounted 2.2 ± 1.5 x 10^6 cm^{-2} and 2.0 ± 0.4 x 10^6 cm^{-2} for *S. aureus* 8325-4 and *S. aureus* DU5883, respectively. Note that Δf and $\Delta\Gamma$ were normalized with respect to the number of adhering bacteria, to yield ($\Delta f/N_{1h}$) and ($\Delta\Gamma/N_{1h}$). Theoretical plots of Δf and $\Delta\Gamma$ for a composite resonator according to the coupled resonance model are given in Figure 3c. Both strains express negative frequency

shifts at all overtones (see Figure 3a), that by comparison with Figure 3c suggest that staphylococci adhering to fibronectin-coated QCM sensor-surfaces possess resonance frequencies well above 65 MHz. *S. aureus* DU5883 yields a frequency shift $\Delta f/N_{1h}$ that is roughly 3 times more negative than of *S. aureus* 8325-4 over the entire range of available QCM-resonance frequencies. In addition $\Delta\Gamma/N_{1h}$ is about twice as large for *S. aureus* DU5883 as for *S. aureus* 8325-4. Although the maximum in $\Delta\Gamma/N_{1h}$ at 25 MHz could indicate the vicinity of a zero-crossing frequency, it is accompanied with a large SD and we therefore decided to neglect this maximum.

Discussion

The influence of fibronectin-binding proteins on the adhesive bond stiffness of staphylococci adhering to fibronectin-coated surfaces has been investigated using a combination of optical microscopy and QCM-D. Fibronectin adsorption as well as staphylococcal adhesion were accompanied by negative frequency shifts, regardless of the absence or presence of FnBPs on the staphylococcal cell surfaces. Neither of the two staphylococcal strains yielded zero-crossing frequencies within the available frequency range (5-65 MHz), and consequently, it is tempting to argue that these negative frequency shifts are indicative of rigid binding of the adhering staphylococci according to a Sauerbrey-type mass-loading. However, the absence of a zero-crossing frequency within the available QCM window of frequencies does not negate a coupled resonance model. Since both *S. aureus* strains are closely related, the only difference being the absence or presence of FnBPs, mass-loading according to Sauerbrey's relation, should have yielded the same $\Delta f/N_{1h}$ and $\Delta\Gamma/N_{1h}$ (see Figure 3). Accordingly, the two strains must adhere with different adhesive bond stiffness according to the coupled resonance model. *S. aureus* 8325-4 possesses FnBPs and its adhesion yields less negative frequency shifts Δf, and is therefore further away from the zero-crossing frequency than *S. aureus* DU5883 and must adhere through a stiffer bond to fibronectin-coatings.

Based on a coupled resonance model, both staphylococcal strains adhere to the fibronectin-coating with a stiff adhesive bond that allows them to resonate at a frequency well above 65 MHz. Therewith these staphylococcal adhesive bonds are dramatically stiffer than the bonds for *Staphylococcus epidermidis* (chapter 4) and *Streptococcus salivarius* (chapter 5) adhering to bare, gold-coated sensor-surfaces, which all yielded positive frequency shifts, implying soft bonding and bacterial resonance frequencies below 5 MHz. It seems counterintuitive at first, that the presence of a soft adsorbed fibronectin-coating can increase the bond stiffness of adhering bacteria. It is likely however, that the increase in stiffness is due to an increased contact area between the bacteria and the soft surface. Alternatively adhering staphylococci may sink into the adsorbed protein layer as illustrated schematically in Figure 3d, to behave more in a conventional mass-loading manner. Specific ligand-receptor bonds between strain 8325-4 and the adsorbed fibronectin-coating clearly yield a stiffer adhesive bond than observed for strain DU5883, as localized ligand-receptor bonds are more efficient in immobilizing an adhering bacterium than non-localized adhesion forces, like for instance the Lifshitz-Van der Waals ones. Without going into details, further support for the above can be found in chapter 7, where equally dramatic effects on the adhesive bond stiffness are observed when soft molecular layers and specific ligand-receptor types of interactions are introduced in the adhesion of silica particles on hard silica and gold surfaces.

In conclusion, here we applied a coupled resonance model in order to compare the adhesive bond stiffness of staphylococci, with and without FnBPs, to a fibronectin-coated sensor-surface in QCM. Staphylococcal adhesion to a soft fibronectin layer yielded a QCM response that more closely resembled mass-loading than adhesion of other strains to a bare sensor-surface. However, adhesion of staphylococci with FnBPs caused the QCM response to shift more in the direction of a coupled resonator than adhesion of staphylococci lacking FnBPs.

Chapter 7

Probing colloid-substrate contact stiffness by acoustic sensing in liquid

Adam L. J. Olsson, Henny C. van der Mei, Diethelm Johannsmann,

Henk J. Busscher, Prashant K. Sharma

Abstract

The Quartz Crystal Microbalance (QCM) is a popular technique to study molecular adsorption in terms of shifts in resonance frequency (Δf) of an oscillating quartz-crystal sensor. Adhesion of colloidal particles (including bio-colloids, such as bacteria or tissue cells) to the QCM surface has been difficult to interpret due to the occurrence of positive frequency shifts, which, according to conventional mass-loading theory, would indicate a loss of mass rather than adsorption. The explanation for positive Δf possibly lies in the fact that particles do not always couple to the sensor surface as a mass, but rather act as "coupled oscillators" of their own. Their oscillation frequency depends on their mass and their adhesive bond stiffness. Positive Δf is observed when the frequency of the coupled resonance is below the QCM resonance frequency, and vice versa. The transition between negative and positive Δf occurs when the QCM resonance frequency equals the particle oscillation frequency and can be observed when Δf is plotted as a function of the QCM resonance frequency, *i.e.* its overtones. If the mass of the particle (m) is known, the particle oscillation frequency can be used to estimate the colloid-substrate spring constant (k). The explanation was verified by monitoring changes in adhesive bond stiffness as a function of adhesive bond energy for silica particles on different surfaces and at different ionic strengths. For silica particles interacting with silica, the stiffness of the adhesive bond is a function of the adhesion energy. In the presence of a molecular film, the stiffness is influenced by the molecular arrangement of this film and by the presence of ligand-receptor interactions, in particular.

Introduction

Colloidal particle adhesion to flat substrates is important in different areas of science. In materials science, colloids are necessary to obtain desired properties required for high data storage, sensory and thermoelectric devices (Talapin & Murray, 2005; Urban et al., 2007). There are biosensor applications where microbial contamination is detected upon direct contact between microorganism and sensor-surface (Buchatip et al., 2010; Serra et al., 2008; Shen et al., 2007). Microbial adhesion causes problems and must be avoided at all costs on both engineering and implant surfaces (Gristina, 1987; Lewin, 1984; Rosan, 1981). The tenacity of adhesion in the form of colloid-substrate stiffness is of importance both for the efficiency and durability of intended colloidal immobilization or to apply the right amount of force for microbial detachment. Centrifugation (Salazar-Banda et al., 2007), rotating disks (Tsai et al., 1991) and flow displacement devices (Gómez Suárez et al., 1999) are used to estimate the force of detachment. Flow displacement devices yield detailed information about colloid adhesion kinetics, while giving only approximate, indirect estimate of the adhesion force at the contact point (Bowen & Epstein, 1979). Atomic force microscopy directly measures the adhesion forces at the interface between a particle and substrate, but it is a destructive technique which requires forced contact, followed by forced detachment for the actual measurement (Bowen et al., 1999). Furthermore, these methods only explore the bond near its failure point *i.e.* bond breakage, without giving information about the bond in its normal state. In order to probe the bond in its natural state, the colloid particle needs to be perturbed non-destructively around its equilibrium position in order to estimate its bond stiffness; one potential technique to do so is the Quartz Crystal Microbalance (QCM).

The QCM is an acoustic sensor which has been widely used to measure the amount and properties of adhering molecular mass at the solid-air and solid-liquid interface by means of shifts in the resonance frequency (Δf) and bandwidth ($\Delta\Gamma$) of an oscillating quartz-crystal-sensor-surface (Macakova et al., 2010; Sauerbrey, 1959). At the heart of QCM, is an AT cut quartz crystal capable to resonating at 5 MHz and its higher overtones. The QCM is capable to sense the weak adhesive bonding of point-like contacts formed between a colloidal particle and a substrate surface via a coupled resonator model (Dybwad, 1985), mathematical details of which are provided in the Modeling section of this paper. Briefly, the Dybwad model predicts two different types of limiting behavior, which we term “inertial loading” and “elastic loading”. When the bond between the

adsorbing particle and the sensor surface is stiff, the particle essentially moves with the resonator, thereby increasing its mass. The frequency of the composite resonator (the crystal and all particles coupled to it) is decreased relative to the frequency of the bare crystal. The situation is well known and equivalent to Sauerbrey-type loading (Sauerbrey, 1959). The force exerted by the sample onto the crystal is the force of inertia. It is proportional to the acceleration and the effective mass of the sample, where the effective mass includes an unknown amount of mass of the ambient liquid dragged along by the spheres. In the opposite limit of weak bonding, the frequency shift is positive. This happens because the spheres in this case do not follow the motion of the crystal. Rather, they are clamped in liquid by inertia. The force exerted onto the crystal now is proportional to the relative displacement and to the stiffness of the bond. The coupling between the crystal and the immobile spheres increase the effective stiffness of the composite resonator, thereby increasing the resonance frequency giving rise to positive frequency shifts. In the high-frequency limit (see theory section) the stiffness of the link is proportional to Δf.

Importantly, the transition between inertial and elastic coupling can be directly observed when comparing the frequency shifts on different overtones. One and the same batch of particles can couple to the sample predominantly via inertia at low harmonics (slow movement, particles follow the crystal) and via elasticity on high harmonics (fast movement, particles do not follow the crystal). As a consequence, Δf is negative on low overtones and positive on high ones. As we will show, the stiffness of the link can be inferred from the "zero-crossing frequency" ω_{ZC}, which is the frequency at which Δf changes sign.

The Dybwad model was derived for attachment in air. Its applicability to adsorbed spheres in a liquid environment is by no means guaranteed. Still, finite element modeling suggests that a similar mechanism is active in liquids, as well (Pomorska et al., 2010). Following this hypothesis, we believe that coupled resonance is the reason behind positive frequency shift observed during colloidal particle adhesion previously reported in literature (Berglin et al., 2008; Fatisson et al., 2009) including bacterial adhesion (Olofsson et al., 2005; Olsen et al., 2003; Olsson et al., 2009 & 2011; Poitras & Tufenkji, 2009b; Su & Li, 2005; Vaughan et al., 2001), adhesion of diatoms (Molino et al., 2008) and of protozoan oocysts (Poitras et al., 2009). Olsen already pointed out that positive frequency shifts in bacterial adhesion are caused by flexible bonding (Olsen et al., 2003), although the mechanism behind the phenomenon was not fully understood. Peculiarly,

the coupled oscillator model has been used numerous times to determine the stiffness of the adhesive bonds in the dry state (Dybwad, 1985; D'Amour et al., 2006; Vittorias et al., 2010), but no attempts to extend the model to liquid environments have yet been made.

The aim of this chapter therefore is to estimate the stiffness k of adhesive bonds between the substrate and colloidal particles of different sizes at the solid-liquid interface. The technique is first validated by modulating the bond stiffness of a silica sphere – silica plate interface via ionic strength. In a second step, it is applied to soft links formed by ligand-receptor (streptavidin-biotin) binding.

Theory

The resonance frequency of a quartz crystal sensor at overtone order n, $f_{Q,n}$, depends on its effective mass and its internal stiffness according to

$$\omega_{Q,n} = 2\pi f_{Q,n} = \sqrt{\frac{K_n}{M}} \qquad (1)$$

where M is one half of the mass of the quartz crystal and $K_n = (n\pi)^2 K_{stat}/2$ is the effective spring constant at overtone n. K_{stat} is the static spring constant of the plate under shear (Johannsmann, 2007). The parameter $\omega_{Q,n}$ occurs in many places in the following text and we often also use the variable ω, for brevity. The periodic stress exerted by the sample onto an oscillating substrate depends on frequency, ω. The corresponding equations apply to all instruments employing acoustic shear waves. When the behavior of the sample is interrogated with a QCM, only the discrete frequencies, ω are available for investigation.

In conventional mass loading theory, small and rigid masses adsorbing to the sensor surface are viewed as an integral part of the crystal, increasing its effective mass M and thereby decreasing the resonance frequency according to Eq. 1.

Large particles adhering to the sensor surface via a small point-contact, on the other hand, possess a frequency of their own that can be mechanically described according to

$$\omega_S = 2\pi f_S = \sqrt{\frac{k}{m}} \tag{2}$$

In Dybwad's original model, m is the mass of the particle, k is the spring constant describing the stiffness of its adhesive bond towards the sensor surface and subscript S stands for sphere and refers to the particle. The model can be generalized to rotational motion. In this case, m is replaced by a moment of inertia (in units of kg m^2) and k becomes the ratio of a torque and angle (units of Nm, for instance a bending stiffness). This second resonance couples to the resonance of the crystal, shifting the frequency and dissipation of the composite resonator with respect to the bare crystal. As always with coupled resonances, these shifts become large, when the resonance frequencies of the two constituent resonators ($f_{Q,n}$ and f_S) have similar values. With regard to the mathematics, we slightly digress from Dybwad's original treatment in that we assume that the frequency shift induced by the spheres is small. The justification for the use of this "small-load approximation" and its merit has been in detail provided in the appendix in Vittorias et al. (2010).

If the sample consists of an assembly of sphere-plate contacts, one can show that the frequency shift is given by (D'Amour et al., 2006)

$$\frac{\Delta f}{f_F} = \frac{1}{\pi Z_q} N_S m\omega \frac{\omega_S^2}{\omega^2 - \omega_S^2} \tag{3}$$

where f_F is the fundamental frequency (f_F = 5 MHz), Z_q is the acoustic impedance of AT-cut quartz, ($Z_q = 8.8 \cdot 10^6$ kg m^{-2} s^{-1}) and N_S is the number of the particles per unit area (particles / cm^2). As such, Eq. 3 applies to all frequencies, ω, but with any given crystal, one can only probe frequencies equal to one of the harmonics ($\omega_{Q,n}$ in Eq. 1).

The experiments reported in (D'Amour et al., 2006) were carried out in air and dissipative processes were minor. Here, we are concerned with spheres embedded in a

liquid medium and the dissipation of energy in the liquid is an important aspect. Before extending Eq. 3 such that it cover spheres in liquids, we briefly comment on how dissipation is measured and quantified with the QCM. The fact that the movement of the sphere relative to the substrate dissipates energy is reflected in the increased resonance bandwidth, termed Γ in the following. More specifically, Γ is the half bandwidth at half maximum. A second parameter is widely used to quantify dissipative processes, which is the "dissipation", D, and its shifts, ΔD. The shift in dissipation, ΔD, is usually displayed in units of 10^{-6}. Γ and D are related by $\Gamma = fD/2$ where f is the frequency of crystal oscillation at a particular overtone, n. For a 5 MHz crystal, one can easily convert from $\Delta D \cdot 10^{-6}$ to $\Delta\Gamma/n$ (note the division by n) by multiplying with 2.5. The reason for using ΔΓ rather than ΔD is the fact the models underlying the QCM can in a rather simple and concise way be written down using complex numbers. In the frame of QCM-modeling, Γ is the imaginary part of a complex frequency. Also, one may plot the shifts in bandwidth versus the shifts in frequency and obtain characteristic shapes. Unless the coupled resonance is highly overdamped, these "polar diagrams" show circles when expressed in terms of ΔΓ vs. Δf (more on this follows later in this section). This characteristic shape is lost when the same data are displayed as ΔD versus Δf. In this study we have consistently used the (un-normalized) frequency shift, Δf, and the bandwidth shift, ΔΓ, which can be calculated from $\Delta f/n$ (the "normalized frequency shift") and ΔD, commonly used for data display by users of the QCM-D.

Equation 3 can be expanded to include dissipation. Essentially, one makes the spring constant, k, complex. In order to cast the equations into a more familiar form, we divide the imaginary part of the spring constant by frequency, ω, and call this parameter ξ. The complex spring constant then is given as $k + i\omega\xi$. ξ is called "drag coefficient" or "friction coefficient" in colloid science. It is the ratio of a force and a velocity. The respective element in a mechanical equivalent circuit is the dashpot. Using these parameters, the complex equivalent to Eq. 3 is

$$\frac{\Delta f^*}{f_F} = \frac{\Delta f + i\Delta\Gamma}{f_F} = \frac{N_S}{\pi Z_q} \frac{m\omega\left(k + i\omega\xi\right)}{m\omega^2 - \left(k + i\omega\xi\right)} \qquad (4)$$

where Δf^* is the complex frequency shift. Both the Dybwad model and Eq. 4 follow the spirit of mechanical equivalent circuits. The experiment is characterized by a vector

field of displacements and a tensor field of local stresses. It is by no means clear that the dynamics of this continuum model can be captures with a small number of discrete elements like point mass, a spring, and a dashpot as shown in figure 1. The potential inadequacies of such a simple model are obvious. Still, equivalent mechanical circuits are transparent and often capture the essentials of the sample's behavior.

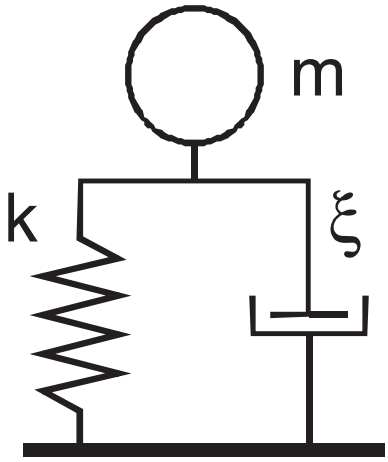

Figure 1. Mechanical equivalent circuit to Eq. 4. The sphere at the top with mass m moves periodically relative to the substrate (at the bottom). It couples to the substrate via a spring with spring constant k and a dashpot with drag coefficient ξ. The force exerted to the substrate is periodic with complex amplitude, F_0. The velocity of the substrate is periodic with the complex amplitude v_0. The complex frequency shift of the sensor surface, $\Delta f^* = \Delta f + i\Delta\Gamma$ is proportional to the number of spheres, N_S, (in units of cm^{-2}) and to the force-velocity ratio, F_0/v_0. The parameter $N_S F_0/v_0$ also carries the name "load impedance".

One might, in principle, allow k and ξ to depend on frequency. In the context of rheology, this would be called "viscoelastic dispersion". Dispersion is connected to relaxation processes inside the material. A second reason for making ξ (or even m) frequency-dependent lies in high-frequency hydrodynamics. The strength of hydrodynamic coupling between the sphere and its environment depends on the penetration depth of the shear wave, which depends on frequency (Kanazawa & Gordon, 1985). For simplicity, k and ξ are fixed parameters independent of frequency in the following.

It is instructive to cast the equation into still another form. In addition to the frequency $\omega_S = (k/m)^{1/2}$ we define a damping rate as $\gamma = \xi/m$ (in of s^{-1}) and write

$$\frac{\Delta f^*}{f_F} = f_{osc}\frac{N_S}{\pi Z_q}\frac{m\omega\left(\omega_S^2 + i\omega\gamma\right)}{\omega^2 - \left(\omega_S^2 + i\omega\gamma\right)} \qquad (5)$$

This is the familiar Lorentz curve describing a forced resonance. Again, Eq. 5 describes a coupled resonance, which shifts the frequency and the bandwidth of the main resonator. Both ω_S and γ will be of the order of a few MHz. When reproducing experimental data with Eq. 5, it is straight forward to insert reasonable guess values for ω_S and γ. For $\gamma << \omega_S$, γ is the half-band full-width of the coupled resonance (in units of radial frequency). One can define a quality factor of the coupled resonance, Q_S, as $Q_S = \omega_S/\gamma = (mk)^{1/2}/\xi$. This parameter will turn out to be convenient.

We have inserted the numerical prefactor f_{osc} into Eq. 5. f_{osc} is the "oscillator strength". One has f_{osc}=1 within the Dybwad formulation. The concept of the oscillator strength is borrowed from molecular spectroscopy, where it quantifies the coupling of any given molecular mode of vibration to the external radiation field. In molecular spectroscopy, f_{osc} is proportional to the square of the transition dipole moment. The transition dipole moment may be zero, and the respective transition then is "forbidden". The term forbidden does not imply that mode would not exist. It only implies that the mode does not couple to electric dipole fields. The Dybwad model was formulated in one dimension and it does not anticipate the possibility of more than one mode of vibration. However a rigid sphere has six degrees of freedom (three translations and three rotations) and there are six corresponding modes of vibration. Four of those are forbidden, which leaves two modes coupling to a periodic translation of the substrate.

The six modes of vibration are;

a) vertical translation (forbidden)

b) wiggling about the point of contact into the *x*-direction (weakly allowed, Figure 2a)

c) wiggling about the point of contact into the *y*-direction (forbidden)

d) rotation about an axis parallel to the *y*-axis, passing through the center of the sphere (allowed, Figure 2b)

e) rotation about an axis parallel to the *x*-axis, passing through the center of the sphere (forbidden)

f) rotation about the vertical axis (torsion, forbidden)

The *x*- and the *y*-axes are parallel and perpendicular to the motion of the substrate. Both are in the substrate plane. The corresponding strains to the link are;

a) extension

b) bending (mode I in fracture mechanics (Anderson, 2005))

c) bending (mode I in fracture mechanics)

d) shear (mode II in fracture mechanics)

e) shear (mode II in fracture mechanics)

f) twist (mode III in fracture mechanics)

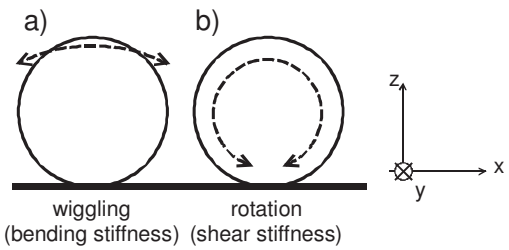

Figure 2. Illustration of the two allowed modes of motion for rigid spheres attached to a substrate via a weak bond. An allowed mode couples to a tangential periodic translation of the substrate in the X direction. The rotation about the center of the sphere directly leads to a displacement of the contact point and therefore strongly couples to a tangential motion of the crystal surface. Wiggling couples to substrate displacement only if the center of rotation is not exactly at the point of contact. The liquid in the neighborhood of the contact point also provides for some coupling.

As in optical spectroscopy, a mode is "allowed" if it couples to the excitation, where the excitation here is a periodic tangential stress into the x-direction at the contact point. Vertical translation, bending into the *y*-direction, rotation about the *x*-axis, and torsion do not induce such stresses and are therefore forbidden. The rotation about the *y*-axis clearly is allowed in this sense (Figure 2b). The situation is less clear for wiggling into the *x*-direction (Figure 2a). If wiggling amounts to a rotation about an axis located at exactly the point of contact, then there is no lateral displacement at the point of contact. However, the exact shape of the mode (which can, for instance be computed with finite element analysis) may be such that the axis of rotation is slightly displaced from the point of contact. In this case, wiggling does couple to a tangential displacement of the substrate. A second factor facilitating wiggling is the presence of the liquid. For the wiggling mode, most of the stress transmitted across the link acts normal to the surface, which does not affect the resonance frequency. A thickness-shear resonator (such as the QCM) only responds to tangential stress. However, if the sphere is embedded in a liquid, wiggling leads to squeeze flow in the neighborhood of the contact and the squeeze flow, in turn, exerts transmits tangential stress. Since there is some coupling of the wiggling mode to the translation of the substrate, we expect the wiggling mode to be "weakly allowed". In mathematical terms, this implies that the oscillator strength in Eq. 5, f_{osc}, is less than unity but still non-zero. It later turns out that we can only reproduce the experimental data if we choose an oscillator strength of the order of 0.1 (see Discussion section). This finding leads us to conclude that these experiments probe the bending stiffness of the contact (as apposed to the shear stiffness). These arguments can further be supported by finite element analysis along the lines described in Pomorska et al. (2010). We elaborate on this model and how it can explain $f_{osc} \sim 0.15$ in the appendix of this chapter. In the following, we account for the possibility of wiggling by introducing the prefactor f_{osc} into Eq. 5 and proceed with the discussion using the mechanical equivalent circuit (Figure 1, the Dybwad model).

Figure 3a - c display Eq. 5 in graphical form. The ratio ω_S/γ (the quality factor, Q_S) was chosen as 10, 2, and 0.9 for the full black line, the black dashed line, and the dash-dotted grey line, respectively. Figure 3c shows the polar diagram. When plotting $\Delta\Gamma$ vs. Δf one finds the circles (or sections of circles) characteristic of resonance phenomena. Importantly, a large value of γ (a low quality factor *i.e.* large dissipation) has two consequences. Firstly, it makes the peak in the plot of $\Delta\Gamma$ vs. ω broad. Secondly, it makes the plots asymmetric. For $\gamma > \omega_S$, Δf does not become positive in the high-frequency limit.

The circles in the polar diagram (Figure 3c) tilt to the left. These coupled resonances are "overdamped".

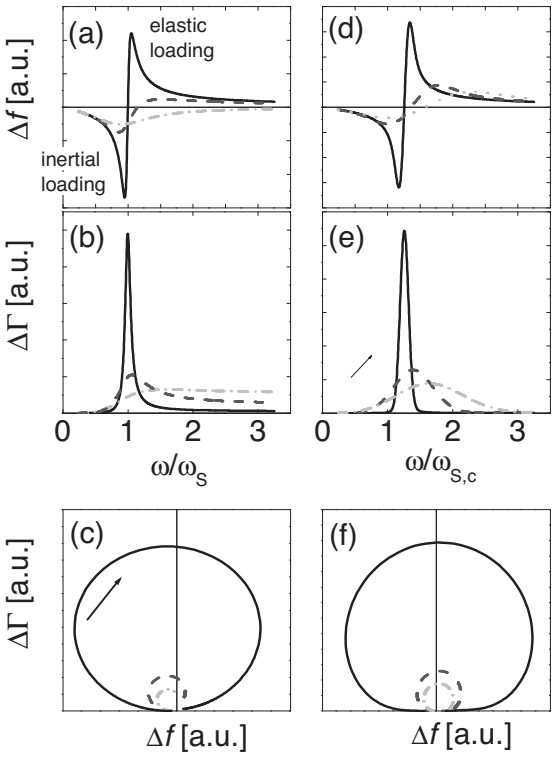

Figure 3. Panels a-c: Shifts of frequency, Δf, and bandwidth, $\Delta\Gamma$, as predicted by Eq. 5. The quality factor of the coupled resonance, Q_S, was chosen as $Q_S = \omega_S/\gamma = 10$, 5, and 0.9 for the full black line, the black dashed line, and the grey dash-dotted line, respectively. If the bandwidth is large, the curves become asymmetric. The circles in polar diagram tilt to the left. For $Q_S < 1$, ($\gamma > \omega_S$, overdamped resonance) the frequency shift never becomes positive. This contrasts to the situation, where the Q-factor of every individual sphere is large, but where the spheres have variable frequencies of the coupled resonance. In the language of spectroscopy, such a situation would be termed "heterogeneous line broadening". This case is shown in panels d – f. The Q-factor of the individual spheres here always was $Q_S = 10$. The frequencies of the coupled resonance followed a Gaussian distribution. The parameter $\omega_{S,c}$ denotes the center of the Gaussian. The width of the Gaussian, σ, varied. Defining the parameter Q^* as $Q^* = \omega_{S,c}/(2\sigma)$ was 10, 5, and 0.9 for the full black line, the black dashed line, and the grey dash-dotted line, respectively. Heterogeneous line broadening also makes the peaks on the plot of $\Delta\Gamma$ versus ω look broader. In contrast to homogeneous line broadening, Δf *does* become positive in the high-frequency limit and the circles in the polar plot do not show tilting.

Another important aspect of coupled resonance for an assembly of particles (rather than a single particle in the Dybwad formulation) is heterogeneous line broadening. If the contact stiffnesses are not the same for all spheres, but rather distributed over a wide range, the peaks in the plots of $\Delta\Gamma$ vs. n become broad, but Δf still becomes positive at high ω. Such a broad distribution of contact stiffnesses is plausible. For sphere-plate contacts between two solids, the contact stiffness strongly depends on the contact radius a (or on a similar effective quantity). In the absence of roughness, a is predicted by the available theories of contact mechanics (Hertz theory being the simplest one) (Popov, 2010). However, these theories neglect roughness. Unless the normal forces are strong (thereby deforming the surface to the extent that local asperities are flattened out), roughness substantially increases the effective contact area and leads to a wide distribution of contact stiffnesses.

In Figure 3d – f, we have accounted for a distribution of contact strengths/stiffnesses. The lines are superpositions of many coupled resonances. Each single coupled resonance follows Eq. 5 but the parameter ω_S was made variable. With regard to the shape of the distribution of ω_S, we chose the Gaussian one for simplicity. The center of the distribution was termed $\omega_{S,c}$. In analogy to the definition of Q_S, we define the parameter Q^* as $Q^* = \omega_S/(2\sigma)$. The values of Q^* in figure 3d – f were $Q^* = 10$, 5, and 0.9 for the full black line, the black dashed line, and the grey dash-dotted line, respectively. The damping rate, γ, was equal to $\gamma = 0.3\ \omega_{S,c}$ in all cases. A broad distribution of values for ω_S makes the peak in the plot of $\Delta\Gamma$ vs. n broad (as does a large γ), but Δf still becomes positive at high n. Positive Δf at high n is the distinctive feature of heterogeneous broadening of the coupled resonance.

Materials and Methods

Particles Preparation

Silica particles as well as streptavidin coated particles with a radius of 0.5 µm and 2.5 µm (Bangs Laboratories, Inc., Fisher, IN, USA) were washed twice by centrifugation in 10 mL of ultrapure water, and diluted to a final concentration of 2×10^8 and 2×10^6 particles per mL, respectively.

Surfaces Preparation

Silica coated QCM-sensor surfaces (Q-sense, Gothenburg, Sweden) were cleaned by submersion into 2% (w/v) sodium dodecyl sulphate (SDS) for 15 min followed by submersion in ultrapure water in a sonicating bath and finally 15 min of UV-ozone treatment. This yielded a hydrophilic silica surface with a zero degrees water contact angle. Biotinylated surfaces where prepared by submerging cleaned gold-plated crystals (Q-sense, Gothenburg, Sweden) into a 0.1 mM solution of biotinylated PEG alkane thiol ($C_{33}H_{63}N_3O_8S_2$) (Nanoscience Instruments, Phoenix, USA) dissolved in ethanol (100%) overnight. These crystals had been cleaned by immersion in a 3:1:1 mixture of ultrapure water, NH_3 and H_2O_2 (Merck, Darmstadt, Germany) at 75°C for 10 min followed by 10 min UV/Ozone treatment and ethanol (70%) rinse.

QCM Measurements

Adhesion of silica particles to QCM-surfaces was followed in a window-equipped QCM-device (E1, Q-sense, Gothenburg, Sweden) together with a metallurgical microscope enabling direct observation of particle adhesion. Potassium chloride (KCl) was dissolved in ultrapure water to final concentrations of 150, 100, 75, 50, 25, 10 and 5 mM. Silica particles were suspended in ultrapure water and introduced into the QCM-chamber. In order to deposit the particles onto the sensor surface, 150 mM KCl was introduced to the chamber whereupon the electrostatic repulsion was effectively shielded during mixing, allowing the particles to instantly adhere to the surface. After particle deposition, the ionic strength was decreased stepwise allowing 3 min for the QCM signal to stabilize at each step. The number of particles per unit area N_S (particles / cm^2) present on the sensor surface at the different ionic strengths was determined from photographs captured from the center of the QCM crystal with a CCD camera mounted on a microscope. In order to correlate adhesive bond stiffness with the adhesive strength, the electrostatic repulsion between silica particles and silica surfaces was calculated for the different ionic strengths using the classical DLVO theory (named after Derjaguin, Landau, Verwey and Overbeek) (Morrison & Ross, 2002).

Results

In these experiments, the silica particles of 0.5 μm radius were deposited onto the surface at an ionic strength of 150 mM. The ionic strength was then gradually decreased. The QCM-experiments are here presented in terms of shifts in frequency (Δf) and bandwidth ($\Delta\Gamma$) divided by the particle density N_S (N per cm^2, Figure 4a and b, respectively) and the corresponding $\Delta f/\Delta\Gamma$-ratios (Figure 4c) as a function of overtone number n. The overall appearance of the curves resembles those of the theoretical predictions for coupled resonance (Figure 3). Δf is negative at low n (*i.e.* low QCM resonance frequencies ω) but changes sign to positive values as n increases. Not only does the magnitude of Δf increase with ionic strength, also the overtone number n at which Δf changes signs (*i.e.* the zero-crossing frequency ω_{ZC}) gradually decrease as the ionic strength decreases (Figure 4a). $\Delta\Gamma$ on the other hand, is always positive and increases with n until it reaches a plateau. Both the magnitude of $\Delta\Gamma$ and the overtone at which $\Delta\Gamma$ reaches its plateau increase with ionic strength. $\Delta f/\Delta\Gamma$-ratios (Figure 4c) yield fairly straight lines as a function of n (or its corresponding resonance frequency ω) which simplifies identifying the zero-crossing frequency (ω_{ZC}).

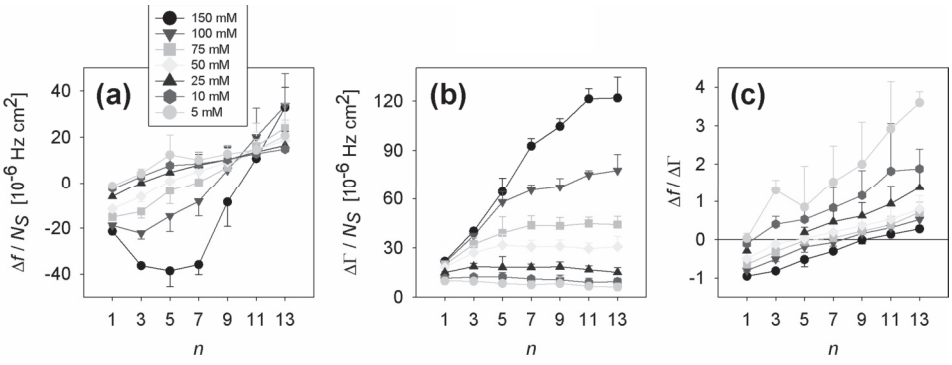

Figure 4. Shift in frequency Δf (panel a), bandwidth $\Delta\Gamma$ (panel b) and the corresponding $\Delta f/\Delta\Gamma$-ratios (panel c) as a function of overtone number n (the corresponding frequencies are the overtone number multiplied by 5 MHz) at different ionic strengths for the adhesion of 0.5 μm radius silica particles to a silica surface. Data are normalized with respect to particle surface density N_S (N per cm^2). Data are averaged values and error bars represent SD over three separate measurements.

Silica particles interacting with silica surfaces represent a hard sphere-plate contact. In order to investigate the stiffness of soft contacts, measurements on biotinylated self assembled mono (SAM) layers were included (Figure 5b and c). The overall appearances are once again similar to those of the theoretical predictions (Figure 3). However, in comparison to the particles adhering directly on silica (Figure 5a) which yielded clear zero-crossing frequencies, the presence of a soft biotin layer (Figure 5b) have dislocated the coupled resonance curve towards higher overtones (*i.e.* only the left part of the coupled resonance curve is detected by the QCM). ω_{ZC} cannot be inferred directly.

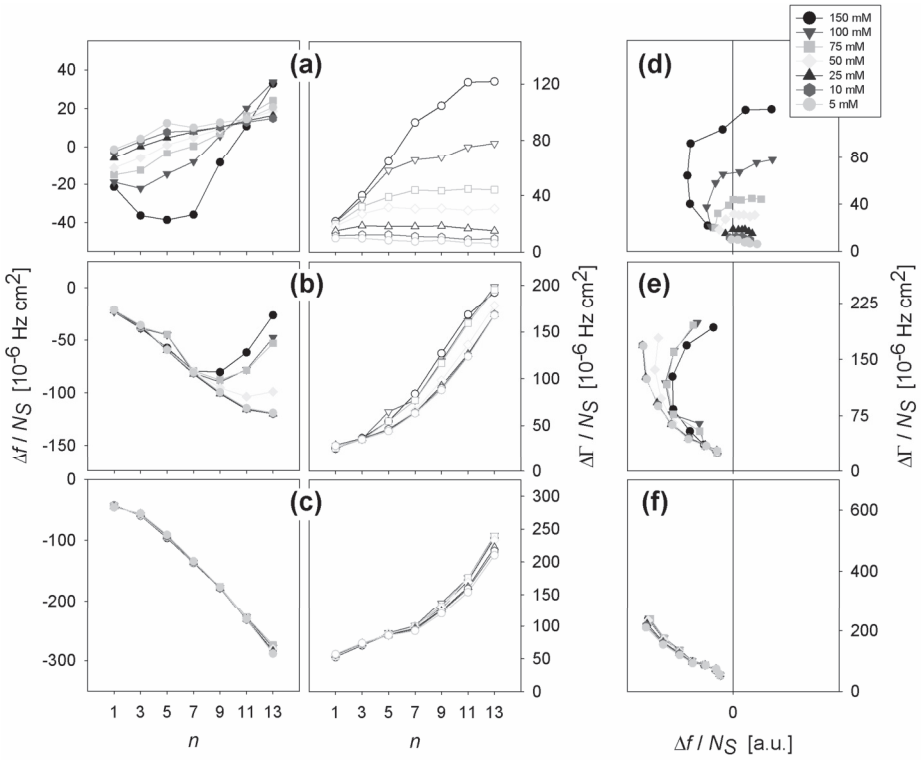

Figure 5. Panels a-c: $\Delta f/N_S$ and $\Delta\Gamma/N_S$ as a function of overtone number (the corresponding frequencies are the overtone number multiplied by 5 MHz) for silica particles on a silica surface (a), silica particles on biotinylated SAM (b) and streptavidin coated silica particles on biotinylated SAM (c). Panels d-f: are the corresponding polar plots. The particle radius was 0.5 μm. Data are averaged values over two separate measurements.

The shape of the curves suggests that there is a hypothetical ω_{ZC} just above the 13th overtone. Δf is clearly ionic strength dependent, ω_{ZC} decrease with increasing ionic strength. For streptavidin-coated particles (Figure 5c) adhering on soft biotin layer the coupled resonance curve is dislocated towards even higher overtones, with ω_{ZC} potentially far above the 13th overtone. $\Delta\Gamma$ is similar for both silica particles and streptavidin-coated particles adhering to biotin. $\Delta\Gamma$ increases with n but never reaches a plateau and does not change as much with ionic strength as silica particles adhering directly on silica. The magnitude of Δf and $\Delta\Gamma$ are also larger for particles adhering to biotin.

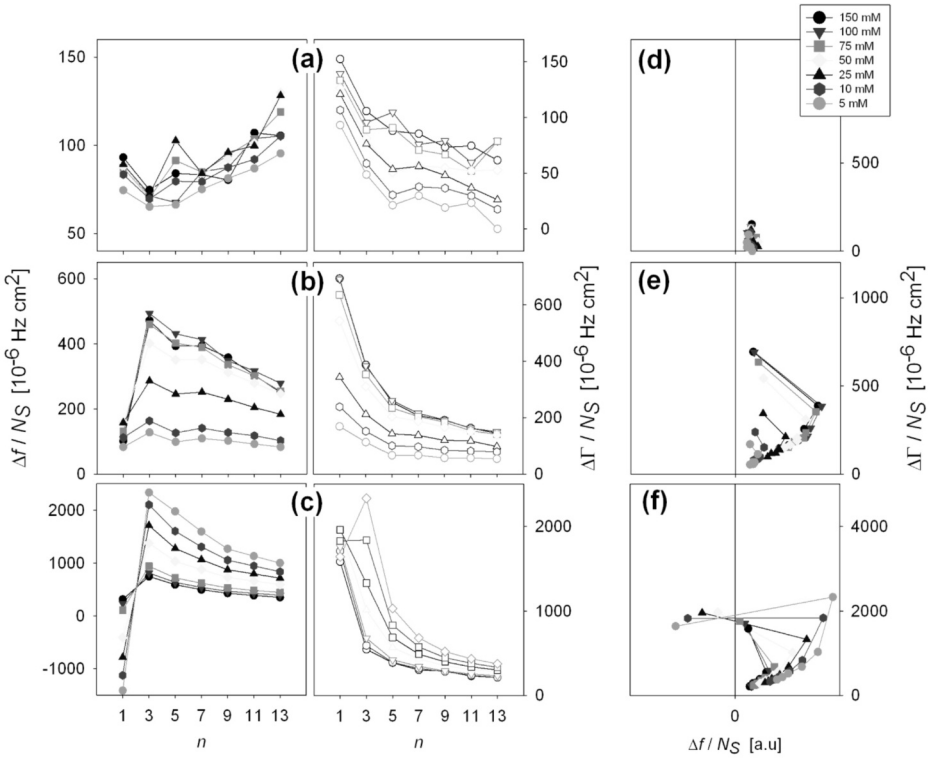

Figure 6. Panels a-c: $\Delta f/N_S$ and $\Delta\Gamma/N_S$ as a function of overtone number (the corresponding frequencies are the overtone number multiplied by 5 MHz) for silica particles on a silica surface (a), silica particles on biotinylated SAM (b) and streptavidin coated silica particles on biotinylated SAM. Panels d-f: are the corresponding polar plots. The particle radius was 2.5 μm. Data are averaged values over two separate measurements.

In the corresponding polar plots (Figure 5d-f) one finds partial circles of varying radius. Silica-silica interaction (Figure 5d) yields the most complete circles but with the smallest radius. The radius increases with ionic strength. Silica-biotin interaction (Figure 5e) yields the second most complete circles with larger radius, but their radius decrease with ionic strength. Streptavidin-biotin interaction (Figure 5f) yields only a quarter of the circle with the largest radius but its radius remains constant with ionic strengths.

In the case of particles with a 2.5 μm radius (Figure 6), the increase in mass, *m*, has dislocated the coupled resonance towards low overtones (*i.e.* only the right hand side of the coupled resonance curve is detected by the QCM). For silica-silica interaction (Figure 6a) Δf is positive at all overtones and slightly increasing with *n*. ΔΓ is also positive, but in contrast to the 0.5 μm radius, ΔΓ has it highest value at the fundamental frequency and decrease with overtone number, indicating the location of ω_{ZC} much lower than the fundamental frequency. The magnitude of both Δf and ΔΓ increase with ionic strength. Presence of a soft biotin layer (Figure 6b) dislocates the coupled resonance curve towards higher overtones. The shape of the curves now suggests that there is a hypothetical ω_{ZC} somewhere just below the fundamental frequency. Δf is still positive at all overtones but has its highest value at the third overtone and then gradually decrease with overtone number. ΔΓ is largest at the fundamental frequency and decreases with ionic strength. The magnitude of both Δf and ΔΓ increase with ionic strength. For streptavidin-coated particles adhering on soft biotin layer (Figure 6c), the coupled resonance curve is further dislocated towards higher overtone numbers. ω_{ZC} is no longer invisible, a zero-crossing frequency can be inferred somewhere between the fundamental frequency and the 3rd overtone. ΔΓ is no longer strictly largest at the fundamental frequency. As the ionic strength decreases, the peak value in ΔΓ moves towards higher overtones. In the corresponding polar plots (Figure 6d-f) the partial circles are now on the right hand side. Silica-silica interaction (Figure 6d) yields a bunch of points and the most incomplete circles. Silica-biotin interaction (Figure 6e) yields less incomplete circles, they are almost half circles, which are larger than for silica-silica, but their radius decrease with ionic strength. Streptavidin-biotin interaction (Figure 6f) yields the most complete circles. They are also the largest, but their radii decrease with ionic strength.

Discussion

Here we have utilized a QCM to investigate the adhesive bond stiffness between different combinations of particles and surfaces. The particles size is varied as well as the softness of the surface. In addition, biotin-functionalized silica surfaces and streptavidin-coated silica particles were used to study the effect of ligand-receptor binding at the interface. All particle-substrate combinations showed evidence of coupled resonance phenomena. Particle adhesive bond stiffness showed dependence to ionic strength, substrate softness and presence of specific interaction.

In the Theory section we described how the original coupled resonance model can be modified to be valid in liquid. Essentially one includes dissipative energy losses by making the frequency shift complex (Eq. 5). Basically one can model the QCM data by Eq. 5. Figure 7 shows an example. The open symbols are the Δf and $\Delta\Gamma$ as obtained with silica/silica contacts at a salt concentration of 150 mM (Figure 5). The parameters used to generate the lines were $\omega_{S,c} = 2\pi$ x 16 MHz, $\sigma = 2\pi$ x 33 MHz, $\gamma = 2\pi$ x 8 MHz, $m = 7/5\ 4\pi/3\ \rho\ R^3$, and $f_{osc} = 0.15$ MHz. The value chosen for γ does not have much effect on the outcome of the model as long as γ is less than about $1/2\ \omega_{S,c}$. The fact that γ is smaller than $\omega_{S,c}$ ($Q_S > 1$) is a conclusion which we draw from the experiment; as long as $Q_S > 1$, Δf turns positive at high frequencies. We justify why this should be so on physical grounds in the appendix of this chapter. The parameters mostly determining the shape of the straight lines in figure 4 are $\omega_{S,c}$ (which sets the frequency where Δf turns from negative to positive values, the zero-crossing frequency, ω_{ZC}), and the width of the distribution, σ, (which sets the width of all features).

The particle density on the surface, N_S, is known from optical imaging and therefore is not a free parameter. For the mass, there is a choice between $2/5\ 4\pi\rho R^3/3$ and $7/5\ 4\pi\rho R^3/3$, which depends on whether the mode is of the rotation type or the wiggling type (see theory section), respectively. One may debate these choices within a factor of 2 or 3. Importantly, the experimental data can in either case only by reproduced if f_{osc} is much less than unity. The combination of parameters $f_{osc}m$ sets the vertical scale. When increasing $f_{osc}m$ by some factor, Δf and $\Delta\Gamma$ increase by this same factor. The shape of the curve does not change. The product of f_{osc} and m is very robust outcome of matching model and experiment. There is a slight cross-correlation between $\omega_{S,c}$ and σ in the sense that an increase in σ also increases the zero-crossing frequency a bit. One can keep ω_{ZC}

constant by increasing σ and decreasing $\omega_{S,c}$ at the same time. For that reason, there is room for debate about the parameter $\omega_{S,c}$. There is little room for debate, however, on the value for $f_{osc}m$. The error bar for this product is 20%, at most. This is important because $f_{osc} << 1$ can only be justified if the resonance is of the wiggling type (Figure 2).

Since we have introduced a distribution of values for ω_S into the model, we do not attempt quantitative fitting. Figure 7 was produced with a Gaussian, but any other distribution might have been used as well. The outcome of the fitting will depend on the shape of the chosen distribution and the derived parameters therefore will not represent a unique solution. We propose a simple semi-quantitative interpretation of the data, which relies on two characteristic features, which are, firstly, the fact that Δf crosses from negative to positive values and the zero-crossing frequency, f_{ZC}, ($f_{ZC} = \omega_{ZC}/2\pi$) and, secondly, the fact that the polar plot produces a section of a circle. The second feature mostly is a cross-check. If the polar plot shows a section of circle, then one trust the coupled oscillator model and proceed with deriving an apparent stiffness from ω_{ZC}.

When the experimental data show a zero-crossing in Δf, one can define an apparent contact stiffness as $k_{app} = m\omega_{ZC}^2$. Comparing to Eq. 2, one sees that this definition amounts to the assumptions that, firstly, k_{app} is a characteristic spring constant, fairly representing the average of the spring constants encountered in the experiment, and that, secondly, ω_{ZC} is not grossly different from ω_S. Both assumptions must be kept in mind when further interpreting the values derived for k_{app} from experiment.

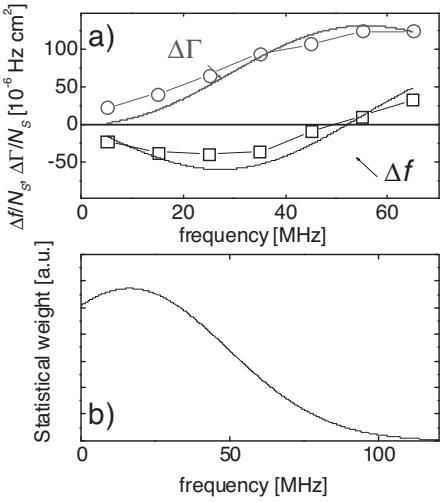

Figure 7. Experimental data for the small spheres (R = 0.5 μm) and a salt concentration of 150 mM (silica/silica), modeled using Eq. 5 (see Theory section). The damping rate was $\gamma = 2\pi$ x 8 MHz. The sample was assumed to be composed of a multitude of spheres with variable contact stiffness. The center of the distribution for ω_S was 2π x 16 MHz. The width was $\sigma = 2\pi$ x 33 MHz. A Gaussian distribution was assumed (panel b). For the mass we used 7/5 $4\pi/3\ \rho\ R^3$. The oscillator strength, f_{osc}, was 0.15.

Clearly, the determination of k_{app} needs an assumption on the parameter m. At this point there is a complication. Since both types of motions are rotations, the parameter m physically must be a moment of inertia, I, which has dimension of kg m^2. Reasonable estimates are $I = 2/5\ MR^2$ for rotation about the center and $I = 7/5\ MR^2$ for rotation about the contact point. In both cases, these estimates do not account for hydrodynamically coupled liquid, and they are therefore lower limits. However, the density of the liquid (1 g/cm^3) is lower than the density of the solid (2.5 g/cm^3) by a factor of 2.5. Also, the penetration depth of shear waves at this frequency is around 0.1 μm, to be compared to a sphere radius of R = 0.5 μm and R = 2.5 μm. We neglect the coupled liquid estimating I.

The fact that the coupled oscillation amounts to a rotation also effects the interpretation of the bond stiffness. The contact exerts a torque and the coordinate describing the motion is an angle. The parameter k therefore must be replaced by a parameter k', which has dimension of Nm. The ratio k'/I (equal to ω_S^2) still has dimension of s^{-2}, as it must be. If the motion is the wiggling type, we have

$$k_{wig,app}' = \frac{7}{5} MR^2 \omega_{ZC}^2 \tag{6}$$

For the rotation, the factor of 7/5 simply is replaced by 2/5. If we apply this simple model to the data set shown in Figure 7 (f_{ZC} = 56 MHz), we find an apparent bending stiffness of $k_{app}' \sim 56$ pN m. This value can be compared to the prediction from Hertz theory, which is (Johnson, 1989)

$$k'_{wig,Hertz} = \frac{32(2-\nu)}{9(3-\nu)} Ga^2R \sim 2Ga^2R \tag{7}$$

Here ν is the Poisson ratio (ν ~ 0.3 for quartz and silica), G is the shear modulus ($G \sim 30$ GPa for quartz and silica), and a is the contact radius. Inputting values, one finds a contact radius of $a_{app} \sim 43$ nm. For rough surfaces, the radius of the contact area is often estimated as $(2\delta_r R)^{1/2}$ with δ_r the vertical scale of roughness. Using $\delta_r \sim 2$ nm, one predicts a contact radius of 40 nm (if the contact radius is dominated by roughness). This shows that the analysis makes sense. The above estimate does not say that the contact radius would be dominated by roughness alone. In fact, the experiments show that this is not the

case. When changing the salt concentration, we shift the balance between Van der Waals attraction and electrostatic repulsion. The zero-crossing frequency, *i.e.* bond stiffness, shifts linearly with electrostatic repulsion (Figure 8). This shift in bond-stiffness is explained by a dependence of the effective contact radius on normal force.

It is instructive to go through the same calculation assuming that the mode is a rotation about the sphere center, rather than a wiggling motion (Figure 2). For rotation, the torque-angle ratio, $k'_{rot,app}$ is given by the shear stiffness of the link times R^2. The apparent shear stiffness as derived from f_{ZC} = 56 MHz comes out to be $k_{shear,app}$ = 64 N/m. Note: this is an ordinary spring constant in units of N/m (no prime as in Eqs. 6 and 7). $K_{shear,app}$ is to be compared to the shear stiffness of the Hertzian contact, which $k_{shear,Hertz} = 4Ga/(2-\nu)$. Inputting values one finds an apparent contact radius of 0.4 nm, which does not make much sense. This calculation further corroborates assigning describing the coupled resonance to the wiggling motion.

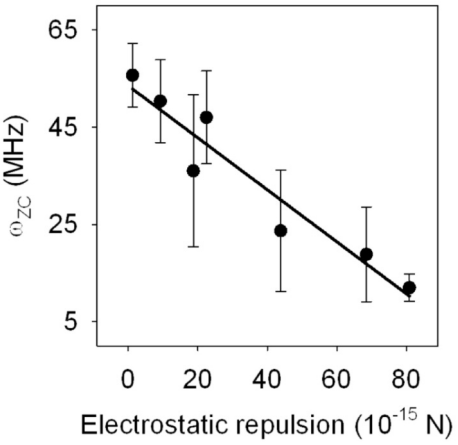

Figure 8. Zero crossing frequency ω_{zc} as a function of electrostatic repulsion, between silica particles of 0.5 µm radius and silica surface at different ionic strengths between 5 and 150 mM KCl. ω_{zc} is an indirect parameter for the adhesive bond stiffness. Thus the adhesive bond stiffness decreases linearly with electrostatic repulsion. Error bars represent SD over three separate experiments. R^2 = 0.92.

Further support for the interpretation of the resonance as a wiggling motion derives from the fact that ΔΓ in almost all cases monotonously increases with frequency. The rotational mode should be higher in frequency than the wiggling mode (see appendix). Possibly, the rotational mode is also very broad, is located to the right of the wiggling mode, and has a low frequency wing extending into experimental frequency range. In this

case the wing of the rotational mode would mask the peak in the plot ΔΓ vs. *n* (Figure 4b), which would otherwise be observed.

A second qualitative feature in the experimental data is the radius of the circles in the polar plot, R_{PD}. As long as $Q_S > 1$, the radius is about ½ times ΔΓ at the zero-crossing frequency. We omit the algebra. For a fixed value of ω_S, one finds

$$\frac{R_{PD}}{N_S} \approx f_{osc} \frac{f_F}{2\pi Z_q} m\omega_S Q_S \qquad (8)$$

We have pulled N_S to the left side of the equation, because results are better displayed in terms of $\Delta f/N_S$ and $\Delta\Gamma/N_S$. In this way, different experiments can more easily be compared (Figure 5 and 6).

As the calculations leading to Figure 3 show, heterogeneous broadening decreases the size of the circle in much the same was as damping. As the distribution becomes broader, the height of the peaks decreases. The details again depend on the distribution chosen, but a reasonable guess amounts to replacing Q_S by Q^*:

$$\frac{R_{PD}}{N_S} \approx f_{osc} \frac{f_F}{2\pi Z_q} m\omega_{S,c} Q^* \approx f_{osc} \frac{f_F}{2\pi Z_q} m\sqrt{\frac{k_{app}'}{I}} Q^* \qquad (9)$$

In most cases, the experimental frequency range does not encompass the zero-crossing frequency, but the polar diagram still shows a section of a circle. If, for given set of experiments, the radius of these circles increases when changing experimental conditions, one may hypothesize that the apparent contact stiffness increases as well. Of course this assumes that Q^*, I, m, and f_{osc}, remain unchanged between experiments.

Such an increase of R_{PD} is seen in Figures. 5 d-e and 6 d-e, when biotin and streptavidin are introduced into the link between particle and surface. It might feel counterintuitive that "soft" biotinylated SAM-layer would form a stiffer contact than the "hard" silica surface. However, using the same lines of arguments used for silica-silica interaction it makes sense, it is all about contact area. Deformation of soft surfaces crates a larger contact area upon contact with particles as compared to hard surface. As the interaction becomes specific (biotin-streptavidin) the particles become even more tightly

adsorbed which invokes an even larger contact area, and thereby and even stiffer bond. Interestingly, for the biotin-silica interaction (b and e) the stiffness decreases with ionic strength. This in direct contrast to the hard sphere-plate contact formed between silica and silica. The explanation lies in the molecular mobility within the biotin-layer. At low ionic strengths the electrostatic repulsion between the silica particle and the gold surface pushes the particle away from the surface, whereupon the biotinlylated PEG-molecules become stretched (or less collapsed). Consequently their mobility decreases and the contact point become stiffer. When salt is added, the electrostatic repulsion decrease and the PEG-molecules retain their freedom of mobility and the stiffness decrease. Ionic strength has no apparent effect on biotin–streptavidin interaction indicating a predominance of specific interactions over non-specific interactions and SAM-layer structural effects.

The frequency of zero-crossing is not only influenced by the contact point stiffness but also by the particle mass (Eq. 2). In experiments done with particle radii of 2.5 μm (Figure 6), the coupled resonance has been dislocated to resonance frequencies close to the fundamental frequency (n=1, 5 MHz) due to increase in mass. Similar to smaller particles, the adhesive bond stiffness increase when introducing biotin and streptavidin. In contrast to smaller particles the silica-biotin interaction becomes stiffer with ionic strength. Possibly, Van der Waals and gravitational forces for particle radii of 2.5 μm overcome the steric hindrance offered by the SAM-layer and thereby the particles come in direct contact with the silica substrate. The adhesive bond stiffness is then governed by non-specific electrostatic interactions rather than the interfacial molecular arrangement. For streptavidin-biotin interaction, on the other hand, stiffness decreases with ionic strength. This can be explained by the fact that streptavidin-coating adds an additional molecular layer at the interface. Additional molecular layer brings further steric hindrance, possibly with a higher hydrostatic pressure than biotinylated SAM alone, which is more difficult to overcome by Van der Waals and gravitational force. The adhesive bond stiffness is again governed by the molecular arrangement at the interface rather than the non-specific electrostatic interactions.

Summary and Conclusions

This study exploits the potential of QCM as a non-destructive method to study changes/differences in the adhesive bond between a particle and a surface, without breaking its bond. We show that a coupled oscillator theory can, under certain conditions

and assumptions, be used to estimate the adhesive bond stiffness between a particle and substrate at the solid-liquid interface. The adhesive bond stiffness for a hard sphere-plate contact is solely determined by non-specific attractive and repulsive forces. In the presence a soft interface, the adhesive bond stiffness is pre-dominantly determined by presence/absence of specific interaction and/or the internal molecular arrangement of the soft layer.

This chapter contains numerous statements on the methodology of data analysis and we summarize the essentials here:

- If the plot of Δf vs. n shows a zero-crossing and if, further, the polar diagram shows a section of a circle, one may analyze the experiments in the frame of the coupled resonator model.
- For spheres with a radius larger than about 0.5 μm one can expect the coupled resonance to be underdamped (see appendix for details). If, on the contrary, the resonances are overdamped, one does not expect a zero-crossing in the Δf vs. n plot.
- The experiments reported here could only be matched by the model if a broad distribution of contact stiffnesses was assumed.
- The amplitude of the coupled resonance was much weaker than expected, which is explained by an oscillator strength being much less than unity. This, in turn, is explained by the coupled resonance being a *wiggling* motion, rather than a rotation about the center of the sphere.
- The radius of the circle sections in the polar plots is predicted by the coupled resonator model, as well. If the zero-crossing frequency is outside the experimental range but the polar plots show still circles sections, one may compare the radii between different experiments. Large radii correspond to large contact stiffness and vice versa.

Appendix

Oscillator Strength of the Wiggling Mode

The Theory section was mostly based on the mechanical circuit shown in Figure 1. From such equivalent circuits, one derives model parameters amenable to intuition. Also, the algebra is straight-forward. Evidently, the real situation is more complicated. The sphere is not a point mass and the liquid is not a dashpot. Stress and strain are 3D tensor fields.

In principle, the one-size-fits-all answer to this problem is finite element modeling (FEM). The disadvantages are well known. For a known geometry one can with good confidence predict the stress distribution (and from this the frequency shift), but it is difficult to run this machine backwards. There is no simple, unique way to interpret experimentally determined frequency shifts in terms of the geometric and viscoelastic parameters entering the FEM calculation. For the case investigated here, there is the further problem that the software package available to us (the Incompressible Navier Stokes Module by COMSOL GmbH, Göttingen) can only do these calculations in 2D. With 2D calculations, one can always make qualitative statements and corroborate certain hypotheses derived from intuition and common sense. Quantitative predictions are more difficult. The question whether or not the wiggling mode can be observed in an experiment is such a qualitative question.

The FEM calculation per se is described in detail in Johannsmann et al. (2008) (Johannsmann et al., 2008). Its application to the coupled resonance is described in (Pomorska et al., 2010). We refer the reader to Pomorska et al. (2010) for details. Figure 9 shows the shifts of frequency and bandwidth versus frequency obtained from this calculation. The frequency scale is in arbitrary units because the sphere size did not match the experiments reported here. Δf and $\Delta\Gamma$ are in arbitrary units for the same reason. The parameter which was varied between the different curves in Figure 9 was the stiffness of the link. The stiffer the link, the higher resonance frequencies the spheres possess. Importantly, one observes two resonances for each stiffness. Figure 9c plots $\Delta\Gamma$ versus ω obtained for the stiffest link on a linear scale. The integral over the peaks is proportional to the oscillator strength. The oscillator strength of the wiggling mode is much weaker than the oscillator strength of the rotational mode. This was true for all cases investigated, but the ratio of the oscillator strengths depended on the stiffness of the link, the width of

the link and the viscosity of the liquid. These dependences are beyond the scope of this work. FEM modeling supports the notion of a wiggling mode being observable with the QCM and, further, suggests that the oscillator strength of this mode is much less than unity.

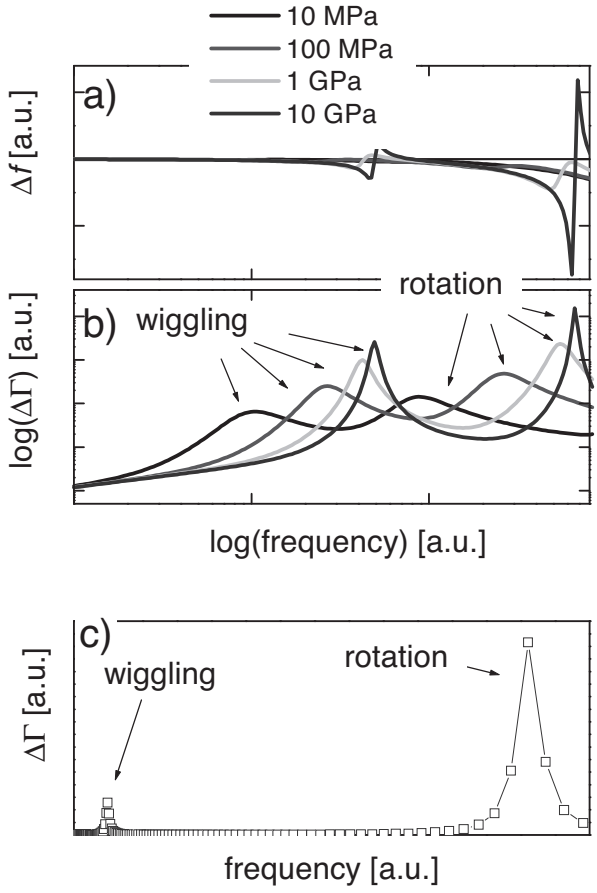

Figure 9. Shifts of frequency and bandwidth as computed from the FEM model. The numbers in the inset denote the stiffness of the link. Importantly, one observes two resonances, which are the wiggling mode and the rotational mode. Panel c shows $\Delta\Gamma$ vs. ω for the highest stiffness on a linear scale. The integral over a peak is proportional to its oscillator strength, f_{osc}.

Quality Factor of the Coupled Resonance, Q_S

In the main text, we argued that coupled resonance was underdamped because we observed positive Δf at high n. Here we demonstrate that such a statement can be corroborated on physical grounds. This is possible because the ratio of ω_S and γ (the quality factors, Q_S) can be estimated from the known equation of hydrodynamics.

The central assumption is that most of the damping originates from the coupling to the bulk liquid. The energy dissipated at the contact is neglected. Further, we assume the radius of the sphere to be larger than then penetration depth of the acoustic shear wave, $\delta = (2\eta/(\rho\omega))$. For a 5 MHz crystal in water, δ is 250 nm / $n^{1/2}$. For the equations below we use $\delta \sim 100$ nm.

For an isolated sphere undergoing periodic translation and/or periodic rotation, the drag coefficient and the effective mass are known (Landau & Lifshitz, 1987). For translation one has

$$\xi = 6\pi\eta\frac{R^2}{\delta}, \quad m = \frac{2\pi}{3}\rho R^3 \tag{10}$$

For rotation, the corresponding equations are

$$\xi' = \pi^2\eta\frac{R^4}{\delta}, \quad I = \frac{2}{5}\frac{4\pi}{3}\rho R^5 \tag{11}$$

ξ has acquired a prime because is the ratio of a torque and a speed of rotation. I is a moment of inertia.

For translation, using $Q_S = (mk)^{1/2}/\xi$ and $\omega_S = (k/m)^{1/2}$, one finds

$$Q_S = \frac{\sqrt{mk}}{\xi} = \frac{m\omega_S}{\xi} = \frac{2\pi\rho R^3/3}{6\pi\eta R^2/\delta}\omega_S = \frac{1}{9}\frac{\rho}{\eta}R\delta\,\omega_S \tag{12}$$

Inserting the density of silica ($\rho \sim 2.5$ g/cm^3), the viscosity of water ($\eta = 1$ mPas), the shear wave penetration depth ($\delta \sim 100$ nm) and a particle resonance frequency $\omega_S = 2\pi\, 50$ MHz and particles radii R 0.5 μm and 2.5 μm, yields $Q_S = 4.4$ and $Q_S = 22$, respectively.

For rotation, again using $Q_S = (mk)^{1/2}/\xi$ and $\omega_S = (k/m)^{1/2}$, one finds

$$Q_S = \frac{\sqrt{Ik'}}{\xi'} = \frac{I\omega_S}{\xi'} = \frac{8\pi\rho R^5/15}{\pi^2\eta R^4/\delta}\omega_S = \frac{8}{15\pi}\frac{\rho}{\eta}R\delta\,\omega_S \qquad (13)$$

k' (in units of Nm) is the ratio of a torque and an angle. Inserting the same values as above yields $Q_S = 6.6$ and $Q_S = 33$ for the small ($R = 0.5$ μm) and the large ($R = 2.5$ μm) silica particle, respectively.

Regardless of the particular mode under consideration, the motion of the sphere is a superposition of rotation and translation. It might be a pure rotation. As long as the dissipation is dominated by the interaction between the sphere and the bulk liquid, one has $Q_S > 1$.

Chapter 8

General discussion

General discussion

In this thesis, we have shown that the explanation for positive frequency shifts during particle adhesion (including adhesion of bacteria) in QCM lies in the fact that particles do not couple to the sensor surface as a mass, but rather as resonators, possessing particle mass and adhesive bond stiffness dependent resonance frequencies. The coupled resonance model was adopted for analysis first upon discovery in chapter 4 and then onwards in chapters 5, 6 and 7. In this chapter we therefore briefly discuss the experimental outcomes of chapters 2 and 3 on the basis of the coupled resonance model.

Streptococcal adhesion in chapter 2, yielded negative frequency shifts at first, which turned positive over time as the number of bacteria present on the sensor-surface increased. The fact that the frequency shifts were positive at the fundamental frequency indicates that fibrillated streptococci adhere to bare gold with relatively soft adhesive bonds allowing for streptococcal resonance frequencies below 5 MHz, which coincide with the results of streptococcal adhesion in chapter 5. On the other hand, the frequency shifts at overtones above the 3rd overtone all yielded negative frequency shifts. In chapter 4 we showed that bacterial extracellular polymeric substances can adhere to the sensor surface and thereby shift the coupled resonance towards negative frequency shifts, similar as for molecular adsorption. Positive frequency shifts at lower overtones in combination with negative frequency shifts at higher overtones, which are far away from a zero-crossing frequency, suggest that the results in chapter 2 are influenced by molecular adsorption. In this respect it is important to notice that molecular adsorption not only arises from bacterial extracellular polymeric substances, but that it may also arise from adsorption of molecular contaminants in a bacterial suspension. This would also explain why the initially negative frequency shifts turn positive with time in some cases. Positive frequency shifts likely occurred first when there were enough bacterial cells on the sensor-surface to balance out the negative shifts caused by molecular adsorption. The risk of substantial influence on the frequency shifts due to adsorption of minor contaminants in a bacterial suspension made us increase the amount of buffer used while washing the harvested bacteria. Although this measure seems to have reduced the influence of molecular adsorption during experiments, one should always remain cautious for the risk of molecular contamination.

In chapter 3, we studied time dependent bacterial bond-maturation by modeling the QCM dissipation-response by an exponentially decaying function, previously used to describe bacterial bond-maturation, which was integrated over the number of adhering bacteria as a function of time. Since we did not understand the reasons for, or even the significance of positive frequency shifts, we only analyzed the dissipation response. We assumed that changes in dissipation were linearly related to the hydration of the bacterium-substratum interface, although we would later discover that, on the basis of the coupled resonance model, dissipation is non-linearly dependent on adhesive bond stiffness. Even though dissipation very well may be associated to the hydration of the interface, it would most definitely be affected by the adhesive bond stiffness as well. This would especially be the case for an adhesive bond stiffness allowing for bacterial resonances that falls within the accessible QCM resonance frequency range, which coincide with peaks in dissipation. This could possibly explain the hump in $\Delta D/N$-values observed between 0 and 200 s in Figure 2 of chapter 3. Based on the non-linear behavior of both frequency and dissipation in the coupled resonance model, we may conclude that it is not very likely that the particular equation chosen in chapter 3 accurately describes the bond-maturation process. Nevertheless, chapter 3 conceptually demonstrates how to tackle unsynchronized adhesion when studying time dependent processes at the level of individual bacteria.

We have just started to understand how we can extract adhesive bond stiffness using QCM by studying zero-crossing frequencies. Since we are limited by the fixed window of available resonance frequencies in QCM, our conclusions have been made from qualitative comparisons of the resonance frequencies of different bacterial strains. Figure 1 summarizes the bacterial and particle resonance frequencies at different surfaces. Note, the resonance frequencies that fall outside the QCM resonance frequencies are only roughly estimated based on the appearance of Δf versus QCM resonance frequency curves. For the time being, we are satisfied that we are able to present a simple analysis of adhesive bond stiffness by comparison of different particle/bacterial resonance frequencies. Assessing bacterial resonance frequencies that fall outside the range of available resonance frequencies in QCM in order to more accurately predict the stiffness of a bacterium-substratum interface requires theoretical modeling. Presently, the measured data can be fitted to the coupled resonance model by varying three different parameters i.e. allowing for a broad-distribution of stiffnesses, allowing for visco-elasticity of the adhesive bond and a coupling factor which describes the degree to which the bending or shear mode of oscillation couples to the sensor-surface. Due to the fact that

such a model relies on three independent parameters, it allows for multiple solutions rather than one unique. In order to make the model more robust, well thought experiments need to be performed to determine the range in which each of these parameters varies, which would make the prediction of bond stiffness more reliable. For future work it is therefore essential to investigate how these parameters may depend on the interfacial properties.

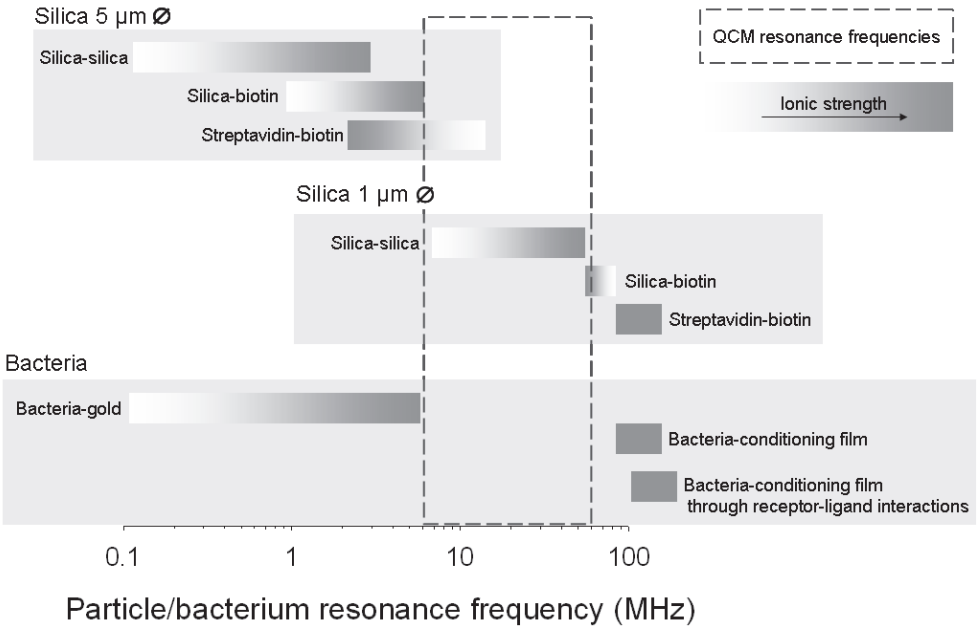

Figure 1. Summary of particle and bacterial resonance frequencies for adhesion to different surfaces, including the influence of ionic strength. The dashed rectangle indicates the range of observable QCM frequencies.

The implications of the coupled resonance model in bioadhesion research and among QCM users in general can only be speculated upon. The question still remains, as to what the practical meaning of adhesive bond stiffness is. Future work should therefore

focus on understanding how the adhesive bond stiffness relates to tenacity of adhesion (i.e. adhesion kinetics), how it relates to the adhesive force, and if it plays a role in the ability of a bacterium to withstand detachment due to an applied force. However, application of the coupled resonance model is not limited to investigations of bacterium-substratum interactions. As we have seen in chapter 7, functionalized sensor-surfaces and surface-functionalized colloidal probes can be used to study the mechanical properties of specific receptor-ligand type of interactions. In chapter 7 we studied biotin-streptavidin bonds, but as long as the molecules can be immobilized on the surface, basically any receptor-ligand combination could be studied. Studying the interaction between different surface modifications does not rely on modeling in the same way as bacterial adhesive bond stiffness does. Whereas the resonance of a bacterium is fixed due to its adhesive bond stiffness and mass, the frequency of a colloidal probe can be tuned into the measurement regime for any adhesive bond stiffness, simply by changing its size or density while keeping its surface unchanged (see Figure 1).

References

References

Abu-Lail, N. I., & Camesano, T. A. (2003). Role of ionic strength on the relationship of biopolymer conformation, DLVO contributions, and steric interactions to bioadhesion of *Pseudomonas putida* KT2442. *Biomacromolecules*, *4*, 1000-1012.

Abu-Lail, N. I., & Camesano, T. A. (2006). Specific and nonspecific interaction forces between *Escherichia coli* and silicon nitride, determined by poisson statistical analysis. *Langmuir*, *22*, 7296-7301.

Allison, D. (2003). The biofilm matrix. *Biofouling*, *19*, 139-150.

Anderson, T. L. (2005). *Fracture mechanics: Fundamentals and applications*. (CRC Press)

Andersson, M., Andersson, J., Sellborn, A., Berglin, M., Nilsson, B., & Elwing, H. (2005). Quartz crystal microbalance-with dissipation monitoring (QCM-D) for real time measurements of blood coagulation density and immune complement activation on artificial surfaces. *Biosensors & bioelectronics*, *21*, 79-86.

Berglin, M., Olsson, A., & Elwing, H. (2008). The interaction between model biomaterial coatings and nylon microparticles as measured with a quartz crystal microbalance with dissipation monitoring. *Macromolecular bioscience*, *8*, 410-416.

Berglin, M., Pinori, E., Sellborn, A., Andersson, M., Hulander, M., & Elwing, H. (2009). Fibrinogen adsorption and conformational change on model polymers: novel aspects of mutual molecular rearrangement. *Langmuir*, *25*, 5602-5608.

Boks, N. P., Busscher, H. J., Van der Mei, H. C., & Norde, W. (2008). Bond-strengthening in staphylococcal adhesion to hydrophilic and hydrophobic surfaces using atomic force microscopy. *Langmuir, 24*, 12990-12994.

Boks, N. P., Kaper, H. J., Norde, W., Busscher, H. J., & Van der Mei, H. C. (2008a). Residence time dependent desorption of *Staphylococcus epidermidis* from hydrophobic and hydrophilic substrata. *Colloids and surfaces B, 67*, 276-278.

Boks, N. P., Norde, W., Van der Mei, H. C., & Busscher, H. J. (2008b). Forces involved in bacterial adhesion to hydrophilic and hydrophobic surfaces. *Microbiology*, *154*, 3122-3133.

Bowen, B. D., & Epstein, N. (1979). Fine particle deposition in smooth parallel-plate channels. *Journal of colloid and interface science*, *72*, 81-61.

Bowen, W. (1999). An atomic force microscopy study of the adhesion of a silica sphere to a silica surface—effects of surface cleaning. *Colloids and surfaces A, 157*, 117-125.

Buchatip, S., Ananthanawat, C., Sithigorngul, P., Sangvanich, P., Rengpipat, S., & Hoven, V. P. (2010). Detection of the shrimp pathogenic bacteria, *Vibrio harveyi*, by a quartz crystal microbalance-specific antibody based sensor. *Sensors and actuators B*, *145*, 259-264.

Camesano, T. A., & Logan, B. E. (2000). Probing bacterial electrosteric interactions using atomic force microscopy. *Environmental science & technology*, *34*, 3354-3362.

Chen, K., Le, D., Zhang, H., Nie, L. H., & Yao, S. Z. (1996). Model of quartz crystal microbe growth sensor and its application to estimation of microbial populations in mineral waters. *Analytica chimica acta*, *329*, 83-89.

Costerton, J. W., Cheng, K. J., Geesey, G. G., Ladd, T. I., Nickel, J. C., Dasgupta, M., & Marrie, T.J. (1987). Bacterial biofilms in nature and disease. *Annual review of microbiology*, *41*, 435-464.

Dabros, T., & Van de Ven, T. G. M. (1982). Kinetics of coating by colloidal particles. *Journal of colloid and interface science*, *89*, 232-244.

De La Fuente, L., Montanes, E., Meng, Y., Li, Yaxin, Burr, T. J., Hoch, H. C., & Wu, M. (2007). Assessing adhesion forces of type I and type IV pili of *Xylella fastidiosa* bacteria by use of a microfluidic flow chamber. *Applied and environmental microbiology*, *73*, 2690-2696.

Dunne, W. M. (2002). Bacterial adhesion : Seen any good biofilms lately ? *Clinical microbiology reviews*, *15*, 155-166.

Dybwad, G. L. (1985). A sensitive new method for the determination of adhesive bonding between a particle and a substrate. *Journal of applied physics*, *58*, 2789-2790.

D'Amour, J., Stålgren, J., Kanazawa, K., Frank, C., Rodahl, M., & Johannsmann, D. (2006). Capillary aging of the contacts between glass spheres and a quartz resonator surface. *Physical review letters*, *96*, 1-4.

Fatisson, J., Domingos, R. F., Wilkinson, K. J., & Tufenkji, N. (2009). Deposition of TiO2 nanoparticles onto silica measured using a quartz crystal microbalance with dissipation monitoring. *Langmuir*, *25*, 6062-6069.

Fowler, T., Wann, E. R., Joh, D., Johansson, S. A., Foster, T. J., & Höök, M. (2000). Cellular invasion by *Staphylococcus aureus* involves a fibronectin bridge between the

bacterial fibronectin-binding MSCRAMMs and host cell beta1 integrins. *European journal of cell biology*, *79*, 672-679.

Gong, K., Mailloux, L., & Herzberg, M. C. (2000). Salivary film expresses a complex, macromolecular binding site for *Streptococcus sanguis*. *The Journal of biological chemistry*, *275*, 8970-8974.

Granéli, A., Edvardsson, M., & Höök, F. (2004). DNA-based formation of a supported, three-dimensional lipid vesicle matrix probed by QCM-D and SPR. *Chemphyschem, 5*, 729-733.

Greene, C., McDevitt, D., Francois, P., Vaudaux, P. E., Lew, D. P., & Foster, T. J. (1995). Adhesion properties of mutants of *Staphylococcus aureus* defective in fibronectin-binding proteins and studies on the expression of fnb genes. *Molecular microbiology*, *17*, 1143-1152.

Gristina, A. (1987). Biomaterial-centered infection: microbial adhesion versus tissue integration. *Science*, *237*, 1588-1595.

Gómez Suárez, C., Noordmans, J., Van der Mei, H. C., & Busscher, H. J. (1999). Detachment of colloidal particles from collector surfaces with different electrostatic charge and hydrophobicity by attachment to air bubbles in a parallel plate flow chamber. *Physical chemistry chemical physics*, *1*, 4423-4427.

He, F., Deng, L., Xie, Q., Nie, L., & Yao, S. (1995). Rapid detection of *Staphylococcus aureus* using a separated electrode piezoelectric crystal sensor. *Analytical letters*, *28*, 213-224.

Heckels, J. E., Blackett, B., Everson, J. S., & Ward, M. E. (1976). The influence of surface charge on the attachment of *Neisseria gonorrhoeae* to human cells. *Journal of general microbiology*, *96*, 359-364.

Hermansson, M. (1999). The DLVO theory in microbial adhesion. *Colloids and surfaces B*, *14*, 105-119.

Hong, S.-R., Choi, S.-J., Jeong, H. D., & Hong, S. (2009). Development of QCM biosensor to detect a marine derived pathogenic bacteria *Edwardsiella tarda* using a novel immobilisation method. *Biosensors & bioelectronics*, *24*, 1635-1640.

Johannsmann, D. (2007). Piezoelectric Sensors. In C. Steinem & A. Janshoff (Eds.). (Springer).

Johannsmann, D., Mathauer, K., Wegner, G., & Knoll, W. (1992). Viscoelastic properties of thin films probed with a quartz-crystal resonator. *Physical review B*, *46*, 7808 - 7815.

Johannsmann, D., Reviakine, I., Rojas, E., & Gallego, M. (2008). Effect of sample heterogeneity on the interpretation of QCM(-D) data: comparison of combined quartz crystal microbalance/atomic force microscopy measurements with finite element method modeling. *Analytical chemistry*, *80*, 8891-8899.

Johnson, K. L. (1989). *Contact mechanics*. (Cambridge University Press).

de Jong, P., te Giffel, M. C., & Kiezebrink, E. A. (2002). Prediction of the adherence, growth and release of microorganisms in production chains. *International journal of food microbiology*, *74*, 13-25.

Kanazawa, K. K., & Gordon, J. G. (1985). The oscillation frequency of a quartz crystal resonator in contact with a liquid. *Analytica chimica acta*, *175*, 99-105.

Kanazawa, K. K., & Gordon, J. G. (1985). Frequency of a quartz microbalance in contact with liquid. *Analytical chemistry*, *57*, 1770-1771.

Katsikogianni, M. G., & Missirlis, Y. F. (2010). Interactions of bacteria with specific biomaterial surface chemistries under flow conditions. *Acta biomaterialia*, *6*, 1107-1118.

Klein, J. D., Clapp, A. R., & Dickinson, R. B. (2003). Direct measurement of interaction forces between a single bacterium and a flat plate. *Journal of colloid and interface science*, *261*, 379-385.

Kwon, K. D., Green, H., Bjöörn, P., & Kubicki, J. D. (2006). Model bacterial extracellular polysaccharide adsorption onto silica and alumina: Quartz Crystal Microbalance with Dissipation monitoring of dextran adsorption. *Environmental science & technology*, *40*, 7739-7744.

Landau, L. D., Lifshitz, E. M. (1987). *Fluid mechanics*. (Butterworth Heinemann).

Lewin, R. (1984). Microbial adhesion is a sticky problem. *Science*, *224*, 375-377.

Long, G., Zhu, P., Shen, Y., & Tong, M. (2009). Influence of extracellular polymeric substances (EPS) on deposition kinetics of bacteria. *Environmental science & technology*, *43*, 2308-2314.

Lowy, Franklin, D. (1998). *Staphylococcus aureus* infections. *The new England journal of medicine*, *339*, 520-532.

Macakova, L., Yakubov, G. E., Plunkett, M. A., & Stokes, J. R. (2010). Influence of ionic strength changes on the structure of pre-adsorbed salivary films. A response of a natural multi-component layer. *Colloids and surfaces B, 77*, 31-39.

Marx, K. A., Zhou, T., Montrone, A., Schulze, H., & Braunhut, S. J. (2001). A quartz crystal microbalance cell biosensor : detection of microtubule alterations in living cells at nM nocodazole concentrations. *Biosensors & bioelectronics, 16*, 773- 782.

Marxer, C. G., Coen, M. C., Bissig, H., Greber, U. F., & Schlapbach, L. (2003). Simultaneous measurement of the maximum oscillation amplitude and the transient decay time constant of the QCM reveals stiffness changes of the adlayer. *Analytical and bioanalytical chemistry*, *377*, 570-577.

Van der Mei, H. C., Rustema-Abbing, M., de Vries, J., & Busscher, H. J. (2008). Bond strengthening in oral bacterial adhesion to salivary conditioning films. *Applied and environmental microbiology*, *74*, 5511-5515.

Van der Mei, H. C., Weerkamp, A. H., & Busscher, H. J. (1987). Physico-chemical surface characteristics and adhesive properties of *Streptococcus salivarius* strains with defined cell surface structures. *FEMS Microbiology letters*, *40*, 15-19.

Molino, P. J., Hodson, O. M., Quinn, J. F., & Wetherbee, R. (2008). The quartz crystal microbalance: a new tool for the investigation of the bioadhesion of diatoms to surfaces of differing surface energies. *Langmuir*, *24*, 6730-6737.

Morikawa, M. (2006). Beneficial biofilm formation by industrial bacteria *Bacillus subtilis* and related species. *Journal of bioscience and bioengineering*, *101*, 1-8.

Morrison, I. D., Ross, S. (2002). *Colloidal dispersions: suspensions, emulsions, and foams.* (Wiley-Interscience).

Muramatsu, H., Watanabe, Y., Hikuma, M., Ataka, T., Kubo, I., Tamiya, E., & Karube, I. (1989). Piezoelectric crystal biosensor system for detection of *Escherichia Coli*. *Analytical letters*, *22*, 2155-2166.

Nivens, D. E., Chambers, J. Q., Anderson, T. R., White, D. C., & James, J. J. (1993). Long-term , on-line monitoring of microbial biofilms using a Quartz Crystal Microbalance. *Analytical chemistry*, *65*, 65-69.

Norde, W. & Lyklema, J. (1989). Protein adsorption and bacterial adhesion to solid surfaces: A colloid-chemical approach. *Colloids and surfaces*, *38*, 1-13.

Olofsson, A., Hermansson, M., & Elwing, H. (2005). Use of a quartz crystal microbalance to investigate the antiadhesive potential of N-acetyl-L-cysteine. *Applied and environmental microbiology*, *71*, 2705-2712.

Olsen, E., Pathirana, S.T., Samoylov., A.M., Barbaree, J.M., Chin, B.A., Neely, W.C., Vodyanoy, V. (2003). Specific and selective biosensor for *Salmonella* and its detection in the environment. *Journal of microbiological methods*, *53*, 273-285.

Olsson, A. L. J., Van der Mei, H. C., Busscher, H. J., & Sharma, P. K. (2010). Novel analysis of bacterium-substratum bond maturation measured using a quartz crystal microbalance. *Langmuir, 26*, 11113-111137.

Olsson, A. L. J., Van der Mei, H. C., Busscher, H. J., & Sharma, P. K. (2009). Influence of cell surface appendages on the bacterium-substratum interface measured real-time using QCM-D. *Langmuir, 25*, 1627-1632.

Olsson, A. L. J., Van der Mei, H. C., Busscher, H. J., & Sharma, P. K. (2011). Acoustic sensing of the bacterium-substratum interface using QCM-D and the influence of extracellular polymeric substances. *Journal of colloid and interface science*, *357*, 135-138.

Van Oss, C. J. (2003). Long-range and short-range mechanisms of hydrophobic attraction and hydrophilic repulsion in specific and aspecific interactions. *Journal of molecular recognition*, *16*, 177-190.

Otto, K, Elwing, H., & Hermansson, M. (1999). Effect of ionic strength on initial interactions of *Escherichia coli* with surfaces, studied on-line by a novel quartz crystal microbalance technique. *Journal of bacteriology*, *181*, 5210-5218.

Otto, K., & Silhavy, T. J. (2002). Surface sensing and adhesion of *Escherichia coli* controlled by the Cpx-signaling pathway. *PNAS*, *99*, 2287-2292.

Otto, K., & Hermansson, M. (2003). Inactivation of ompX causes increased interactions of type 1 fimbriated *Escherichia coli* with abiotic surfaces. *Journal of bacteriology*, *186*, 226-234.

Pavey, K. D., Barnes, L., Hanlon, G. W., Olliff, C. J., Ali, Z., & Paul, F. (2001). A rapid, non-destructive method for the determination of *Staphylococcus epidermidis* adhesion to surfaces using quartz crystal resonant sensor technology. *Letters in applied microbiology*, *33*, 344-348.

Peacock, S. J., Foster, T. J., Cameron, B. J., & Berendt, A. R. (1999). Bacterial fibronectin-binding proteins and endothelial cell surface fibronectin mediate adherence of

Staphylococcus aureus to resting human endothelial cells. *Microbiology*, *145*, 3477-3486.

Poitras, C., Fatisson, J., & Tufenkji, N. (2009). Real-time microgravimetric quantification of *Cryptosporidium parvum* in the presence of potential interferents. *Water research*, *43*, 2631-2638.

Poitras, C., & Tufenkji, N. (2009). A QCM-D-based biosensor for *E. coli* O157:H7 highlighting the relevance of the dissipation slope as a transduction signal. *Biosensors & bioelectronics*, *24*, 2137-2142.

Pomorska, A., Shchukin, D., Hammond, R., Cooper, M. A., Grundmeier, G., & Johannsmann, D. (2010). Positive frequency shifts observed upon adsorbing micron-sized solid objects to a quartz crystal microbalance from the liquid phase. *Analytical chemistry*, *82*, 2237-2242.

Popov, V. L. (2010). *Contact mechanics and friction: Physical principles and applications*. (Springer).

Prakobphol, A,, Burdsal, C. A., & Fisher, S. J. (1995). Quantifying the strength of bacterial adhesive interactions with salivary glycoproteins. *Journal of dental research*, *74*, 1212-1218.

Rasmussen, M. B., Oddershede, L. B., & Siegumfeldt, H. (2008). Optical tweezers cause physiological damage to *Escherichia coli* and *Listeria* bacteria. *Applied and environmental microbiology*, *74*, 2441-2446.

Rawle, R. J., Selassie, C. R. D., & Johal, M. S. (2007). Creation of mammalian single- and double-stranded DNA surfaces: a real-time QCM-D study. *Langmuir*, *23*, 9563-9566.

Reipa, V., Almeida, J., & Cole, K. D. (2006). Long-term monitoring of biofilm growth and disinfection using a quartz crystal microbalance and reflectance measurements. *Journal of microbiological methods*, *66*, 449-459.

Rijnaarts, H. (1995). Reversibility and mechanism of bacterial adhesion. *Colloids and Surfaces B*, *4*, 5-22.

Rodahl, M., & Kasemo, B. (1996). A simple setup to simultaneously measure the resonant frequency and the absolute dissipation factor of a quartz crystal microbalance, *Review of scientific instruments, 67*, 3238-3241.

Rosan, B. (1981). Microbial adhesion to surfaces. *Science*, *214*, 902-3.

Salazar-Banda, G. R., Felicetti, M. A, Gonçalves, J. A. S., Coury, J. R., & Aguiar, M. L. (2007). Determination of the adhesion force between particles and a flat surface, using the centrifuge technique. *Powder technology*, *173*, 107-117.

Saravia-Otten, P., Müller, H. P., & Arvidson, S. (1997). Transcription of *Staphylococcus aureus* fibronectin binding protein genes is negatively regulated by agr and an agr-independent mechanism. *Journal of bacteriology*, *179*, 5259-5263.

Sauerbrey, G. (1959). Verwendung von schwingquarzen zur wagung dunner schichten und zur mikrowagung. *Zeitschrift für physik, 155*, 206-222.

Schofield, A. L., Rudd, T. R., Martin, D. S., Fernig, D. G., & Edwards, C. (2007). Real-time monitoring of the development and stability of biofilms of *Streptococcus mutans* using the quartz crystal microbalance with dissipation monitoring. *Biosensors & bioelectronics*, *23*, 407-413.

Serra, B., Gamella, M., Reviejo, A. J., & Pingarrón, J. M. (2008). Lectin-modified piezoelectric biosensors for bacteria recognition and quantification. *Analytical and bioanalytical chemistry*, *391*, 1853-1860.

Shen, Z., Huang, M., Xiao, C., Zhang, Y., Zeng, X., & Wang, P. G. (2007). Nonlabeled quartz crystal microbalance biosensor for bacterial detection using carbohydrate and lectin recognitions. *Analytical chemistry*, *79*, 2312-2319.

Sonohara, R., Muramatsu, N., Ohshima, H., & Kondo, T. (1995). Difference in surface properties between *Escherichia coli* and *Staphylococcus aureus* as revealed by electrophoretic mobility measurements. *Biophysical chemistry*, *55*, 273-277.

Su, X.-L., & Li, Y. (2005). A QCM immunosensor for *Salmonella* detection with simultaneous measurements of resonant frequency and motional resistance. *Biosensors & bioelectronics*, *21*, 840-848.

Sutherland, I. (2001). Biofilm exopolysaccharides: a strong and sticky framework. *Microbiology*, *147*, 3-9.

Talapin, D. V., & Murray, C. B. (2005). PbSe nanocrystal solids for n- and p-channel thin film field-effect transistors. *Science*, *310*, 86-89.

Tsai, C.-J inn, Pui, D. Y. H., & Liu, B. Y. H. (1991). Particle detachment from disk surfaces of computer disk drives. *Journal of aerosol science, 22,* 737-746.

Tsuneda, S., Aikawa, H., Hayashi, H., Yuasa, A., & Hirata, A. (2003). Extracellular polymeric substances responsible for bacterial adhesion onto solid surface. *FEMS Microbiology letters*, *223*, 287-292.

Urban, J. J., Talapin, D. V., Shevchenko, E. V., Kagan, C. R., & Murray, C. B. (2007). Synergism in binary nanocrystal superlattices leads to enhanced p-type conductivity in self-assembled PbTe/Ag2 Te thin films. *Nature materials*, *6*, 115-121.

Vadillo-Rodríguez, V., Busscher, H. J., Norde, W., de Vries, J., & Van der Mei, H. C. (2004). Atomic force microscopic corroboration of bond aging for adhesion of *Streptococcus thermophilus* to solid substrata. *Journal of colloid and interface science*, *278*, 251-254.

Vaudaux, P. E., Waldvogel, F. A., Morgenthaler, J. J., & Nydegger, U. E. (1984). Adsorption of fibronectin onto polymethylmethacrylate and promotion of *Staphylococcus aureus* adherence. *Infection and immunity*, *45*, 768-774.

Vaudaux, P., Suzuki, R., Waldvogel, F. A., Morgenthaler, J. J., & Nydegger, U. E. (1984). Foreign body infection: role of fibronectin as a ligand for the adherence of *Staphylococcus aureus*. *The Journal of infectious diseases*, *150*, 546-553.

Vaughan, R. D., Sullivan, C. K. O., & Guilbault, G. G. (2001). Development of a quartz crystal microbalance (QCM) immunosensor for the detection of *Listeria monocytogenes*. *Enzyme and microbial technology*, *29*, 635- 638.

Vigeant, M. A., Ford, R. M., Wagner, M., & Tamm, L. K. (2002). Reversible and irreversible adhesion of motile *Escherichia coli* cells analyzed by Total Internal Reflection Aqueous Fluorescence Microscopy. *Applied and environmental microbiology, 68*, 2794-2801.

Vigeant, M. A., Wagner, M., Tamm, L. K., & Ford, R. M. (2001). Nanometer distances between swimming bacteria and surfaces measured by Total Internal Reflection Aqueous Fluorescence Microscopy. *Langmuir*, *17*, 2235-2242.

Vittorias, E., Kappl, M., Butt, H.-J., & Johannsmann, D. (2010). Studying mechanical microcontacts of fine particles with the quartz crystal microbalance. *Powder technology*, *203*, 489-502.

Voinova, M. V., Jonson, M., & Kasemo, B. (1997). Dynamics of viscous amphiphilic films supported by elastic solid substrates. *Journal of physics: Condensed matter*, *9*, 7799-7808.

Voinova, M. V., Jonson, M., & Kasemo, B. (2002). " Missing mass " effect in biosensor ' s QCM applications. *Biosensors and Bioelectronics*, *17*, 835-841.

Voinova, M. V., Rodahl, M., Jonson, M., & Kasemo, B. (1999). Viscoelastic acoustic response of layered polymer films at fluid-solid interfaces: Continuum mechanics approach. *Physica scripta*, *59*, 391-396.

Vörös, J. (2004). The density and refractive index of adsorbing protein layers. *Biophysical journal*, *87*, 553-561.

Walz, J. Y. (1997). Measuring particle interactions with total internal reflection microscopy. *Current opinion in colloid & interface science*, *2*, 600-606.

Zhu, P., Long, G., Ni, J., & Tong, M. (2009). Deposition kinetics of extracellular polymeric substances (EPS) on silica in monovalent and divalent salts. *Environmental science & technology*, *43*, 5699-5704.

Summary

Summary

Microbial adhesion and subsequent biofilm formation occur on virtually all natural or man made surfaces and constitute problems in many fields of human endeavor. Biofilms that form on biomedical implants do not only create great discomfort for patients by impairing the function of the implant but also cause severe infections that are potentially lethal, requiring revision surgery. In order to develop new antifouling-strategies and -surfaces, precise understanding of the interfacial properties of bacterium-substratum interactions is essential. Although the most popular techniques to study microbial adhesion continuously reveal new knowledge and improve our understanding about microbial adhesion phenomena, the details about the complex interactions occurring within the interface between microbes and substratum surfaces are poorly understood. At present, no methods are able to study the mechanics of bio-interfaces in a non-invasive and non-destructive manner. This thesis therefore investigates the potential use of an acoustic sensing technique called Quartz Crystal Microbalance (QCM) for non-invasive and non-destructive study of mechanical properties of interfaces formed upon interactions between microorganisms and surfaces.

Chapter 1 gives a brief introduction to bacterial adhesion, methods currently used to study bacterial adhesion as well as the aim of this thesis. Chapter 1 also briefly introduces what has hitherto been done with QCM in the field of bioadhesion. In short and outspokenly, even though a fair number of publications have been published on the subject, their impact on the understanding of bacterial adhesion has been limited. QCM has indeed been forwarded as a promising technique to study bacterium-substratum interfaces, but the interpretation of the experimental outcome has usually been difficult and the researchers have ended up with qualitative presumptions that are difficult to validate. Therefore, the aim of this thesis is to develop a full and unambiguous interpretation model for bacterial adhesion in QCM.

In chapter 2, a window equipped QCM device was, for the first time, used in combination with a microscope to study bacterial adhesion. As a first step to develop an understanding of how to interpret QCM-signals caused by adhering bacteria, the adhesion of five *Streptococcus salivarius* strains with well characterized surface morphology was studied. All strains examined were hydrophilic but possessed cell surface appendages (*i.e.* fibrils) of different lengths and surface densities. Streptococcal adhesion did not follow

the conventional mass-loading theory, *i.e.* that an adhering mass yields a proportional negative frequency shift. Only a "bald" mutant, completely devoid of all cell surface appendages, yielded a negative shift after four hours of adhesion. All other strains, possessing cell surface appendages, yielded positive frequency shifts even though they adhered in higher numbers. A relation between fibril length and the QCM-signal generated by individual bacteria suggested that the QCM responds to bacterial cell-surface morphology rather than the mass of the adhering bacteria.

Chapter 3 describes a methodology to study time dependent processes occurring within the interface between adhering bacteria and the substratum using QCM. It is known that the bond between bacteria and substratum matures *i.e.* becomes stronger with time. Since bacterial adhesion is a continuous process, the QCM-signal is the sum of all the individual bacteria that adhered to the surface at different points in time. In order to evaluate bond-maturation at the level of single bacteria, the QCM-signal was modeled by a previously proposed equation that was integrated over the number of bacteria that adhered at each point in time, as described by the measured bacterial adhesion kinetics. Although the variation was large, all bacteria yielded a characteristic bond-maturation time constant of roughly 1 min which is comparable to the bond-maturation time constants observed with atomic force microscopy. Rigid silica particles, on the other hand, did not show any change in dissipation over time. This suggests that bacterial bond-maturation is due to a re-conformation of appendages present on the bacterial cell surface.

In chapter 4, we investigate the effect of extracellular polymeric substances (EPS) on the QCM-signal. EPS is excreted by certain bacterial strains upon their adhesion and plays an important role in their adhesion to surfaces and subsequent biofilm formation. The major components of EPS are exopolysaccharides, nucleic acids, proteins, glycoproteins and phospholipids. In this chapter, the adhesion of EPS-producing and non-EPS-producing *Staphylococcus epidermidis* strains was studied in QCM. It was once again concluded that bacterial adhesion does not follow conventional mass loading theory. Both strains yielded positive frequency shifts in line with the experimental outcome in chapter 2. The positive frequency shifts were explained by a coupled resonance model, first described by Dybwad in 1985 for particles adhering to a QCM-sensor in air. The explanation of positive frequency shifts during bacterial adhesion lies in the fact that colloidal particles do not always couple to the sensor surface as a mass. Instead, particles behave as coupled resonators that possess resonance frequencies of their own. The resonance frequency of the particles depends on their mass and their adhesive bond stiffness. If the particle

resonance frequency is below the QCM-sensor frequency, then positive frequency shifts are observed, and vice versa. A change from negative to positive frequency shift occurs when the frequency of the particle matches the resonance frequency of the QCM-sensor. Thus, QCM has the ability to study the stiffness of the adhesive bond between bacteria and a substratum. In chapter 4, we made no attempts to quantify the adhesive bond stiffness but introduced the coupled resonance model as a qualitative explanation for the occurrence of positive frequency shifts. Although both *S. epidermidis* strains yielded positive frequency shifts, the non-EPS-producing strain yielded approximately two-fold higher positive frequency shifts than the EPS-producing strain. This difference between these strains was attributed to EPS adsorption on the sensor surface. Thus, it was concluded that although bacteria adhere according to the coupled resonance model, bacterial adhesion can be accompanied by molecular adsorption influencing the QCM-signal in the negative direction. EPS adsorption as little as only a few percent of the bacterial weight significantly influenced the QCM-signal. This is an important finding not only relating to EPS production of bacteria during adhesion, but since it illustrates how only a small amount of molecular contamination present in a bacterial suspension can cause a positive frequency shift to a negative one, which consequently could lead to miss-interpretation of the results.

In chapter 5, we further elaborate on the concept of coupled resonance by studying differences in the resonance frequency of two streptococcal strains, possessing cell surface appendages of different length and density, at different ionic strengths. It was found that the resonance frequency of streptococci was dictated by their surface morphology, and further influenced by ionic strength. More specifically, it could be concluded that the stiffness of the streptococcal adhesive bond is determined by the packing density of cell surface appendages within the bacterium-substratum interface.

Chapter 6 describes how the adhesive bond stiffness differs between staphylococci that adhere non-specifically and staphylococci that adhere specifically via specific receptor-ligand interactions to an adsorbed fibronectin film. It was found that specific adhesion caused a stiffer bond than non-specific adhesion. Interestingly, both staphylococci adhered to fibronectin with stiffer bonds than streptococci that adhere to bare gold in chapter 5. This is likely due to deformation of the fibronectin film, which may create an even denser packing density of molecules present within the interface.

In chapters 5 and 6, bacterial adhesive bond stiffness was studied indirectly, simply by comparing the bacterial resonance frequencies. In chapter 7, we developed a more

extensive model to extract the bond stiffness for particles adhering at the solid-liquid interface. In short, the coupled resonance model, as valid in air, was extended for use in liquid by considering the contact point as being visco-elastic rather than only elastic, i.e. by adding a damping element (dashpot) next to the already present elastic element (spring). In addition, we introduced the coupled oscillator strength, describing how well the particle resonance coupled to the sensor, and allowed for a distribution of contact-point stiffnesses. We validated the model by monitoring changes in adhesive bond stiffness for silica particles on different surfaces at different ionic strengths. For silica particles interacting with a hard surface (silica), the stiffness of the adhesive bond was directly influenced by the adhesion energy, whereas in presence of a conditioning film the stiffness was influenced by the molecular arrangement and the presence/absence of ligand-receptor interactions (streptavidin-biotin). These findings are all in agreement with the conclusions drawn in chapters 5 and 6, regarding the interpretation of the QCM response to bacterial adhesion. Furthermore, the fact that the experiments could only be reproduced by modeling while assuming weak coupled oscillator strengths, strongly suggests that the particle resonances were of the wiggling-type (i.e. rotation around its contact point) rather than of shear-type (i.e. rotation around its central axis).

In chapter 8 we discuss the potential impact of the QCM-technique on the field of bioadhesion as well as suggest for future work, how to improve the coupled resonance model. We conclude that, by applying the coupled resonance model to bacterial adhesion in QCM, we have developed a method to study the stiffness of adhesive bonding between bacteria and substratum surfaces. The advantage over other techniques, such as flow displacement devices and atomic force microscopy, is that QCM collects its information from a large number of bacteria, simultaneously and in real-time, without breaking their adhesive bonds with the substratum surface.

Samenvatting

Samenvatting

Op vrijwel alle natuurlijke of door de mens gemaakte oppervlakken, vindt microbiële hechting plaats met daaropvolgend de vorming van een biofilm en dit leidt veelal tot problemen. Biofilms op biomedische implantaten zorgen voor ongemak voor patiënten, niet alleen doordat het functioneren van het implantaat vermindert, maar kunnen ook aanleiding geven tot ernstige infecties met potentieel dodelijke afloop, waardoor revisie chirurgie noodzakelijk is. Om bacteriële adhesie te verminderen is bij de ontwikkeling van zogenaamde antifouling-technieken een goed begrip van bacterie-substraat interacties noodzakelijk. Hoewel gangbare technieken steeds nieuwe kennis onthullen, dat ons begrip over microbiële adhesie mechanismen heeft doen toenemen, worden de details van de interacties in het grensvlak tussen microben en oppervlakken slecht begrepen. Op dit moment bestaan er geen methoden om de mechanica van briogrensvlakken op een niet-invasieve en niet-destructieve manier te bestuderen. Dit proefschrift onderzoekt daarom de mogelijkheid om, gebruik makend van een techniek genaamd Quartz Crystal Microbalans (QCM), met akoestische waarnemingen op een niet-invasieve en niet-destructieve manier de mechanica van grensvlakken gevormd bij de interactie tussen bacteriën en oppervlakken in kaart te brengen

Hoofdstuk 1 bestaat uit een korte introductie over bacteriële hechting, een uiteenzetting van hedendaagse methoden ter analyse van bacteriële hechting en het doel van dit proefschrift. Ook introduceert hoofdstuk 1 kort wat er tot nu toe gedaan is met QCM op het gebied van bioadhesie. Publicaties over QCM zijn verre van schaars, maar hebben tot op heden niet geleid tot een beter begrip van bacteriële hechting. De techniek is ooit geïntroduceerd als een veelbelovende techniek om bacterie-substraat grensvlakken te bestuderen, maar deze verwachting is flink bijgesteld door gecompliceerde interpretaties van experimentele data en kwalitatieve, slecht te valideren hypothesen. Daarom is het doel van dit proefschrift het ontwikkelen van een volledig en eenduidig model ter interpretatie van bacteriële hechting in de QCM.

In hoofdstuk 2 wordt een QCM apparaat, voorzien van een transparant venster, voor de eerste keer gebruikt in combinatie met een microscoop om bacteriële adhesie te bestuderen. Als een eerste stap op weg naar een begrip hoe QCM-signalen, veroorzaakt door aangehechte bacteriën, moeten worden geïnterpreteerd, is de hechting van vijf Streptococcus salivarius stammen met een goed gekarakteriseerde oppervlakte

structuren bestudeerd. Alle vijf stammen waren hydrofiel, maar fibrillen op het celoppervlak varieerden in lengte en oppervlaktedichtheid. Hechting van de streptokokken volgde niet de conventionele “mass-loading”-theorie, welke ervan uit gaat dat een hechtende massa een proportionele negatieve frequentie verschuiving veroorzaakt. Alleen een zogenaamde "kale" mutant, zonder fibrillen, leverde een negatieve verschuiving op na vier uur hechting. Alle andere stammen veroorzaakten positieve frequentie verschuivingen ondanks aanhechting in groten getale. Een relatie tussen fibril lengte en het QCM-signaal, gegenereerd door de afzonderlijke bacteriën, suggereert dat de QCM reageert op bacteriële oppervlakte structuren in plaats van op de massa van de hechtende bacteriën.

Hoofdstuk 3 beschrijft een methode om met behulp van de QCM tijdsafhankelijke processen, die plaatsvinden binnen het grensvlak tussen hechtende bacteriën en het substraat, te bestuderen. Het is bekend dat de binding tussen bacteriën en substraat sterker wordt met de tijd. Aangezien bacteriële adhesie een continu proces is, is het QCM-signaal de som van alle individuele aangehechte bacteriën op verschillende tijdstippen. Om de toename van de bindingsterkte per individuele bacterie te evalueren, is het QCM-signaal geëvalueerd met een model overgenomen uit de theorie voor deeltjes depositie. Ondanks de grote variatie leverden alle bacteriën een karakteristieke tijdconstante voor de toename van de bindingsterkte op van ongeveer één minuut, vergelijkbaar met de tijdconstanten voor de versterking van de hechtingskracht, waargenomen met ”atomic force” microscopie. Rigide silica deeltjes vertoonden echter geen verandering van dissipatie in de tijd, hetgeen bevestigt dat de toename in bindingsterkte tijdens bacteriële hechting het gevolg is van een herrangschikking van bacteriële oppervlakte structuren.

In hoofdstuk 4 onderzoeken we het effect van extracellulair polymere stoffen (EPS) op het QCM-signaal. EPS wordt uitgescheiden door bepaalde bacteriestammen volgend op hun aanhechting en het speelt een belangrijke rol in hun hechting aan oppervlakken en de daaropvolgende biofilmvorming. De belangrijkste componenten van EPS zijn exopolysacchariden, nucleïnezuren, eiwitten, glycoproteïnen en fosfolipiden. In dit hoofdstuk werd de hechting van EPS-producerende en niet-EPS-producerende Staphylococcus epidermidis stammen bestudeerd in de QCM. Er werd wederom geconcludeerd dat bacteriële hechting niet de conventionele “mass-loading”-theorie volgt. Beide stammen veroorzaakten positieve frequentie verschuivingen in overeenstemming met de experimentele resultaten in hoofdstuk 2. De positieve frequentie verschuivingen werden verklaard met een gekoppeld resonantie model, het eerst beschreven door

Dybwad in 1985 voor hechtende deeltjes aan een QCM-sensor in de lucht. De verklaring van positieve frequentie verschuivingen tijdens bacteriële hechting is dat colloïdale deeltjes niet altijd als een massa koppelen aan het sensoroppervlak. In plaats daarvan gedragen deeltjes zich als gekoppelde resonatoren die resonantiefrequenties van zichzelf bezitten. De resonantiefrequentie van de deeltjes is afhankelijk van hun massa en de rigiditeit van de binding. Als de resonantiefrequentie van het deeltje lager is dan de QCM-sensor frequentie, dan worden positieve frequentie verschuivingen waargenomen, en vice versa. Een verandering van negatief naar positief frequentie verschuiving treedt op wanneer de frequentie van het deeltje overeenkomt met de resonantiefrequentie van de QCM-sensor. Zo geeft de QCM de mogelijkheid om de rigiditeit van de binding tussen bacteriën en substraat te bestuderen. In hoofdstuk 4 hebben we niet getracht de rigiditeit te kwantificeren, maar het gekoppeld resonantie model als een kwalitatieve verklaring voor het ontstaan van positieve frequentie verschuivingen geïntroduceerd.

Hoewel beide *S. epidermidis* stammen positieve frequentie verschuivingen veroorzaakten, veroorzaakte de niet-EPS-producerende stam ongeveer een twee keer zo grote positieve frequentie verschuiving dan de EPS-producerende stam. Dit verschil werd toegeschreven aan EPS adsorptie op het sensoroppervlak en geconcludeerd dat, hoewel bacteriën zich volgens het gekoppeld resonantie model hechten, bacteriële hechting gepaard kan gaan met moleculaire adsorptie die het QCM-signaal kan doen verschuiven in de negatieve richting. EPS adsorptie, slechts enkele procenten van het gewicht van de bacterie, kan het QCM-signaal significant beïnvloeden. Dit is een belangrijke bevinding, welke niet alleen betrekking heeft op EPS productie van bacteriën tijdens aanhechting, aangezien dit aantoont dat slechts een kleine hoeveelheid moleculaire adsorptie vanuit een bacteriële suspensie een positieve frequentie verschuiving kan doen veranderen in een negatieve, mogelijk leidend tot foutieve interpretatie van de resultaten.

In hoofdstuk 5 wordt nader ingegaan op het concept van gekoppelde resonantie door het bestuderen van verschillen in resonantiefrequentie van twee streptokokken-stammen, die oppervlakte structuren bezitten van verschillende lengte en dichtheid. Experimenten werden uitgevoerd bij verschillende ion sterkten van de bacterie suspensie. De resonantiefrequentie van streptokokken bleek bepaald te worden door oppervlaktestructuren en werd verder beïnvloed door ion sterkte. Concluderend, rigiditeit van de binding wordt bepaald door de dichtheid van de oppervlakte structuren in het bacterie-substraat grensvlak.

In hoofdstuk 6 wordt beschreven hoe de bindingsrigiditeit verschilt tussen stafylokokken die wel dan niet specifiek hechten aan een geadsorbeerde fibronectine film, via specifieke receptor-ligand interacties. Specifieke aanhechting bleek te resulteren in een sterkere binding dan niet-specifieke aanhechting. Beide stafylokokken hechtten met een sterkere binding aan fibronectine dan streptokokken hechtten aan goud (hoofdstuk 5). Dit is waarschijnlijk vanwege de vervorming van de fibronectine film, resulterend in een nog hogere dichtheid van moleculen aanwezig in het grensvlak.

In hoofdstuk 5 en 6 werd bacteriële bindingsrigiditeit indirect onderzocht door het vergelijken van de bacteriële resonantiefrequenties. In hoofdstuk 7 ontwikkelden we een uitgebreider model ter evaluatie van de rigiditeit van de binding van deeltjes in het vaste stof-vloeistof grensvlak. Samenvattend is het gekoppeld resonantie model, net als in de lucht, toepasbaar voor gebruik in vloeistof door het contactpunt meer als visco-elastisch in plaats van elastisch te beschouwen. Dit kan door bijvoorbeeld een dempend element (een soort schokdemper) toe te voegen aan het reeds aanwezige elastisch element (veer). Daarnaast introduceerden we de gekoppelde oscillerende kracht, welke beschrijft hoe goed de deeltjesresonantie relateert aan de sensor, leidend tot een distributie van de rigiditeit van de contactpunten.

We hebben het model gevalideerd door waarnemingen van de veranderingen in de rigiditeit van de binding tussen silica deeltjes en verschillende oppervlakken bij verschillende ion sterkten. Voor de interactie van silica deeltjes met een hard oppervlak (silica), wordt de rigiditeit van de binding direct beïnvloed door de adhesie-energie, terwijl in aanwezigheid van een zogenaamde conditioning-film de stijfheid van de hechting beïnvloed wordt door moleculaire rangschikking en aan- of afwezigheid van ligand-receptor interacties (streptavidine-biotine). Deze bevindingen komen wat betreft de interpretatie van het QCM respons op bacteriële hechting overeen met de conclusies getrokken in hoofdstukken 5 en 6. Ook het feit dat de experimenten alleen kon worden gereproduceerd door het modelleren onder de veronderstelling van zwak gekoppelde oscillerende krachten, suggereert dat de deeltjesresonantie van een schuddend (dwz roterend rond het contactpunt) type is, en niet schuivend (dwz rotatie rond de centrale as).

In hoofdstuk 8 bespreken we de mogelijke impact van de QCM-techniek op het gebied van bioadhesie en worden suggesties gegeven ter verbetering het gekoppelde resonantie model. We concluderen dat, door toepassing van het gekoppeld resonantie model van bacteriële hechting in QCM, we een methode hebben ontwikkeld om de

rigiditeit van de binding tussen bacteriën en substraten te bestuderen. De voordelen ten opzichte van andere technieken, zoals “atomic-force”-microscopie of instrumenten welke de vloeistofstroming beïnvloeden, zijn groot doordat QCM gelijktijdig en real-time informatie verzamelt over een groot aantal bacteriën, zonder de binding met het substraat te verbreken.

Acknowledgements

Yes, we finally made it!

It won't be the prettiest nor the ugliest thesis ever to be seen. Yet here, balancing in your hands, is the proof that I will obtain a PhD degree. It has not always been easy, but after four years of hard work, frustration and sometimes even despair, we did reach the end. Some may ask themselves, why does he refer to himself as 'we'? Well, the answer is simple. The realization of this thesis does not depend on me alone, but also on the help and support from others. In an attempt to show my appreciation to these people, here are my words.

Prashant, thank you for being my supervisor; you have been an excellent one. Not only have you been there to discuss work-related topics, but more importantly, you have always been there as a friend.

Henk and **Henny**, as promotors you have been most essential for the realization of this thesis. Thank you for the time and effort you both have put into my project. I truly appreciate it!

Diethelm, working across disciplines was sometimes a challenge, but in the end very rewarding. I have learned a lot from you. Thank you very much for our collaboration which led to chapter 7.

Hans and **Arun,** I enjoy collaborations, and ours was no different. In fact, it was a lot of fun! Thank you for your contributions to chapter 5.

Danielle and **Otto**, thank you for translating my summary into Dutch.

The reading committee: **Prof. dr. Herrmann, Prof. dr. ir. van Loosdrecht and Prof. dr. ir. Norde,** thank you for taking the time to evaluate my thesis.

The Interface Biophysics group at Gothenburg University deserves acknowledgment for being a source of inspiration to pursue research, which finally led me here. Thank you!

Whether named or not, all colleagues at the department of Biomedical Engineering are acknowledged; some of you for administrative support, others for work-related help, and all of you for just being a part of the good atmosphere. With time, certain of you became more than 'just' colleagues; you became good friends. **Gerwin, Arina, Guru, Das, Brandon, Jan, Isa, Deepak, Agnieszka, Anton H, Daniëlle, Eefje, Jesse, Marieke,** thank you for all the fun!

Speaking of friends, what would life be without friends? Regardless if its about having a couple of drinks, playing ice hockey, making a Swedish road trip or just simply going to the movies, a rich social life made my Groningen experience unforgettable. No one mentioned, no one forgotten. This paragraph is meant for all of you that, in one way or another, have enriched my life outside the walls of the department.

Mom, Dad and **Nina,** we are far apart and I wish we could meet more often. Luckily, nowadays it is quite simple to stay in touch. Your support has been, is, and will always be important to me. Thank you!

Dear **Magda**, the life as *us*, instead of me, just seems so much simpler. In Groningen, my life became our life, and so shall it be. For that I will always be grateful.